GEOCHEMICAL CHARACTERIZATION OF SHALLOW SEDIMENTS FROM THE GROUNDING ZONE OF THE WHILLANS ICE STREAM

by

Kimberly Anne Roush

A thesis submitted in partial fulfillment
of the requirements for the degree

of

Master of Science

in

Land Resources and Environmental Sciences

MONTANA STATE UNIVERSITY
Bozeman, Montana

April 2019

ACKNOWLEDGEMENTS

This work has been the result of a collaboration including multiple people. To start, I want to thank my advisor, John Priscu, for taking me on, a geologist, as a student, entertaining many days of editing, and reminding me to wear deodorant; Mark Skidmore for his enthusiasm and shared story over many a field season; and John Dore for entertaining my wandering questions with respect to the fascinating field of oceanography. Thank you to Alex Michaud and Tristy Vick-Majors for all that you taught me at the bench, sharing your intrigue for polar science and entertaining my never ending stream of recently coded figures. Thank you to Carrie, Wei, Gus and Amy for their enduring inspiration, support in communicating with R, working with the IC, and creating more organization, structure and logical flow to my presentation abilities. Thank you to my family for seeding my curiosity in science and supporting me in this endeavor.

TABLE OF CONTENTS

TABLE OF CONTENTS CONTINUED

TABLE OF CONTENTS CONTINUED

LIST OF TABLES

LIST OF FIGURES

LIST OF FIGURES CONTINUED

ABSTRACT

The research presented in this thesis focused on subglacial flow beneath the West Antarctic Ice Sheet (WAIS) and its potential influence near the grounding zone. Antarctic grounding zones are of specific scientific interest because they can impact the stability of the continental ice sheet and its breakup, potentially resulting in significant sea level rise. My major objective was to determine whether there was influence of subglacial water at the Whillans Grounding Zone (WGZ) on the Siple Coast of the WAIS. A gravity corer was used to collect a 70 cm sediment core through 780 m of ice borehole drilled using a hot water clean access drilling system. The core was collected in a marine embayment adjacent to the WGZ beneath a 10 m water column. I used a combination of geochemical, isotopic and organic matter analyses to characterize the benthic sediments, porewater and water column. The geochemical and isotopic data showed the influence of subglacial freshwater on sediment porewater at specific depths in the 70 cm core. Vertical gradients of chloride and sulfate between surficial sediment and the overlying water column indicated ion diffusion from porewater to the column water. Dissolved organic matter concentration of sediment porewater and the overlying water column also indicated upward diffusion occurs from porewater to the overlying seawater. Sediment particulate carbon and nitrogen data showed that benthic sediments were more depleted in nitrogen than the overlying seawater. Sediment particulate carbon and nitrogen data showed that benthic sediments were more depleted in nitrogen than the overlying seawater. Geochemical, isotopic and organic matter data supports the influence of subglacial freshwater at the WGZ.

CHAPTER ONE

AN INTRODUCTION TO THE WHILLANS GROUNDING ZONE

Since the late 1970's, the role that the ocean plays in regulating climate has been increasingly revealed. The deleterious impacts of climate change are being manifested via diminished freshwater supply and resource availability (Schewe et al. 2014), increased intensity of wet and dry areas (Trenberth 2011), disruption of predictable weather patterns (Milly et al. 2015), loss of ice (Pritchard et al. 2012), decrease in pH (Dore et al. 2009) and sea-level rise (Herr and Galland, 2009).

The increase in global ocean temperature has had major impacts on ice, salinity and ocean circulation. Recent studies document an increase in the volume of freshwater runoff in the Arctic, which is linked to an intensification in large-scale anticyclonic winds and freshening of the upper stratigraphic marine layer. This intensification results in an increase in the volume of a lower salinity water layer in the ocean; changes in the halocline depth and depth of the underlying layer which impacts vertical temperature gradients, heat fluxes and the sea-ice cover (Pemberton and Nilsson 2016). Atmospheric temperature increases are causing freshwater glacial melt globally (Hood et al. 2015), thus altering ocean stratification. In addition, research suggests that the locations of tropical cyclones are reaching their maximum intensity closer to the poles compared to the last 30 years due to the expanding zone of the Hadley circulation cell (Lucas et al. 2014). These impacts are detectable at high latitudes in the southern hemisphere, a region that displays early signs of a changing global climate (Robinson et al. 2018; Rintoul et al. 2018; Sharmila et al. 2018).

Antarctica contains 90% of glacier ice on Earth (Hood et al. 2015). Characterizing the rapidly retreating West Antarctic Ice Sheet (WAIS) grounding zones (Rignot et al. 2014; Khazendar et al. 2016; Milillo et al. 2017) provides an indicator of the rate and extent of hydrologic change associated with glaciers. Freshwater subglacial melt from the WAIS has been found to flow under the ice sheet and flow into the sea (Carter et al. 2012; Horgan et al. 2013). Historically, evidence of episodic subglacial flow has been detected on the Kamb Ice Stream on the Siple Coast (Gray et al. 2005), in the Adventure subglacial trough near Dome C of the East Antarctic Ice Sheet (Wingham et al. 2006) and on Byrd Glacier (Stearns et al. 2008). Focusing on the WAIS, the most climatically-sensitive regions lie at the transition from grounded ice sheet to floating ice shelf. This transition point is sensitive to warm ocean waters eroding the ice and creating uncontrolled retreat of the marine-based WAIS. The development of seismic applications for ice (Siegfried et al. 2016; Siegfried and Fricker 2018) and marine systems (Hamilton 1976; Blankenship et al. 1986, 1987), satellite altimetry and ground-based GPS stations has enabled us to more closely probe the conditions for life at the Whillans Grounding Zone (WGZ) on the Siple Coast, an important point where subglacial water mixes with marine water. Technological developments have enabled us to make discoveries we were not able to make previously in environments that are extremely difficult to access (Priscu et al. 2013b).

Sampling at the WGZ in January 2015 was part of a multi-year collaboration known as Whillans Ice Stream Subglacial Access Research Drilling (WISSARD). WISSARD brought together glaciologists, biologists and geologists to study ice sheet interactions with water, either at the basal boundary where the where ice streams come in contact with active subglacial hydrologic systems (Christner et al. 2014) or at the marine margin where the ice sheet is exposed to tidal forcing (Siegfried and Fricker 2018). The overarching hypothesis of WISSARD was that dynamic glaciological, sedimentological, and geochemical processes act synergistically to influence ice sheet dynamics and control the structure and function of microorganisms inhabiting the Whillans subglacial environment. My research addresses the geochemistry of shallow marine sediments present at the grounding zone. Specifically, I examined the sediments to determine the influence of subglacial freshwater influence and whether the sediment porewaters provide a diffusive source of organic matter to the overlying water column. My research is significant because it is the first to examine the influence of subglacial flow on marine sediments adjacent to the Whillans Ice Stream GZ.

Structure of the Thesis

Chapter 1 highlights the significance of my research, introduces the overarching hypothesis and sub-hypotheses, and introduces Antarctic glaciomarine systems. Chapter 2 focuses on the application of stable isotope and geochemical analysis to determine the extent of subglacial influence on marine sediments at the WGZ. Chapter 3 characterizes particulate carbon and dissolved organic carbon and determines if marine sediments are influenced by a freshwater subglacial component and if the sediment is a diffusive source of dissolved organic carbon to the water column.

Hypothesis and Objectives

The overarching question addressed in my thesis is:

"Is there an influence of subglacial waters on sediments of the Whillans Grounding Zone (WGZ)?"

"Influence" refers to parameters which show characteristics of subglacial waters, such as water previously analyzed in upstream Subglacial Lake Whillans. Subglacial and marine characteristics were obtained using geochemical measurements of water chemistry (stable isotopes, ion chemistry, organic carbon and inorganic nutrients).

My thesis focused on testing the following specific hypotheses:

Hypothesis 1: Porewater geochemistry at the WGZ is subglacially-influenced.

Associated Objectives:

1. Measure stable isotopes of water ($\delta^{18}O$ and δD).
2. Measure concentrations of major cations (Li^+, Na^+, K^+, NH_4^+, Mg^{2+}, Ca^{2+}), and major anions (F^-, Cl^-, Br^-, SO_4^{2-}), and acetate.
3. Compute fluxes of selected ions between sediment porewater and the overlying water column.

4. Construct a two-component mixing model, using SLW water and sub-ice shelf seawater as end-members, to determine the extent of subglacial influence.

*Hypothesis 2: WGZ s*ediments and porewaters at the WGZ are enriched in organic matter relative to overlying seawater.

Associated Objectives:

1. Quantify particulate carbon and particulate nitrogen in WGZ sediments and overlying seawater.
2. Measure dissolved organic carbon of WGZ sediment porewater and overlying seawater.
3. Determine concentrations of total dissolved nitrogen of sediment porewater.
4. Compute vertical flux calculations of dissolved organic carbon between sediment porewater and the overlying water column.

Significance of My Research

My research was part of the WISSARD project and focuses on the first direct acquisition of a sediment core and seawater from an Antarctic grounding zone, the Whillans Grounding Zone (WGZ), on Antarctica's Siple Coast. The first oceanographic measurements (Clough and Hansen 1979; Jacobs et al. 1979a, 1979b; Gilmour 1979; Williams and Robinson 1979) from beneath the Ross Ice Shelf, which abuts the Siple Coast, were collected at J9 with the Ross Ice Shelf Project in 1977.

Evidence of microbial life (Azam et al. 1979; Lipps et al. 1979) and dark inorganic carbon activity was thought to be associated with nitrifying organisms (Horrigan 1981). My data will provide important new insight in characterizing subglacial geochemistry in glaciomarine systems. The sediment core was located ~110 km downstream from Subglacial Lake Whillans (SLW) and about 13 km on the marine side of the grounding line on Antarctica's Siple Coast (Figure 1.1). The 76 0m thick Ross Ice Shelf (RIS) was hot water drilled providing access to the 10 m deep marine water cavity. A gravity corer was then used to extract sediment cores; the core used in my study was 70 cm long.

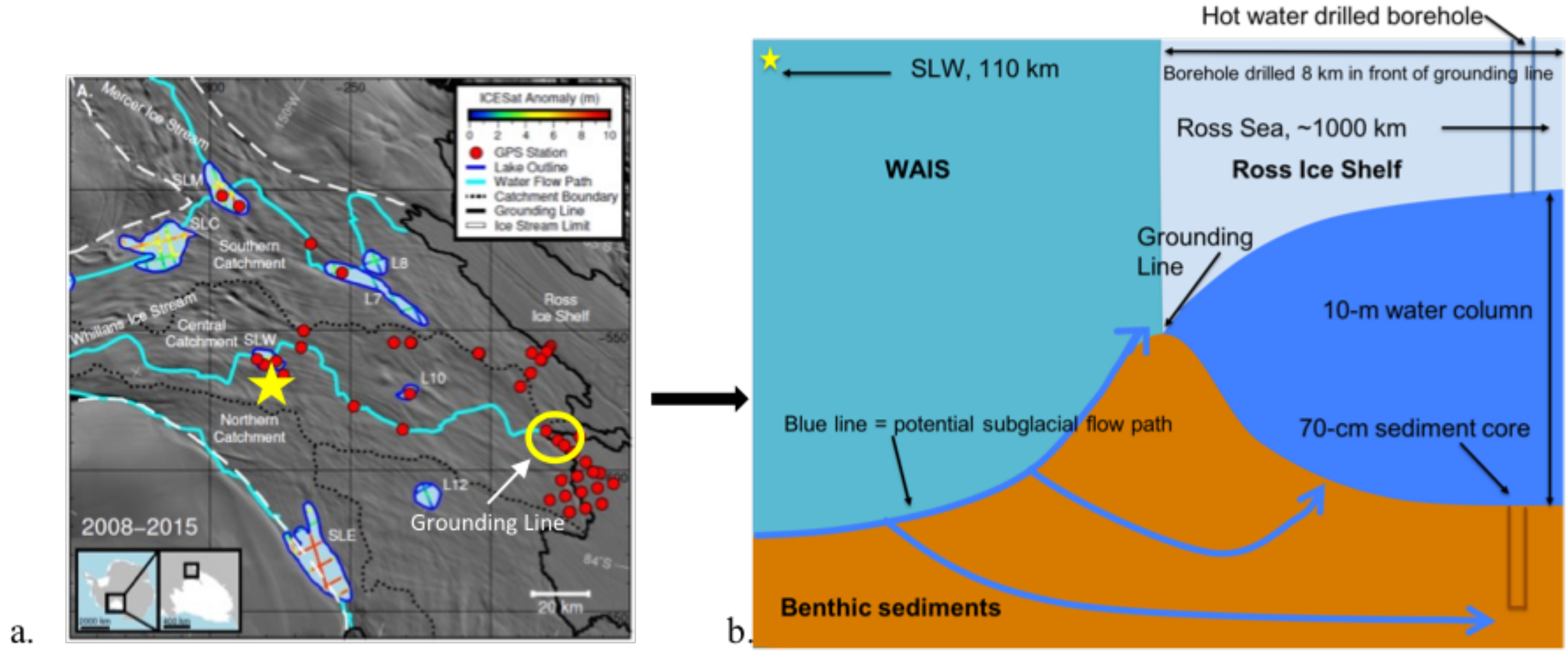

Figure 1. 1 a. The yellow circle indicates the Whillans Grounding Zone (WGZ), where the sediment core was extracted (left). The yellow star indicates SLW. The figure depicts the location where subglacial flow enters into the Ross Ice Shelf Cavity (modified after Siegfried et al., 2014). b. My conceptual working model (right) showing a 3-D cross section of the WGZ. Blue arrows indicate subglacial flow.

Located beneath ~760 m of ice in cold, aphotic conditions, the WGZ is an important transitional environment between the freshwater subglacial WAIS network and the marine RIS cavity. Until recently, logistical and technological challenges prevented the acquisition of samples from sediment and water beneath hundreds of meters of ice; a monumental stride forward was the ability to extract contaminant free samples while protecting these pristine environments (Priscu et al. 2013).

The ice sheet – ice shelf grounding zone is an important environment because it: (i) impacts ice sheet stability and the rate at which ice flows out of the grounded part of the ice sheet (Simkins et al. 2018); (ii) reveals evidence of diurnal tides (Williams and Robinson 1979); and (iii) encompasses the nutrient and geochemical transition from a fresh- to marine dominated system on the way to the Ross Sea, where Antarctica Bottom Water (ABW) is formed. ABW gets passed to the Southern Ocean where it impacts global oceanic circulation and global weather patterns. Consequently, research at the WGZ will provide new information on processes that impact how the WAIS interfaces with Ross Ice Shelf cavity and the Ross Sea.

While McMurdo Sound ANDRILL data collected in 2006 and 2007 (Harwood et al. 2007) suggests a partial collapse of the WAIS as recently as 400,000 years ago (Bamber et al. 2009; Scherer et al. 1998; Kingslake et al. 2018), the retreat of the WAIS is predicted to have a continued impact on global sea level throughout the 21st century (Rignot et al. 2011). Complete collapse of the WAIS has been estimated to result in a global, eustatic sea level rise of 3.3 m (Bamber et al. 2009), which was adapted for regional geographical variation. Previous studies, which did not account for regional variation, estimated a 5- to 6-m rise in sea level (Tol et al. 2006). Due to uncertainty about future atmospheric and oceanic warming and an incomplete understanding of the complex processes and feedback mechanisms that cause sea level to rise, a large degree of uncertainty surrounds projections of global sea-level rise (Horton et al. 2014). The minimal warming scenario (<2°C by 2300 AD) estimates sea level to rise by 0.4 to 0.6 m while the most aggressive warming scenario (8°C by 2300 AD) estimates sea level to rise 2.0 to 3.0 m (Horton et al. 2014).

My study focused on the influence of subglacial flow on the Siple Coast (Figure 1.2) grounding zone environment. Specifically, I analyzed the variation in stable water isotopes, geochemistry and organic matter composition in sediment porewater throughout a 70-cm sediment core and overlying water column to determine if subglacial discharge influences the coastal marine environment at the WGZ.

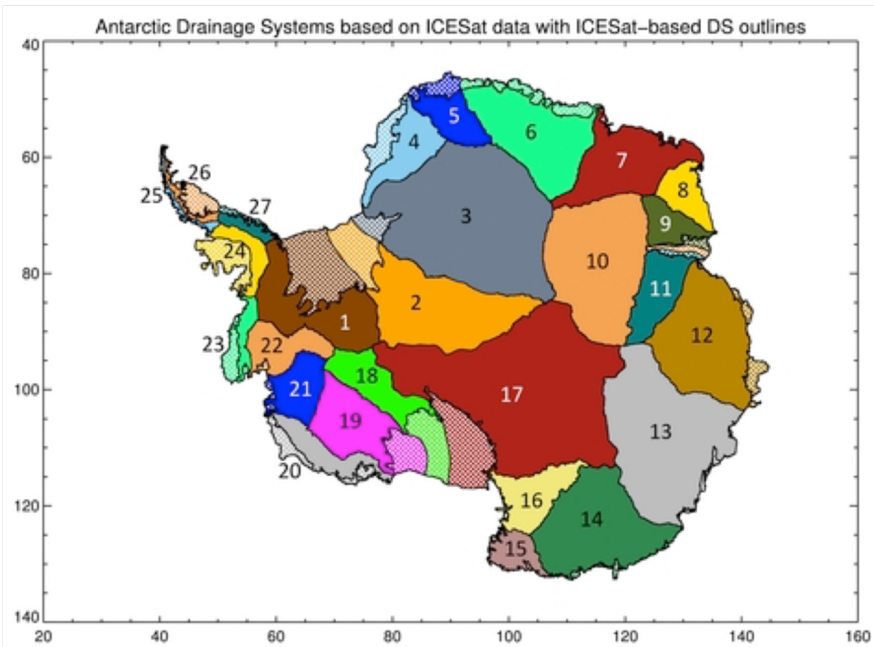

Figure 1. 2 Map shows how NASA split Antarctica into different hydrologic units. The Siple Coast is contained by Unit 18.
https://icesat4.gsfc.nasa.gov/cryo_data/ant_grn_drainage_systems.php

Background: Antarctic Marine Environments

Ice Shelves and Ice Shelf Basal Melt

Previous airborne radio echo-sounding (RES) analysis estimated that 44% of Antarctica was dominated by coastline (Drewry et al. 1982), while satellite imagery reveals that floating ice shelves are thought to account for 75% of the Antarctica's coastline (Swithinbank 1988; Rignot et al. 2013). Ice shelves gain mass through inflow from the grounded ice sheet and lose mass through iceberg calving and surface and basal melting (Smethie and Jacobs 2005). Basal melt has been found to cause rapid mass loss from West Antarctic ice shelves and is recognized as the dominant ablation process in Antarctica, exceeding iceberg calving (Depoorter et al. 2013; Rignot et al. 2013;

Pritchard et al. 2012). As such, basal melt can strongly influence the mass balance of the WAIS (Stewart 2018).

The theory of inclined plumes has provided much insight into the processes of ocean circulation and basal ice shelf melt since its first application (MacAyeal 1984). Large scale water masses created and transported by water density layer stratification (Jenkins 2011). Driven by heat transfer from the ocean to the ice base, the basal melt rate is constrained by the circulation which influences oceanographic conditions within the ice shelf cavity (Stewart 2018). Melt water from the ice sheet in ice shelf cavities aids sea ice growth (Langhorne et al. 2015) and influences large scale sea ice trends (Hellmer 2004). Basal melt rates at the grounding zone are increased by the flux of subglacial freshwater as the freshwater buoyant plume increases the rate at which ocean heat is made available to the ice base through entrainment of recent melt (Stewart 2018). Flow beneath the currently stable Ross Ice Shelf were observed to be moving at 22.2 ± 0.2 m a^{-1} at 1.7 km seaward of the Mercer/Whillans Ice Stream grounding line (Marsh et al. 2016; Jacobs 2004; Jenkins 2011; Jacobs et al. 2011).

Compared to ice-free continental shelves, few observations have been made in the ice shelf cavity (Jacobs et al. 1979a; Pillsbury and Jacobs 1985; Vick-Majors et al. 2016b). In addition to density driven stratification, the wind and tides (barotropic flow), power open ocean circulation while ice shelf cavities are also subject to a buoyancy forcing at multiple locations (MacAyeal 1984). Buoyancy forcing can occur: where subglacial freshwater enters the system from ice-sheet network, where melting occurs at the ice shelf base; or as loss at the surface on the adjacent open continental shelf during winter (Figure 1.3). Where the ice shelf base slopes, the ISW (Ice Shelf Water) forms a buoyant plume, flowing up the base of the shelf (MacAyeal 1984). Sustained by continual fresh meltwater input balanced by entrainment of more saline water from below, the water can become "supercooled" and frazil ice can precipitate upward to the ice base (Holland and Feltham 2006). Known as the "ice pump" (Lewis and Perkin 1986), this mechanism can accrete masses of basal marine ice up to 300 m thick (Lambrecht et al. 2007).

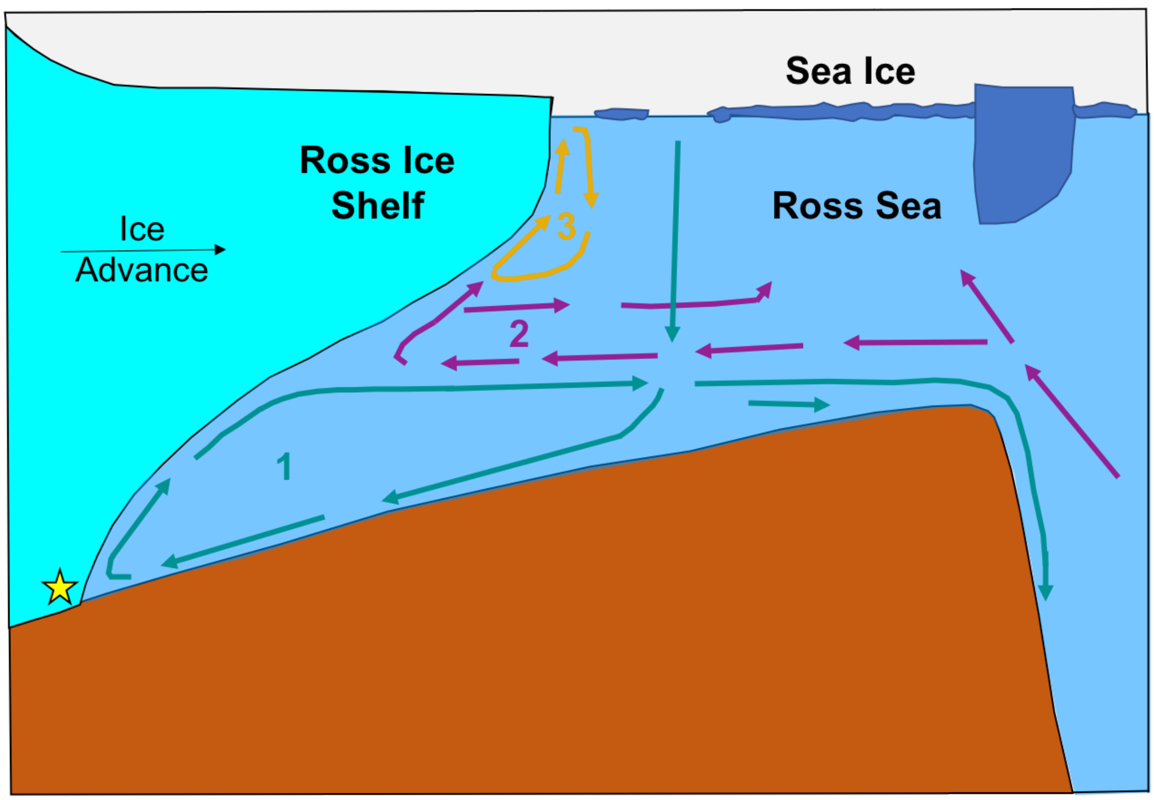

Figure 1.3 The yellow star indicates the location of the grounding line (sediment core GC3 was drilled and extracted seaward from the grounding line). Numbers 1, 2 and 3 refer to modes of sub-ice-shelf cavity melting related to ocean circulation (Jacobs et al. 1992). Mode 1 initiates thermohaline convection in which dense shelf water evolves into cold, fresh Ice Shelf Water (ISW), mode 2 is associated with intermediate-depth "warm" inflows from the slope-front region and mode 3 is associated with relatively shallow bases and where melting is high due to tidal pumping and seasonal coastal currents.

Temperature and salinity control the stratification and flow of major currents in the global oceans. Research shows that Modified Circumpolar Deep Water (MCDW) recirculates out of the Ross Ice Shelf cavity and High Salinity Shelf Water (HSSW) accesses deeper regions of the cavity (Smethie and Jacobs 2005). Using temperature and salinity concentrations from CTD profiles along the ice front in conjunction with chlorofluorocarbon analyses, Smethie and Jacobs estimated a Ross Ice Shelf cavity residence time of 3.5 years and net basal melt rates of 55 Gt yr^{-1} based on the salinity budget, and 18 Gt yr^{-1} based on thermal energy budget assuming an inflow of pure HSSW (Smethie and Jacobs 2005). Reddy et al. (2010) used chlorofluorocarbon concentrations to determine a 2.2-year residence time in the Ross Ice Shelf cavity and a 10 cm yr^{-1} melt rate. This discrepancy suggests that the mean source water for melting is either warmer or fresher the HSSW (Stewart 2018).

Grounding Zones

While the grounding zone refers to the transitional region between a fully grounded ice sheet and a free-floating ice shelf, the grounding line represents the location where an ice sheet (overlying the continental crust) decreases in thickness and transitions to an ice shelf (Parizek et al. 2013). The WGZ refers to the region inland of the grounding line where ice sheet transitions from overriding a continental landmass to an ice shelf floating over marine water, in this case the Ross Sea. The grounding zone associated with the Whillans Ice Stream where samples from the WISSARD project were collected is a marine dominated system located under ~760 m of ice, impenetrable to light (Figure 1.4).

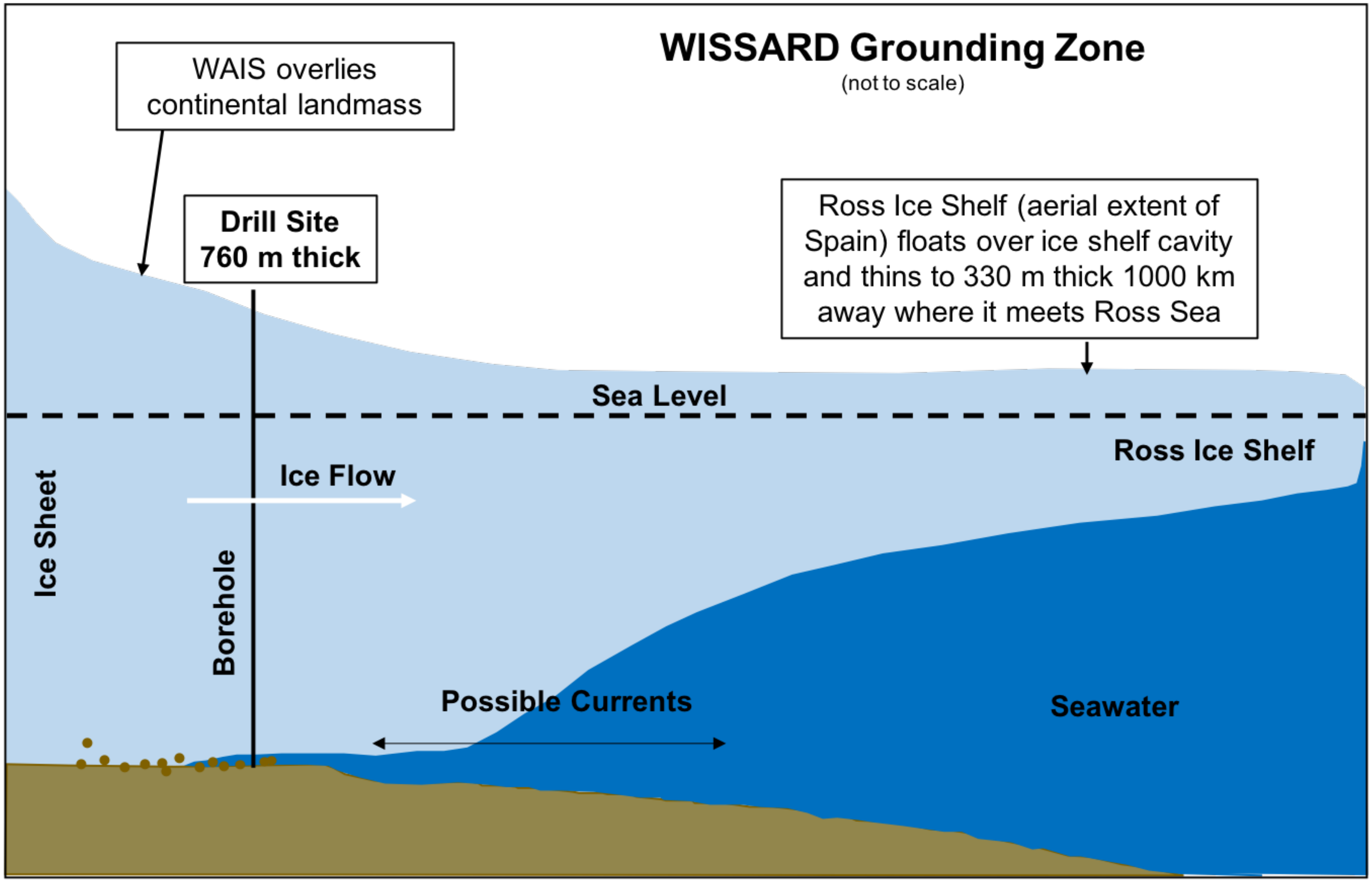

Figure 1.4 Cross section view of the grounding zone. Sediment core was extracted from ~8 km seaward from the actual grounding zone. Redrawn from http://www.wissard.org/

The WGZ is also an indicator of the stability of the RIS and the greater WAIS (Carter and Fricker 2012). For an ice shelf to be stable, the mass losses (mostly due to basal melt near the grounding line, ice fronts and iceberg calving) must be approximately equal to the mass gained through the influx of grounded ice, precipitation and basal refreezing downstream of the grounding line melt zone (Schoof 2007).

Mechanically, the grounding zone represents a transition between grounded ice sheet flow dominated by vertical shear and ice shelf flow dominated by longitudinal stretching and lateral shearing. The two types of flow couple together across a complex mechanical transition zone near the grounding line in which longitudinal and shear stresses are important. The dynamic role of this transition zone is that it controls the rate of outflow of ice across the grounding line. In order to comprehend the dynamics of the grounded part of a marine ice sheet, it is necessary to understand the behavior of the sheet-shelf transition zone (Schoof 2007).

Historic Importance and Significance

Like many ice streams draining the WAIS, Ice Stream C/Kamb Ice Stream (KIS; north of WIS) is characterized by large fluctuations in velocity, which may have implications for ice sheet stability. The KIS was blocked by crevasses (surface crevasses at the time of the blockage) imaged by radar. These crevasses may have blocked the KIS multiple times (from 30 to 140 years ago) throughout the recordable hydrologic history (Retzlaff and Bentley 1993; Smith et al. 2002). It is hypothesized that the blockage could be caused by changes in subglacial water drainage or due to basal freeze-on, resulting in a

10 to 15 m thick accretionary basal ice layer that formed over several thousand years and a decrease in flow (from a high rate comparable to modern day Ice Stream B and D at ~700 m a^{-1} to <10 m a^{-1}) (Anandakrishnan and Alley 1997; Vogel 2004). A blockage such as that on KIS could have major implications for altering subglacial water flow and geochemical concentrations downstream in the GZ region.

Grounding Line

The grounding line designates the geomorphological and geophysical boundary where ice transitions from overlying the continental landmass to overlying the Ross Sea (Ross Ice Shelf Cavity). Multiple conditions and processes, including buoyancy, bed topography, water depth, the modulating effects of glacial-isostatic adjustment and mass balance, determine the location and stability of the grounding line and ultimately, the ice sheet (Thomas and Bentley 1978; Schoof 2007; Katz and Grae Worster 2010; Gomez et al. 2010). The modern grounding line at the WGZ occurs where the seabed drastically increases in depth (Anandakrishnan et al. 2007).

Parameters which impact ice flux to the grounding line include the: flow structure of the ice sheet (Rignot et al. 2011; Bamber et al. 2000), basal thermal regime (Kleman and Glasser 2007), basal slipperiness due to the distribution and style of meltwater drainage (Stearns et al. 2008), cyclical responses of subglacial till rheology due to tides (Doake et al. 2002; Anandakrishnan et al. 2003; Gudmundsson 2007), and effects of ice shelf buttressing (Rignot and Steffen 2008; Hulbe et al. 2008; Simkins et al. 2018).

The Whillans grounding line has been one of the most intensively studied active grounding lines in Antarctica and is characterized by an accreting grounding zone wedge (Anandakrishnan et al. 2007), channelized meltwater delivery (Horgan et al. 2013), till compaction up-dip of the grounding line due to low amplitude tidal flexure (Christianson et al. 2013), and basal melt-out of englacial debris (Christianson et al. 2016). All of these are thought to contribute to grounding line dynamics (Simkins et al. 2018).

Grounding Zone Wedge

The grounding zone wedge (GZW) is a wedge shaped deposit composed predominantly of glacial diamict or till, which is formed by high rates of sediment delivery to the grounding zone by fast-flowing fluvial inputs (Batchelor and Dowdeswell 2015). Sediments fall out of suspension and bounce along the sediment water interface. The wedge has a stabilizing influence on the lateral position of the grounding line against rising sea level (Alley et al. 2007).

Geophysical analyses of grounding zone environments in Antarctica have led to major advances characterizing landforms and processes through the application of: seismic (Blankenship et al. 1986, 1987; Horgan et al. 2013a, 2013b; Christianson et al. 2012; Bart et al. 2017), gravity, ground and airborne radio echo sounding (Oswald and Robin 1973; Vaughan et al. 2007; Scambos et al. 2011), and repeat track satellite altimetry measurements of the ice surface (Gray et al. 2005; Wingham et al. 2006; Fricker et al. 2007). In addition, Powell et al. (1996) used a remotely operated vehicle

(ROV) to investigate the grounding zone processes at Mackay Glacier in McMurdo Sound (north of the McMurdo Dry Valleys).

A global survey of high latitude GZWs found structures to be, on average, <15km long and 15-100 m thick (Batchelor and Dowdeswell 2015). Formed by fast flowing ice streams (Figure 1.6), GZWs accrete where floating ice shelves constrain vertical accommodation space immediately beyond the GZ line (Figure 1.7). The long-term stability of the grounding zone wedge is thought to be controlled by ice-sheet mass balance (Simkins et al. 2018). This suggests that the geomorphology of the grounding zone wedge indicates an episodic style of ice-stream retreat (Batchelor and Dowdeswell 2015).

The presence of GZWs were first hypothesized following the discovery of a 6 m till layer beneath WIS in West Antarctica (Blankenship et al. 1987b; Alley et al. 1987). Boundary conditions used to create Siple Coast ice sheet-shelf models of location and movement include: the shape of surface ice sheet, ice sheet thickness, surface accumulation and density, temperature and fabric within the ice, structure of the ice sheet's base, thermal state at the base (frozen or thawed), geothermal flux, ice thickness of shelves and glacial fronts, and bathymetry of sub-ice shelf cavities and adjacent Amundsen Sea out to the continental shelf break (Scambos et al. 2017).

Identification of SLW and the WGZ

Ice-penetrating radio-echo sounding (RES) surveys from the 1950s provided an early understanding of subglacial lakes in Antarctica (Robin et al. 1970). Subsequent surveys have identified a total of almost 400 subglacial lakes (Siegert et al. 2005; Bell et al. 2007; S. P. Carter et al. 2007; Popov and Masolov 2007). SLW was identified in 2006 (Fricker et al. 2007) using surface elevation observations from the GLAS (Ground Laser Altimeter System) aboard the Ice, Cloud and land Elevation Satellite (ICESat).

Beginning in 1983, a glaciology program was initiated to study West Antarctic ice streams that flow into the Ross Ice Shelf (Blankenship et al. 1986). A key aspect of the study was to analyze the contact zone between the Ice Stream B /Whillans Ice Stream, WIS) and its bed to determine how water permitted the high rates of ice flow at WIS. Through this research, Blankenship et al. (1986) observed a *hump* on seismic profiles (Blankenship et al. 1986), which was later identified as the till delta or grounding zone wedge (Alley et al. 2007). Identifying the fast flow Ice Stream B was an early indication of the active subglacial water network that underlies the WAIS (Alley et al. 1987). Early maps of the Whillans grounding line were published by Rose (1979) and later by Shabtaie and Bentley (1987).

Satellite and airborne altimetry detected high intensity, high volume subglacial discharge events associated with perturbed ice dynamics in Antarctica, at Byrd Glacier in East Antarctica (Stearns et al. 2008) and Crane Glacier on the Antarctic Peninsula (Scambos et al. 2011). The WISSARD (Whillans Ice Stream Subglacial Access Research Drilling) project used satellite altimetry, interferometric radar and GPS height data to detect ice surface height changes (to an accuracy of 0.02 m and precision of 0.06 m) at SLW that are associated with basal water storage and movement (Siegfried et al. 2016; Siegfried et al. 2017; Siegfried and Fricker 2018). SLW was originally thought to be created by geothermal influence and/or the rapid movement of ice over a bed of varying basal traction so as to create depressions in the ice surface that resulted in hydropotential depressions at the ice base and later filled with water (Carter and Fricker 2012).

The WISSARD project was a collaborative, multidisciplinary research project aimed at characterizing: 1) marine ice sheet stability and the potential for the WAIS to make a large contribution to near-future global sea level rise, and 2) the presence and activities of microorganisms in dark and cold subglacial aquatic environments. The WISSARD Project drilled and sampled the subglacial environment in SLW and the lower Whillans Ice Stream near the WGZ to determine whether drainage from SLW entered the marine environment. Uncertainty over ice sheet dynamics and vulnerability (IPCC, 2007) further motivated glaciological and subglacial hydrologic analysis. The WISSARD project was designed to collect and analyze data on the active subglacial lake using satellite remote sensing, surface geophysics, borehole sensors, and analyzing recovered subglacial water, sediment and basal ice samples. Changes to the WAIS mass balance could ultimately impact the mechanical and geochemical dynamics of the WGZ.

Importance of the Siple Coast

Recently, the Goddard Ice Altimetry Group mapped Antarctic drainage systems according to ice provenance with separation of drainage along the Transantarctic Mountains (Figure 1.4). The Siple Coast, underlain by a deep sediment- and volcanic-structure laden basin (van Wyk de Vries et al. 2017) characterized by a relatively high geothermal heat flux (Fisher et al. 2015), is of utmost interest because it is a major outlet for the WAIS, responsible for draining approximately one-third of the ice from the WAIS (Figure 1.5). Historically, the WAIS has been known to flow into three major outlets (Weddell Sea, Pine Island Bay, Ross Sea), but the Ross Sea is of greatest interest because fast moving ice streams transport the grounded (non-floating) interior across the Siple Coast grounding line (Parizek et al. 2003). More recently, it has been found that glaciers on the Amundsen Coast of the WAIS (Thwaites, Haynes and Pine Island) are producing the majority of Antarctica's contribution to sea level rise (Rignot and Steffen 2008; Joughin et al. 2014).

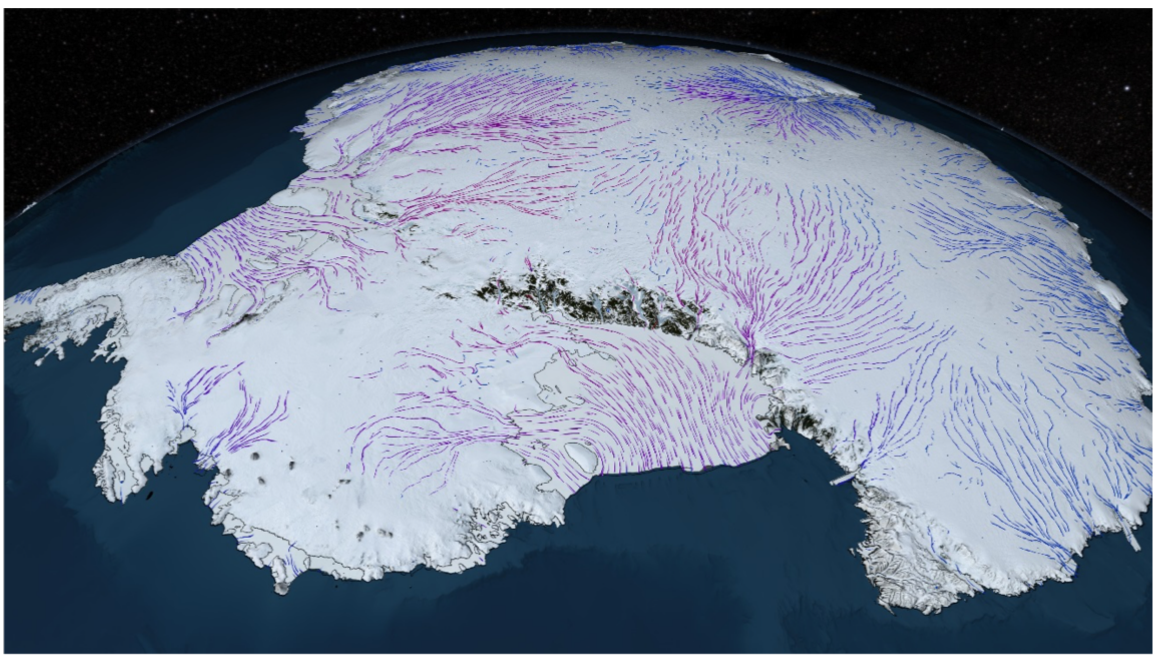

Figure 1. 5 Blue to magenta lines show the magnitude of flow (low to high) and delineate motion of the ice sheet. The Antarctic Ice Sheet over the BedMap2 (British Antarctic Survey, NASA ICESat; Operation IceBridge) with the grounding line shown by a black dashed line. https://svs.gsfc.nasa.gov/cgi-bin/details.cgi?aid=4060

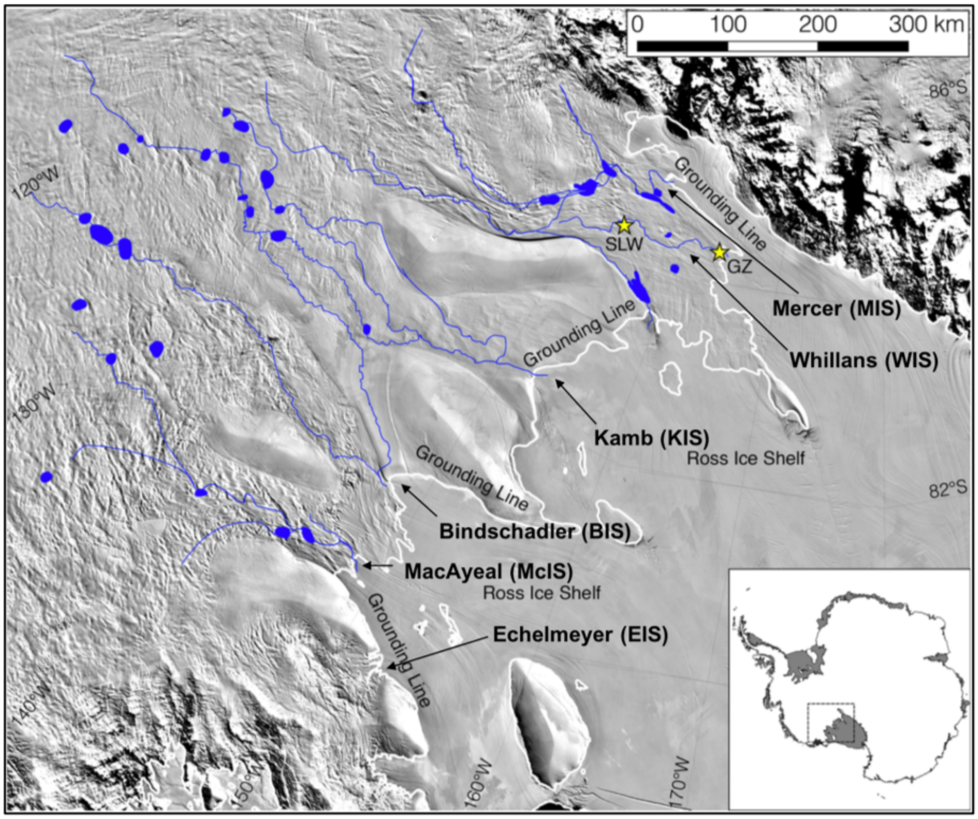

Figure 1.6 Blue denotes the subglacial network of rivers and lakes across the Siple Coast. Major fluvial systems are labeled by arrows. The yellow stars indicate where SLW and the GZ/WGZ WISSARD sampling sites are located. (Figure adapted from Tristy Vick-Majors et al. in revision.)

Dominant ice streams terminate at the Siple, Gould and Shirase Coasts. Ice streams were originally named, from south to north, Ice Stream A through F in the 1980s. Ice streams range from 30 to 80 km in width and 300 to 500 km in length (Oppenheimer 1998). Renamed in 2003 (Catania, 2004), the ice streams received the following names to honor glaciologists who devoted much effort to further our understanding of ice sheet processes (Figure 1.6): 1) Ice Stream A, or Mercer Ice Stream (MIS), is sourced at the base of the Transantarctic Mountains where East Antarctic Plateau's Reedy Glacier turns into the Shimizu Ice Stream; 2) Ice Stream A partially contributes to Ice Stream B, or Whillans Ice Stream (WIS), upstream of the grounding zone at a region 100 km in width;

3) Ice Stream C, or Kamb Ice Stream (KIS), experienced a blockage ~140 years ago (Rose 1979) in the lower reaches, but the upper reaches are still flowing; 4) Ice Stream D, or Bindschadler Ice Stream (BIS), is sourced near the Byrd Station region and joins with 5) Ice Stream E (MacAyeal Stream), near the Ross Ice Shelf (Armstrong, 2008); and 6) Echelmeyer Ice Stream (EIS). These six ice streams are of interest because they represent low-angle end-members amongst Antarctic ice streams. Extensive research shows that the ice streams are characterized by high frequency, asynchronous discharge with rapidly evolving lateral boundaries (Parizek et al. 2003).

These six ice streams are responsible for the greatest ice volume loss and highest grounding zone retreat (1300 km) in Antarctica since the Last Glacial Maximum, ~14,000 years ago (Parizek et al. 2003). While the cause of ice streams has been debated, the major ice stream formation models include: till deformation; till deformation in concert with basal sliding; and basal sliding (Armstrong, 2008). Understanding the subsurface structure and processes are fundamental to understanding the continuing evolution of the WAIS and its contribution to sea level (Christianson et al. 2012). Research along the Siple Coast initially investigated ice stream flow paths, ice stream margins, relict margins, the shutdown of subglacial ice streams and how they contribute to the greater ice sheet dynamics (Catania, 2004).

The Siple Coast is also important because it encompasses an environment which includes various components of the glaciomarine system (GS). The GS includes subglacial ice streams, estuaries, grounding zone wedges, and grounding zone lines and is defined as a marine setting that shows signs and indications of subglacial influence

(Molnia 1983; Domack and Powell 2017). These environments and subglacial structures provide insight as to how the WAIS subglacial network interfaces with the Ross Sea.

Physical Controls on Marine Sedimentation

Dominant physical controls that determine marine sedimentation include particle type/source (i.e., terrigenous, biogenic, authigenic, volcanogenic and cosmogenic), rate of erosion and sedimentation, and the average grain size (Burdige 2006). The rate of sedimentation at the WGZ is determined by the velocity and sediment concentration within the subglacial flow and lateral advection associated with Ross Sea and Ice Shelf Cavity flow (Burdige 2006).

Sediments in the western Ross Sea, beneath the McMurdo Ice Shelf (MIS), contain large quantities of intact biogenic particles, particularly diatoms (Carter et al. 1981). Ice shelf sediments contain siliceous sponge spicules, which have the propensity to form mats that trap planktic foraminifers, bryozoans, mollusks, echinoids, ostracods, and display polychaete worm tubes (Carter et al. 1981; Scherer et al. 2016).

The Ross Ice Shelf J9 drill site (Figure 1.7) (Clough and Hansen 1979), located 600 km south of the MIS sample location, contained less terrigenous sediment particulate matter and more biogenic sediment particulate matter than sediment sampled under the MIS. The higher concentration of biogenic matter is thought to be associated with the intrusion of phytoplankton-bearing waters advected from the Ross Sea and/or liberated from sea ice. J9 sediment is known to contain: a large fraction of platy clays; feldspar and quartz; a smaller fraction of terrigenous material; a biogenic component dominated by degraded diatom frustules and amorphous particles of organic material dominated by siliceous fragments (Clough and Hansen 1979; Gilmour 1979; Jacobs et al. 1979a, 1979b; Lipps et al. 1979; Azam et al. 1979; Carter et al. 1981).

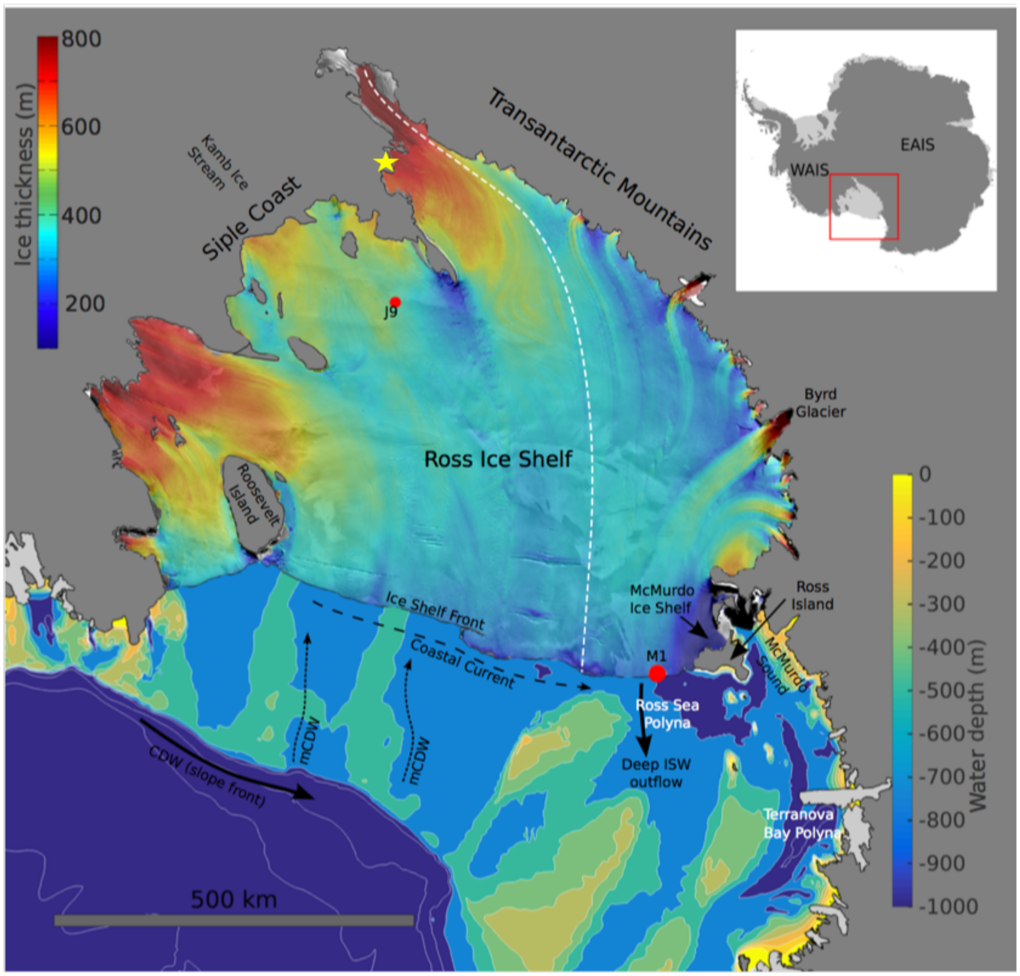

Figure 1. 7 The map depicts the Ross Ice Shelf thickness (Griggs and Bamber 2011), bathymetry (Davey 2004) and the background ice shelf imagery is from the MODIS Mosaic of Antarctica (T. Scambos et al. 2007). Sample locations (red circles) from RISP J9 (Clough and Hansen 1979) and M1, annotate a four year ice shelf and ice cavity study (Stewart 2017). This study at the WGZ is represented by the yellow star.

Sediments recovered in the 1989 CIROS-1 drilling operation in the McMurdo Sound were identified as upper Oligocene to lower Miocene sediments and include illite and chlorite, a clay mineral assemblage associated with physical weathering. Deeper Oligocene sediments included greater quantities of smectite, whose composition is known to be dominated by beidellite, an Fe-rich smectite known to form in forest or scrubland soils under cool to cold temperate climates (Ehrmann et al. 1992). The Ferrar Dolomite was identified as a source material for lower Oligocene deposits (Claridge et al. 1989). Finer sediments along the Siple Coast are likely terrestrially sourced with a lithology of volcanic origin that has undergone weathering, however a substantial amount of dropstones are present due to basal fallout from the overlying ice shelf.

During the season of 2006/2007, a 1285 m long sediment drill core (AND-1B) was extracted from beneath the McMurdo Ice Sheet (MIS) in conjunction with ANDRILL (Scopelliti et al. 2013). The core included alternating sections of diamictites, diatomites and volcaniclastic sediments that spanned the last 14 Ma (Scopelliti et al. 2013). An 80-m thick diatomite interval from the Pliocene (~4.5 to 3.0 million years ago) is considered to be the most recent interval with a climate warmer than today (Scopelliti et al. 2013). For this reason, the interval is widely studied as an analogue for the effects of anthropogenic warming (Pollard and DeConto 2009).

Subglacial Fluvial Inputs

Fresh-water glacial discharge across the grounding line is a source of basal melt to the marine environment in Alaskan and Greenland fjords, and is known to impact sedimentation (Motyka et al. 2003, 2011). Basal melt rates at the grounding zone in these environments are increased by the flux of subglacial freshwater as circulation associated with the buoyant plume increases the rate at which ocean heat is made available to the ice base through turbulent entrainment (Jacobs et al. 1992). Jenkins presented a model (2011) which unified the concept of convention driven melting (Motyka et al. 2003) with the more general concept of melt driven convection. The only distinction between the two main subglacial buoyancy melt models was whether the primary buoyancy source is at the origin or generated by the subsequent flow of the resulting plume (Jenkins 2011). Jenkins (2011) characterized the role of freshwater discharge and basal melt rate in driving the motion of the grounding line in Rutford Ice Stream at the Filcher-Ronne Ice Shelf and the WIS. Carter and Fricker (2012) examined spatial and temporal variability in subglacial water supply by combining volume estimates feeding the grounding zone derived from the Ice, Cloud and land Elevation Satellite (ICESat) data with a model for subglacial transport to identify six major grounding zones along the Siple Coast.

Ross Sea Circulation, Advection and the Ross Ice Shelf Cavity

The Southern Ocean is a significant site of Antarctic Bottom Water (AABW) formation (Figure 1.8) (Freeman and Lovenduski 2016), sourced by the Weddell Sea (50% contribution), the run-off from Wilkes Land (~30%) and the Ross Sea (~20%). The Southern Ocean is dominated by two major gyres, the Weddell Gyre and the Ross Sea Gyre (Figure 1.9). The Ross Sea Gyre is a well-defined cyclonically circulating feature (low pressure relative to surroundings; clockwise pattern) that borders the Ross Sea

Polyna, whose strong, wind-forced, upper-ocean flow opposes baroclinic circulation (Reid 1989; Locarnini 1994). Michel et al. (1979) used geochemical tracers to estimate circulation between the sub-Ross Ice Shelf and the open Ross Sea to occur on a six year cycle (Smethie and Jacobs 2005; Jacobs 2004; Jacobs et al. 2003).

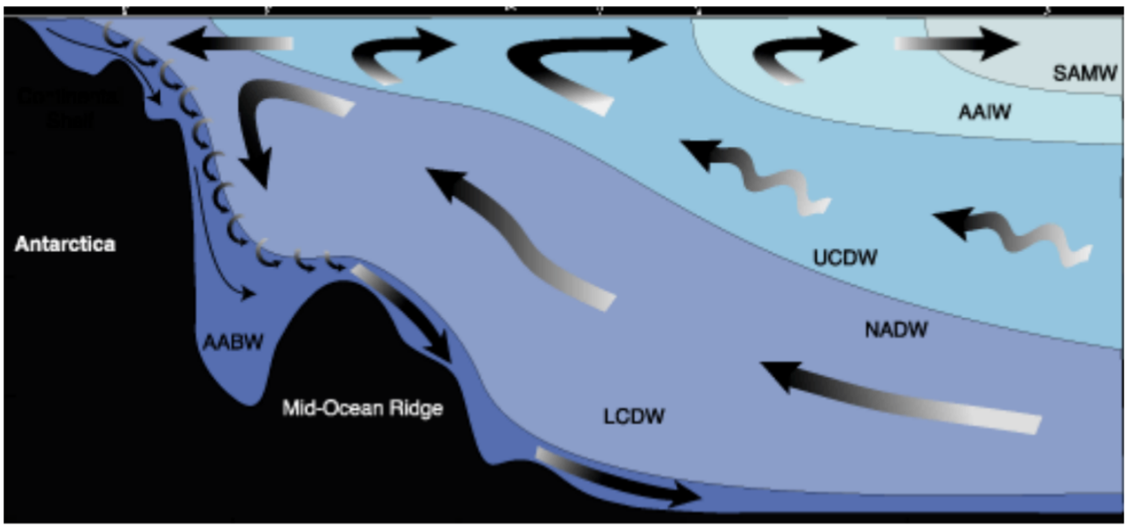

Figure 1.8 The figure depicts the continental shelf and typical currents off the Antarctic coast transitioning to the Southern Ocean (Turner et al., 2009). (PF – Polar Front; SAF – SubAntarctic Front; and STF – Subtropical Front), and water masses (AABW – Antarctic Bottom Water; LCDW and UCDW, Lower and Upper Circumpolar Deep Waters; NADW – North Atlantic Deep Water; AAIW – Antarctic Intermediate Water and SAMW – Sub- Antarctic Mode Water).

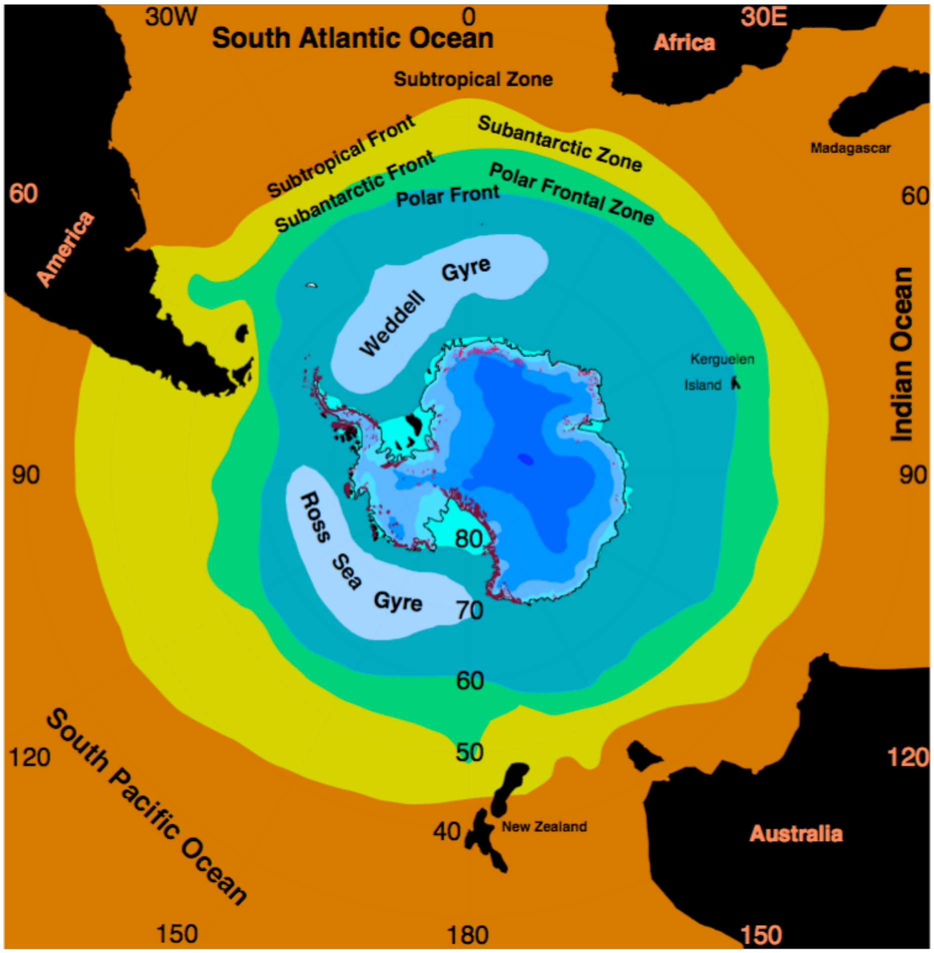

Figure 1.9 The Polar Front, Polar Front Zone, Subantarctic Zone and Subtropical Zone are shown surrounding Antarctica. The Weddell Gyre and the Ross Sea Gyre are the two major oceanographic features surrounding Antarctica (permission obtained; Grobbe, 2007).

Early studies identified the prevailing water mass in McMurdo Sound to have salinity ranging from 34.6-34.9‰ and temperatures around -1.9°C, with seasonal melt impacting the upper 100 m of the water column on an annual basis (Littlepage 1965; Heath 1971; Gilmour 1975). Sub-ice shelf currents between Ross Island and RISP J9

(Ross Ice Shelf Project, 1977-1978), displayed a wide range of velocities (0.9 – 33 cm s^{-1}) that varied with tides (Williams and Robinson 1979).

Sub-ice shelf circulation and the associated rates of melting and freezing are strongly influenced by the shape (determined by ice draft and bathymetry) of the sub-ice shelf cavity, as was documented for the Amery Ice Shelf, East Antarctica (Galton-Fenzi et al. 2008); Pine Island Ice Shelf (Davies et al. 2017), and the Larsen Ice Shelf (Schaffer et al. 2016). As previously described, subglacial ice streams and GZs on the Siple Coast have been mapped in detail (Fricker et al. 2007; Carter and Fricker 2012; Christianson et al. 2013; Horgan et al. 2013b). While radio-echo mapping of the seafloor beneath the Ross Ice Shelf only provides a crude image of major bathymetric features (Neal 1979), seismic data has provided an estimate of the depth to bedrock (n=25, 113 ± 5 m to 783 ± 5 m) and identification of a seafloor unconformity beneath the Ross Sea (Robertson and Bentley 1990).

A history of glaciation has incised a deeper continental shelf (~1000 m) offshore of the Antarctic coast compared to other global coastal shelves (~200 m) (Alder et al. 2016). Although the WGZ grounding zone is ~1000 km from the edge of the Ross Ice Shelf, depending on the season, tidal currents could laterally advect nutrients southward into the Ross Ice Shelf Cavity (Jacobs et al. 1979a, 1979b). Tidal currents have been identified as the most energetic stirring process throughout the sub-ice-shelf cavity (Holland et al. 2003). Numerical models (Holland et al. 2003) have played an increasing role in characterizing the thermodynamics of the Ross Ice Shelf and the associated impact on the Ross Sea. Numerical simulations suggest that tidal currents in the sub-ice-shelf regions mix the water column, destroy stratification and promote contact between the ice and warm water near the seabed and create thermohaline circulation by meltwater production in regions of strong vertical mixing that may ventilate deeper regions of the sub-ice-shelf cavity (MacAyeal, 1984).

As previously mentioned, ice shelf cavities are subject to deep buoyancy input, or freshwater ice melt at the ice shelf base. As basal melting of the shelves freshens underlying water, seawater properties evolve to create a melt water mixing line, or Gade line, established by the latent heat of fusion, the specific heat capacity of water and the salinity difference between the ice melt and seawater (Gade 1979). Jacobs et al. (1992) identified three modes (HSSW flows beneath the ice shelf where the coast is extremely deep and two warm water mass flows that melt the surface) of melt that characterize overturning circulation in the sub-ice shelf. The HSSW flow is considered to be the dominant mode of melting under ice shelves and is responsible for large masses of marine ice observed beneath the Ross (Neal 1979), Ronne (Lambrecht et al. 2007) and the Amery (Fricker et al. 2001) ice shelves. The other two modes of circulation described by Jacobs and others (Jacobs et al. 1992) involve warmer water masses which can cause melting at the ice shelf-water interface (Stewart 2018).

Relocation of sediment solids and pore waters relative to the sediment water interface can be caused by particle sedimentation, compaction upon burial, bioturbation or by an externally impressed flow (groundwater, hydrothermal flow, or fluvial input as addressed above) (Burdige 2006).

Basal Fallout

Basal melting occurs when warmer ocean water melts ice, creating a buoyant, cold and comparatively fresh plume that can carry entrained sediment mass away from the grounding zone (Jacobs et al. 2003). Basal melting is governed by the Coriolis-influenced transport and vertical mixing of ocean heat, the pressure dependence of the freezing point of seawater, and the sea floor and cavity morphology (Rignot et al. 2013). The highest rates of basal melt occur at the Ronne Ice Shelf and at Getz Glacier (Rignot et al. 2013). Ocean water can be delivered to the grounding zone through thermohaline circulation and by advection created by processes external to the sub-ice-shelf cavity (Jacobs et al. 1979a; 1979b). Antarctic sub-ice-shelf cavities are subject to a wide range of ocean flows, ranging from the very warm Circumpolar Deep Water (CDW) to High Salinity Shelf Water (HSSW)(Payne et al., 2004; Payne et al., 2007).

Bioturbation

Benthic macro- and meiofauna rework surficial sediments through bioirrigation and bioturbation and also affect redox conditions in the region of the sediment they inhabit (Burdige 2006; Hemer et al. 2007). Sediments collected off the Amery Ice Shelf in the Prydz Bay were found to contain foraminifera, ostracods, radiolaria, diatoms, and pteropods (Post et al. 2007).

Synthesis

The GZ interface between Antarctic ice sheet and ice shelf environments: 1) impacts the stability (Simkins et al. 2018) of the ice sheet and the circulation, stratification and flow beneath the Ross Ice Shelf and 2) has been shown to contain microorganisms and metabolic activities in a cold, dark environment that had never been explored. The location, logistical requirements and resource investment make sub-ice shelf environments difficult to study. Interdisciplinary research such as that done by the WISSARD project (Christner et al. 2014; Purcell et al. 2014; Vick-Majors et al. 2016a; 2016b; Michaud et al. 2016) in conjunction with the recent development of technologies (Priscu et al. 2013; Tulaczyk et al. 2014) has enabled us to better understand sub-ice sheet processes in a way that has not been previously possible. Given their increasing instability and importance to sea level rise, ice sheets, and in particular, ice streams and associated grounding zones are being studied at an increasing rate. My thesis, which was a component of the WISSARD project, focuses on a shallow sediment core associated with the WGZ. Data from my study on sediment character, stable isotopic variation, and organic and inorganic geochemistry provides new information on this little studied ecosystem. Specifically, I constrained the influences of subglacial freshwater in a sub ice shelf environment and show how the sediments interact with the overlying marine water column.

Bibliography

Achberger, A. M., B. C. Christner, A. B. Michaud, J. C. Priscu, M. L. Skidmore, T. J. Vick-Majors, and WISSARD Science Team. 2016. “Microbial Community Structure of Subglacial Lake Whillans, West Antarctica.” *Frontiers in Microbiology* 7: 1457. https://doi.org/10.3389/fmicb.2016.01457.

Alder, V., M. Azzaro, R. Hucke-Gaete, R. Mosetti, J. L. Orgeira, L. Quartino, A. R. Rey, L. Schejter, M. Vecchione, and E. R. Marschoff. 2016. “Chapter 36H. Southern Ocean.” *Chapter 36H. Southern Ocean*, 1–41.

Alley, R. B., S. Anandakrishnan, T. K. Dupont, B. R. Parizek, and D. Pollard. 2007. “Effect of Sedimentation on Ice-Sheet Grounding-Line Stability.” *Science* 315.

Alley, R. B., D. D. Blankenship, C. R. Bentley, and S. T. Rooney. 1987. “Till beneath Ice Stream B: 3. Till Deformation: Evidence and Implications.” *Journal of Geophysical Research* 92 (B9): 8921. https://doi.org/10.1029/JB092iB09p08921.

Anandakrishnan, S., and R. B. Alley. 1997. “Stagnation of Ice Stream C, West Antarctica by Water Piracy.” *Geophysical Research Letters* 24 (3): 265–68. https://doi.org/10.1029/96GL04016.

Anandakrishnan, S., G. A. Catania, R. B. Alley, and H. J. Horgan. 2007. “Discovery of Till Deposition at the Grounding Line of Whillans Ice Stream.” *Science* 315: 1835–38. https://doi.org/10.1126/science.1138393.

Anandakrishnan, S., D. E. Voigt, R. B. Alley, and M. A. King. 2003. “Ice Stream D Flow Speed Is Strongly Modulated by the Tide beneath the Ross Ice Shelf.” *Geophysical Research Letters* 30 (7). https://doi.org/10.1029/2002GL016329.

Anderson, S. P., J. I. Drever, and N. F. Humphrey. 1997. “Chemical Weathering in Glacial Environments.” *Geology* 25 (5): 399–402. https://doi.org/10.1130/0091-7613(1997)025<0399:CWIGE>2.3.CO.

Armstrong, M. 2008. “West Antarctic Ice Streams - A Review of the Proposed Mechanisms of Ice Streaming.” *Literature Review*, 1–13. https://ir.canterbury.ac.nz/bitstream/handle/10092/13920/GCAS_11_Lit_Armstrong.pdf?sequence=1.

Arrigo, K. R., G. van Dijken, and M. Long. 2008. “Coastal Southern Ocean: A Strong Anthropogenic CO_2sink.” *Geophysical Research Letters* 35 (21). https://doi.org/10.1029/2008GL035624.

Arrigo, K. R., G. L. van Dijken, and S. Bushinsky. 2008. “Primary Production in the Southern Ocean, 1997–2006.” *Journal of Geophysical Research* 113 (C8): C08004. https://doi.org/10.1029/2007JC004551.

Arrigo, K. R., D. H. Robinson, D. L. Worthen, R. B. Dunbar, G. R. DiTullio, M. VanWoert, and M. P. Lizotte. 1999. “Phytoplankton Community Structure and the Drawdown of Nutrients and CO_2 in the Southern Ocean.” *Science (New York, N.Y.)* 283 (5400): 365–67. https://doi.org/10.1126/SCIENCE.283.5400.365.

Asper, V. 2003. “The Distribution of Particulate Organic Carbon and Its Dynamics in the Southern Ross Sea.” In *Biogeochemistry of the Ross Sea Antarctic Research Series*.

https://doi.org/10.1029/078ARS15.
Azam, F., J. R. Beers, L. Campbell, A. F. Carlucci, O. Holm-Hansen, F. M. H. Reid, and D. M. Karl. 1979. "Occurrence and Metabolic Activity of Organisms Under the Ross Ice Shelf, Antarctica, at Station J9." *Science* 203 (4379): 451–53. https://doi.org/10.1126/science.203.4379.451.
Bamber, J. L., R. E. M. Riva, B. L. A. Vermeersen, and A. M. LeBrocq. 2009. "Reassessment of the Potential Sea-Level Rise from a Collapse of the West Antarctic Ice Sheet." *Science (New York, N.Y.)* 324 (5929): 901–3. https://doi.org/10.1126/science.1169335.
Bamber, J. L., D. G. Vaughan, and I. Joughin. 2000. "Widespread Complex Flow in the Interior of the Antarctic Ice Sheet." *Science* 287 (5456): 1248–50.
Bart, P. J., and J. B. Anderson. 1997. "Grounding Zone Wedges on the Antarctic Continental Shelf, Antarctic Peninsula." In *Glaciated Continental Margins*, 96–97. Dordrecht: Springer Netherlands. https://doi.org/10.1007/978-94-011-5820-6_36.
Bart, P. J., B. J. Krogmeier, M. P. Bart, and S. Tulaczyk. 2017. "The Paradox of a Long Grounding during West Antarctic Ice Sheet Retreat in Ross Sea." *Scientific Reports* 7 (1): 1262. https://doi.org/10.1038/s41598-017-01329-8.
Batchelor, C. L., and J. A. Dowdeswell. 2015. "Ice-Sheet Grounding-Zone Wedges (GZWs) on High-Latitude Continental Margins." *Marine Geology* 363: 65–92. https://doi.org/https://doi.org/10.1016/j.margeo.2015.02.001.
Bell, R. E., M. Studinger, C. A. Shuman, M. A. Fahnestock, and I. Joughin. 2007. "Large Subglacial Lakes in East Antarctica at the Onset of Fast-Flowing Ice Streams." *Nature* 445 (22 February 2007): 904–7. https://doi.org/10.1038/nature05554.
Blankenship, D. D., C. R. Bentley, S. T. Rooney, and R. B. Alley. 1987a. "Till beneath Ice Stream B: 1. Properties Derived from Seismic Travel Times." *Journal of Geophysical Research* 92 (B9): 8903. https://doi.org/10.1029/JB092iB09p08903.
Blankenship, D. D., C. R. Bentley, S. T. Rooney, and R. B. Alley. 1986. "Seismic Measurements Reveal a Saturated Porous Layer beneath an Active Antarctic Ice Stream." *Letters to Nature* 322 (3): 54–57.
Blankenship, D. D., C. R. Bentley, S. T. Rooney, and R. B. Alley. 1987b. "Till beneath Ice Stream B: 1. Properties Derived from Seismic Travel Times." *JOURNAL OF GEOPHYSICAL RESEARCH* 92 (10): 8903–11. https://doi.org/10.1029/JB092iB09p08903.
Boudreau, B. P. 1996. "The Diffusive Tortuosity of Fine-Grained Unlithified Sediments." *Geochimica et Cosmochimica Acta* 60 (16): 3139–42. https://doi.org/10.1016/0016-7037(96)00158-5.
Boyd, E. S., R. K. Lange, A. C. Mitchell, J. R. Havig, T. L. Hamilton, M. J. Lafrenière, E. L. Shock, J. W. Peters, and M. Skidmore. 2011. "Diversity, Abundance, and Potential Activity of Nitrifying and Nitrate-Reducing Microbial Assemblages in a Subglacial Ecosystem." *Applied and Environmental Microbiology* 77 (14): 4778–87. https://doi.org/10.1128/AEM.00376-11.
Burdige, D. 2006. *Geochemistry of Marine Sediments*. Princeton, N.J.: Princeton University Press.
Canfield, D. E., and J. Farquhar. 2009. "Animal Evolution, Bioturbation, and the Sulfate

Concentration of the Oceans." *PNAS* 106 (20): 8123–27. www.pnas.org/cgi/content/full/.

Carlson, C. A., and D. A. Hansell. 2003. "The Contribution of Dissolved Organic Carbon and Nitrogen to the Biogeochemistry of the Ross Sea" 78: 123–42. https://doi.org/10.1029/078ARS08.

Carter, L., J. S. Mitchell, and N. J. Day. 1981. "Suspended Sediment beneath Permanent and Seasonal Ice, Ross Ice Shelf, Antarctica." *New Zealand Journal of Geology and Geophysics* 24 (2): 249–62. https://doi.org/10.1080/00288306.1981.10422716.

Carter, Sasha P., D. D. Blankenship, M. E. Peters, D. A. Young, J. W. Holt, and D. L. Morse. 2007. "Radar-Based Subglacial Lake Classification in Antarctica." *Geochemistry, Geophysics, Geosystems* 8 (3). https://doi.org/10.1029/2006GC001408.

Carter, S. P., and H. A. Fricker. 2012. "The Supply of Subglacial Meltwater to the Grounding Line of the Siple Coast, West Antarctica." *Annals of Glaciology* 53 (60): 267–80. https://doi.org/10.3189/2012AoG60A119.

Catania, G. A. 2004. "Dynamic History of the Kamb Ice Stream, West Antarctica: Controls on Streaming Behavior and Ice Stream Shutdown." University of Washington.

Christianson, K., R. W. Jacobel, H. J. Horgan, S. Anandakrishnan, and R. B. Alley. 2012. "Subglacial Lake Whillans — Ice-Penetrating Radar and GPS Observations of a Shallow Active Reservoir beneath a West Antarctic Ice Stream." *Earth and Planetary Science Letters* 331–332: 237–45. https://doi.org/10.1016/j.epsl.2012.03.013.

Christianson, K., B. R. Parizek, R. B. Alley, H. J. Horgan, R. W. Jacobel, S. Anandakrishnan, B. A. Keisling, B. D. Craig, and A. Muto. 2013. "Ice Sheet Grounding Zone Stabilization Due to till Compaction." *Geophysical Research Letters* 40 (20): 5406–11. https://doi.org/10.1002/2013GL057447.

Christianson, K, J. Robert, J. H. Horgan, R. B. Alley, S. Anandakrishnan, M. D. Holland, and K. DallaSanta. 2016. "Basal Conditions at the Grounding Zone of Whillans Ice Stream, West Antarctica, from Ice-penetrating Radar." *Journal of Geophysical Research: Earth Surface* 121 (11): 1954–83. https://doi.org/10.1002/2015JF003806.

Christner, B. C., J. C. Priscu, A. M. Achberger, C. Barbante, S. P. Carter, K. Christianson, A. B. Michaud, et al. 2014. "A Microbial Ecosystem beneath the West Antarctic Ice Sheet." *Nature* 512 (7514): 310–13. https://doi.org/10.1038/nature13667.

Claridge, G. G. C, and J. B. Campbell. 1989. "Clay Mineralogy." Edited by P.J. Barrett. *Antarctic Cenozoic History from the CIROS-1 Drillhole, McMurdo Sound. DSIR Bull.*

Clarke, B. G. 2008. "Physical Characteristics of Subglacial Tills." *Géotechniques* 58 (1): 67–76. https://doi.org/10.1680/geot.2008.58.1.67]67.

Cloern, J. E., A. D. Jassby, T. S. Schraga, E. Nejad, and C. Martin. 2017. "Ecosystem Variability along the Estuarine Salinity Gradient: Examples from Long-Term Study of San Francisco Bay." *Limnology and Oceanography* 62 (S1): S272–91. https://doi.org/10.1002/lno.10537.

Clough, J. W., and B. L. Hansen. 1979. "The Ross Ice Shelf Project." *Science* 203 (4379): 433–34.

Craig, H., and L. Gordon. 1965. *Deuterium and Oxygen 18 Variations in the Ocean and the Marine Atmosphere*. *Stable Isotopes in Oceanographic Studies and Paleotemperatures*.

Davies, D., R. G. Bingham, A. G. C. Graham, M. Spagnolo, P. Dutrieux, D. G. Vaughan, A. Jenkins, and F. O. Nitsche. 2017. "High-Resolution Sub-Ice-Shelf Seafloor Records of Twentieth Century Ungrounding and Retreat of Pine Island Glacier, West Antarctica." *Journal of Geophysical Research: Earth Surface* 122 (9): 1698–1714. https://doi.org/10.1002/2017JF004311.

Depoorter, M. A., J. L. Bamber, J. A. Griggs, J. T. M. Lenaerts, S. R. M. Ligtenberg, M. R. Van Den Broeke, and G. Moholdt. 2013. "Calving Fluxes and Basal Melt Rates of Antarctic Ice Shelves." *Nature* 502 (3 October 2013): 89–93. https://doi.org/10.1038/nature12567.

Doake, C. S. M., H. F. J. Corr, K. W. Nicholls, A. Gaffikin, A. Jenkins, W. I. Bertiger, and M. A. King. 2002. "Tide-Induced Lateral Movement of Brunt Ice Shelf, Antarctica." *Geophysical Research Letters* 29 (8): 67-1-67–4. https://doi.org/10.1029/2001GL014606.

Domack, E., and R. Powell. 2017. *Chapter 8: Modern Glaciomarine Environments and Sediments*. https://doi.org/http://dx.doi.org/10.1016/B978-0-08-100524-8.00030-0.

Doran, P. T., J. C. Priscu, W. B. Lyons, J. E. Walsh, A. G. Fountain, D. M. McKnight, D. L. Moorhead, et al. 2002. "Antarctic Climate Cooling and Terrestrial Ecosystem Response." *Nature*, 517–20. https://doi.org/10.1038/nature710.

Dore, J. E., R. Lukas, D. W. Sadler, M. J. Church, and D. M. Karl. 2009. "Physical and Biogeochemical Modulation of Ocean Acidification in the Central North Pacific." *PNAS*. Vol. 106. http://www.pnas.org/content/pnas/106/30/12235.full.pdf.

Drewry, D. J., S. R. Jordan, and E. Jankowski. 1982. "Measured Properties of the Antarctic Ice Sheet: Surface Configuration, Ice Thickness." *Annals of Glaciology*. Vol. 3.

Egli, T. 2015. "Microbial Growth and Physiology: A Call for Better Craftsmanship." *Frontiers in Microbiology* 06 (April): 287. https://doi.org/10.3389/fmicb.2015.00287.

Ehrmann, W. U., M. Melles, G. Kuhn, and H. Grobe. 1992. "Significance of Clay Mineral Assemblages in the Antarctic Ocean." *Marine Geology* 107: 249–73.

Emerson, S., and J. Hedges. 2008. *Chemical Oceanography and the Marine Carbon Cycle*. New York.

Epstein, S, and T. Mayeda. 1953. "Variation of O^{18} Content of Waters from Natural Sources." *Geochimica et Cosmochimica Acta* 4 (5): 213–24. https://doi.org/10.1016/0016-7037(53)90051-9.

Fisher, A. T., K. D. Mankoff, S. M. Tulaczyk, S. W. Tyler, N. Foley, and and the WISSARD Science Team. 2015. "High Geothermal Heat Flux Measured below the West Antarctic Ice Sheet." *Science Advances* 1 (6): e1500093. https://doi.org/10.1126/sciadv.1500093.

Freeman, N. M., and N. S. Lovenduski. 2016. "Mapping the Antarctic Polar Front:

Weekly Realizations from 2002 to 2014." *Earth Syst. Sci. Data* 8: 191–98. https://doi.org/10.5194/essd-8-191-2016.

Fricker, H. A., S. Popov, I. Allison, and N. Young. 2001. "Distribution of Marine Ice beneath the Amery Ice Shelf." *Geophysical Research Letters* 28 (11): 2241–44. https://doi.org/10.1029/2000GL012461.

Fricker, H. A., T. Scambos, R. Bindschadler, and L. Padman. 2007. "An Active Subglacial Water System in West Antarctica Mapped from Space." *Science (New York, N.Y.)* 315 (5818): 1544–48. https://doi.org/10.1126/science.1136897.

Gade, H. G. 1979. "Melting of Ice in Sea Water: A Primitive Model with Application to the Antarctic Ice Shelf and Icebergs." *Journal of Physical Oceanography* 9 (1): 189–98. https://doi.org/10.1175/1520-0485(1979)009<0189:MOIISW>2.0.CO;2.

Gaidos, E., B. Lanoil, T. Thorsteinsson, A. Graham, M. Skidmore, S. Han, T. Rust, and B. Popp. 2004. "A Viable Microbial Community in a Subglacial Volcanic Crater Lake, Iceland." *Astrobiology* 4 (3): 327–44. https://doi.org/10.1089/ast.2004.4.327.

Galton-Fenzi, B. K., C. Maraldi, R. Coleman, and J. Hunter. 2008. "The Cavity under the Amery Ice Shelf, East Antarctica." *Journal of Glaciology*. Vol. 54.

Gambi, M. C., M. C. Buia, L. Mazzella, M. Lorenti, and M. B. Scipione. 2000. "Spatio-Temporal Variability in the Structure of Benthic Populations in a Physically Controlled System off Terra Nova Bay: The Shallow Hard Bottoms." In *Ross Sea Ecology: Italiantartide Expeditions (1987--1995)*, edited by Francesco Maria Faranda, Letterio Guglielmo, and Adrianna Ianora, 527–38. Berlin, Heidelberg: Springer Berlin Heidelberg. https://doi.org/10.1007/978-3-642-59607-0_38.

Gilmour, A. E. 1975. "McMurdo Sound Hydrological Observations, 1972–73." *New Zealand Journal of Marine and Freshwater Research* 9 (1): 75–95. https://doi.org/10.1080/00288330.1975.9515548.

Gilmour, A E. 1979. "Ross Ice Shelf Sea Temperatures." *New Series*. Vol. 203. https://www.jstor.org/stable/pdf/1747127.pdf?refreqid=excelsior%3A41fb498256acb7477c861af97eb24ea5.

Gomez, N., J. X. Mitrovica, M. E. Tamisiea, and P. U. Clark. 2010. "A New Projection of Sea Level Change in Response to Collapse of Marine Sectors of the Antarctic Ice Sheet." *Geophys. J. Int* 180: 623–34. https://doi.org/10.1111/j.1365-246X.2009.04419.x.

Goodwin, I. D. 1988. "The Nature and Origin of a Jokulhlaup near Casey Station, Antarctica." *Journal of Glaciology* 34 (116): 95–101. https://doi.org/10.1017/S0022143000009114.

Gooseff, M. N., W. B. Lyons, D. M. McKnight, B. H. Vaughn, A. G. Fountain, and C. Dowling. 2006. "A Stable Isotopic Investigation of a Polar Desert Hydrologic System, McMurdo Dry Valleys, Antarctica." *Arctic, Antarctic, and Alpine Research* 38 (1): 60–71. https://doi.org/10.1657/1523-0430(2006)038[0060:ASIIOA]2.0.CO;2.

Gordon, D. A., J. Priscu, and S. Giovannoni. 2000. "Origin and Phylogeny of Microbes Living in Permanent Antarctic Lake Ice." *Microbial Ecology* 39 (3): 197–202. https://doi.org/10.1007/s002480000016.

Gray, L., I. Joughin, S. Tulaczyk, V. B. Spikes, R. Bindschadler, and K. Jezek. 2005.

"Evidence for Subglacial Water Transport in the West Antarctic Ice Sheet through Three-Dimensional Satellite Radar Interferometry." *Geophysical Research Letters* 32 (3): L03501. https://doi.org/10.1029/2004GL021387.

Gudmundsson, G. H. 2007. "Tides and the Flow of Rutford Ice Stream, West Antarctica." *Journal of Geophysical Research* 112 (F4): F04007. https://doi.org/10.1029/2006JF000731.

Hamilton, E. L. 1976. "Shear-Wave Velocity versus Depth in Marine Sediments: A Review." *Geophysics* 41 (5): 983–96. https://library.seg.org/doi/pdf/10.1190/1.1440676.

Hansell, D. A., and C. A. Carlson. 1998. "Deep-Ocean Gradients in the Concentration of Dissolved Organic Carbon." *Nature* 395 (6699): 263–66. https://doi.org/10.1038/26200.

Harwood, D. M., F. Florindo, R. H. Levy, C. R. Fielding, S. F. Pekar, M. A. Speece, and SMS Science Team. 2007. "ANDRILL Southern McMurdo Sound Project." Lincoln. https://doi.org/0-9723550-2-2.

Heath, R. A. 1971. "New Zealand Journal of Marine and Freshwater Research Circulation and Hydrology under the Seasonal Ice in McMurdo Sound, Antarctica." https://doi.org/10.1080/00288330.1971.9515400.

Hellmer, H. H. 2004. "Impact of Antarctic Ice Shelf Basal Melting on Sea Ice and Deep Ocean Properties." *Geophysical Research Letters* 31 (L10307): 1–4. https://doi.org/10.1029/2004GL019506.

Hemer, M. A., A. L. Post, P. E. O'Brien, and M. Craven. 2007. "Sedimentological Signatures of the Sub-Amery Ice Shelf Circulation." *Antarctic Science* 19 (4): 497–506. https://doi.org/10.1017/S0954102007000697.

Herndl, G. J., T. Reinthaler, E. Teira, H. van Aken, C. Veth, A. Pernthaler, and J. Pernthaler. 2005. "Contribution of Archaea to Total Prokaryotic Production in the Deep Atlantic Ocean." *Applied and Environmental Microbiology* 71 (5): 2303–9. https://doi.org/10.1128/AEM.71.5.2303-2309.2005.

Herr, D., and G. R. Galland. 2009. "The Ocean and Climate Change Tools and Guidelines for Action IUCN Global Marine Programme." *Multilateral Office*.

Hoefs, J. 2015. *Stable Isotope Geochemistry*. https://doi.org/10.1007/978-3-319-19716-6.

Holland, D. M., S. S. Jacobs, and A. Jenkins. 2003. "Modelling the Ocean Circulation beneath the Ross Ice Shelf." *Antarctic Science* 15 (1): S0954102003001019. https://doi.org/10.1017/S0954102003001019.

Holland, P. R., and D. L. Feltham. 2006. "The Effects of Rotation and Ice Shelf Topography on Frazil-Laden Ice Shelf Water Plumes." https://journals.ametsoc.org/doi/pdf/10.1175/JPO2970.1.

Hood, E., T. J. Battin, J. Fellman, S. O'Neel, and R. G. M. Spencer. 2015. "Storage and Release of Organic Carbon from Glaciers and Ice Sheets." *Nature Geoscience* 8 (2): 91–96. https://doi.org/10.1038/ngeo2331.

Horgan, H. J., K. Christianson, R. W. Jacobel, S. Anandakrishnan, and R. B. Alley. 2013. "Sediment Deposition at the Modern Grounding Zone of Whillans Ice Stream, West Antarctica." *Geophysical Research Letters* 40 (15): 3934–39. https://doi.org/10.1002/grl.50712.

Horgan, H. J., R. B. Alley, K. Christianson, R. W. Jacobel, S. Anandakrishnan, A. Muto, L. H. Beem, and M. R. Siegfried. 2013. "Estuaries beneath Ice Sheets." *Geology* 41 (11): 1159–62. https://doi.org/10.1130/G34654.1.

Horrigan, S. G. 1981. "Primary Production under the Ross Ice Shelf , Antarctica" 26 (2): 378–82.

Horton, B. P., S. Rahmstorf, S. E. Engelhart, and A. E. Kemp. 2014. "Expert Assessment of Sea-Level Rise by AD 2100 and AD2300." *Quaternary Science Reviews* 84: 1–6. https://ac.els-cdn.com/S0277379113004381/1-s2.0-S0277379113004381-main.pdf?_tid=9c93f213-1f46-4ef9-a169-9f77660bedbb&acdnat=1539458362_1132352ebf123b63f0bd7ce71ea9de30.

Hulbe, C. L., T. A. Scambos, T. Youngberg, and A. K. Lamb. 2008. "Patterns of Glacier Response to Disintegration of the Larsen B Ice Shelf, Antarctic Peninsula." *Global and Planetary Change* 63 (1): 1–8. https://doi.org/10.1016/J.GLOPLACHA.2008.04.001.

Iversen, N., and B. B. Jørgensen. 1993. "Diffusion Coefficients of Sulfate and Methane in Marine Sediments: Influence of Porosity." *Geochimica et Cosmochimica Acta* 57 (3): 571–78. https://doi.org/10.1016/0016-7037(93)90368-7.

Jacobs, S. S. 2002. "Freshening of the Ross Sea During the Late 20th Century." *Science* 297 (5580): 386–89. https://doi.org/10.1126/science.1069574.

Jacobs, S. S., W. M. Smethie, K. M. Assmann, D. M. Holland, and A. Bergamasco. 2003. "Melting and Freezing Under the Ross Ice Shelf: Lessons From an Impacted Cavity." In *American Geophysical Union, Fall Meeting 2003, Abstract Id. C41A-03*. http://adsabs.harvard.edu/abs/2003AGUFM.C41A..03J.

Jacobs, S. S. 2004. "Bottom Water Production and Its Links with the Thermohaline Circulation." *Antarctic Science* 16 (4): 427–37. https://doi.org/10.1017/S095410200400224X.

Jacobs, S. S., A. L. Gordon, and A. F. Amos. 1979. "Effect of Glacial Ice Melting on the Antarctic Surface Water." *Nature* 277 (8): 469–71. https://www.nature.com/articles/277469a0.pdf.

Jacobs, S. S., H. H. Helmer, C. S. M. Doake, A. Jenkins, and R. M. Frolich. 1992. "Melting of Ice Shelves and the Mass Balance of Antarctica." *Journal of Glaciology* 38 (130): 375–87. https://doi.org/10.3189/S0022143000002252.

Jacobs, S. S, A. Jenkins, C. F. Giulivi, and P. Dutrieux. 2011. "Stronger Ocean Circulation and Increased Melting under Pine Island Glacier Ice Shelf." *Nature Geoscience* 4. https://doi.org/10.1038/NGEO1188.

Jacobs, S. S., A. L. Gordon, and J. L. Ardai. "Circulation and Melting beneath the Ross Ice Shelf." *Science* 203 (4379): 439–43. https://doi.org/10.1126/science.203.4379.439.

Jenkins, A. 2011. "Convection-Driven Melting near the Grounding Lines of Ice Shelves and Tidewater Glaciers." *Journal of Physical Oceanography* December: 2279–94. https://doi.org/10.1175/JPO-D-11-03.1.

Joughin, I., B. Smith, and B. Medley. 2014. "Marine Ice Sheet Collapse Potentially Under Way for the Thwaites Glacier Basin, West Antarctica." *Science* 344 (6185): 735–38. https://doi.org/10.1126/science.1249055.

Jouzel, J., L. Merlivat, and C. Lorius. 1982. “Deuterium Excess in an East Antarctic Ice Core Suggests Higher Relative Humidity at the Oceanic Surface during the Last Glacial Maximum.” *Nature* 299 (5885): 688–91. https://doi.org/10.1038/299688a0.

Kamb, B. 2001. “Basal Zone of the West Antarctic Ice Streams and Its Role in Lubrication of Their Rapid Motion.” In *The West Antarctic Ice Sheet: Behavior and Environment*, 157–99. American Geophysical Union (AGU). https://doi.org/10.1029/AR077p0157.

Katz, R. F, and M. G. Worster. 2010. “Stability of Ice-Sheet Grounding Lines.” *Proc. R. Soc. A* 466: 1597–1620. https://doi.org/10.1098/rspa.2009.0434.

Kendall, B., R. A. Creaser, C. T. Reinhard, T. W. Lyons, and A. D. Anbar. 2015. “Transient Episodes of Mild Environmental Oxygenation and Oxidative Continental Weathering during the Late Archean.” *Science Advances* 1 (10): 1–7. https://doi.org/10.1126/sciadv.1500777.

Kendall, C., E. Caldwell, and D. Snyder. 2004. “Resources on Isotopes.” USGS. 2004. https://wwwrcamnl.wr.usgs.gov/isoig/period/o_iig.html.

Khazendar, A., E. Rignot, D. M. Schroeder, H. Seroussi, M. P. Schodlok, B. Scheuchl, J. Mouginot, T. C. Sutterley, and I. Velicogna. 2016. “Rapid Submarine Ice Melting in the Grounding Zones of Ice Shelves in West Antarctica.” *Nature Communications* 7 (1): 13243. https://doi.org/10.1038/ncomms13243.

Kingslake, J., R. P. Scherer, T. Albrecht, J. Coenen, R. D. Powell, R. Reese, N. D. Stansell, S. Tulaczyk, M. G. Wearing, and P. L. Whitehouse. 2018. “Extensive Retreat and Re-Advance of the West Antarctic Ice Sheet during the Holocene.” *Nature* 558 (7710): 430–34. https://doi.org/10.1038/s41586-018-0208-x.

Kleman, J., and N. F. Glasser. 2007. “The Subglacial Thermal Organisation (STO) of Ice Sheets.” *Quaternary Science Reviews* 26: 585–97. https://doi.org/10.1016/j.quascirev.2006.12.010.

Lambrecht, A., H. Sandha, D. G. Vaughan, and C. Mayer. 2007. “New Ice Thickness Maps of Filchner-Ronne Ice Shelf, Antarctica, with Specific Focus on Grounding Lines and Marine Ice.” https://doi.org/10.1017/S0954102007000661.

Langhorne, P. J., K. G. Hughes, A. J. Gough, I. J. Smith, M. J. M. Williams, N. J. Robinson, C. L. Stevens, et al. 2015. “Observed Platelet Ice Distributions in Antarctic Sea Ice: An Index for Ocean-Ice Shelf Heat Flux.” *Geophysical Research Letters* 42 (13): 5442–51. https://doi.org/10.1002/2015GL064508.

Lanoil, B., M. Skidmore, J. C. Priscu, S. Han, W. Foo, S.W. Vogel, S. Tulaczyk, and H. Engelhardt. 2009. “Bacteria beneath the West Antarctic Ice Sheet.” *Environmental Microbiology* 11 (3): 609–15. https://doi.org/10.1111/j.1462-2920.2008.01831.x.

Lerman, A. 1978. “Chemical Exchange Across Sediment-Water Interface.” *Annual Review of Earth and Planetary Sciences* 6: 281–303. www.annualreviews.org.

Lewis, A. R., D. R. Marchant, D. E. Kowalewski, S. L. Baldwin, and L. E. Webb. 2006. “The Age and Origin of the Labyrinth, Western Dry Valleys, Antarctica: Evidence for Extensive Middle Miocene Subglacial Floods and Freshwater Discharge to the Southern Ocean.” *Geology*, no. 7: 513–16. https://doi.org/10.1130/G22145.1.

Lewis, E. L., and R. G. Perkin. 1986. “Ice Pumps and Their Rates.” *Journal of Geophysical Research: Oceans (1978–2012)* 91 (C10): 11756–62.

https://doi.org/10.1029/JC091iC10p11756.
Lipps, J. H., T. E. Ronan, and T. E. DeLaca. 1979. "Life Below the Ross Ice Shelf." *New Series*. Vol. 203. https://www.jstor.org/stable/pdf/1747131.pdf?refreqid=excelsior%3A926308beb36cf31fb706d979c5dceebb.
Littlepage, J. L. 1965. "Oceanographic Investigations in Mcmurdo Sound, Antarctica." In *Biology of the Antarctic Seas II, Volume 5*, edited by George A. Llano, 1–37. American Geophysical Union (AGU). https://doi.org/10.1029/AR005p0001.
Locarnini, R. A. 1994. "Water Masses and Circulation in the Ross Gyre and Environs - Ricardo Alejandro Locarnini - Google Books." Texas A&M University. https://books.google.com/books/about/Water_Masses_and_Circulation_in_the_Ross.html?id=qroQAQAAIAAJ.
Lucas, C., B. Timbal, and H. Nguyen. 2014. "The Expanding Tropics: A Critical Assessment of the Observational and Modeling Studies." *Wiley Interdisciplinary Reviews: Climate Change* 5 (1): 89–112. https://doi.org/10.1002/wcc.251.
MacAyeal, D. R. 1984. "Thermohaline Circulation below the Ross Ice Shelf: A Consequence of Tidally Induced Vertical Mixing and Basal Melting." *Journal of Geophysical Research: Oceans (1978–2012)* 89 (C1): 597–606. https://doi.org/10.1029/JC089iC01p00597.
Mangoni, O., V. Saggiomo, F. Bolinesi, F. Margiotta, G. Budillon, Y. Cotroneo, C. Misic, P. Rivaro, and M. Saggiomo. 2017. "Phytoplankton Blooms during Austral Summer in the Ross Sea, Antarctica: Driving Factors and Trophic Implications." *Plos One* 12 (4): 1–23. https://doi.org/10.1371/journal.pone.0176033.
Manheim, F. T., and L. S. Waterman. 1974. "32. Diffusimetry (Diffusion Constant Estimation) on Sediment Cores." http://deepseadrilling.org/22/volume/dsdp22_32.pdf.
Marsh, O. J., H. A. Fricker, M. R. Siegfried, K. Christianson, K. W. Nicholls, H. F. J. Corr, and G. Catania. 2016. "High Basal Melting Forming a Channel at the Grounding Line of Ross Ice Shelf, Antarctica." *Geophysical Research Letters* 43 (1): 250–55. https://doi.org/10.1002/2015GL066612.
Martiny, A. C., J. A. Vrugt, F. W. Primeau, and M. W. Lomas. 2013. "Regional Variation in the Particulate Organic Carbon to Nitrogen Ratio in the Surface Ocean." *Global Biogeochemical Cycles* 27 (3): 723–31. https://doi.org/10.1002/gbc.20061.
Martiny, A. C., J. A. Vrugt, and M. W. Lomas. 2014. "Concentrations and Ratios of Particulate Organic Carbon, Nitrogen, and Phosphorus in the Global Ocean." *Scientific Data* 1 (December): 140048. https://doi.org/10.1038/sdata.2014.48.
McElroy, M. B. 2007. *Ocean Biogeochemical Dynamics*. *Physics Today*. Vol. 60. Princeton, N.J.: Princeton University Press. https://doi.org/10.1063/1.2754608.
Menzies, J., J. W. M van der Meer, and W. W. Shilts. 2018. "Subglacial Processes and Sediments." In *Past Glacial Environments*, 105–58. Amsterdam: Elsevier.
Merlivat, L., and J. Jouzel. 1979. "Global Climatic Interpretation of the Deuterium-Oxygen 18 Relationship for Precipitation." *Journal of Geophysical Research* 84 (C8): 5029. https://doi.org/10.1029/JC084iC08p05029.
Michaud, A. B., M. L. Skidmore, A. C. Mitchell, T. J. Vick-Majors, C. Barbante, C.

Turetta, W. Van Gelder, and J. C. Priscu. 2016. "Solute Sources and Geochemical Processes in Subglacial Lake Whillans, West Antarctica." *Geology* 44 (5): 347–50. https://doi.org/10.1130/G37639.1.

Michaud, A. B., M. L. Skidmore, A.C. Mitchell, T. J. Vick-Majors, C. Barbante, C. Turetta, W. Vangelder, and J. C. Priscu. 2016. "Solute Sources and Geochemical Processes in Subglacial Lake Whillans, West Antarctica." *Geology* 44 (5). https://doi.org/10.1130/G37639.1.

Michel, R. L., T. W. Linick, and P. M. Williams. 1979. "Tritium and Carbon-14 Distributions in Seawater from under the Ross Ice Shelf Project Ice Hole." *Science (New York, N.Y.)* 203 (4379): 445–46. https://doi.org/10.1126/science.203.4379.445.

Mikucki, J. A., C. M. Foreman, B. Sattler, W. Berry Lyons, and J. C. Priscu. 2004. "Geomicrobiology of Blood Falls: An Iron-Rich Saline Discharge at the Terminus of the Taylor Glacier, Antarctica." *Aquatic Geochemistry* 10 (3–4): 199–220. https://doi.org/10.1007/s10498-004-2259-x.

Mikucki, J. A., P. A. Lee, D. Ghosh, A. M. Purcell, A. C. Mitchell, K. D. Mankoff, A. T. Fisher, et al. 2016. "Subglacial Lake Whillans Microbial Biogeochemistry: A Synthesis of Current Knowledge." https://doi.org/10.1098/rsta.2014.0290.

Milillo, P., E. Rignot, J. Mouginot, B. Scheuchl, M. Morlighem, X. Li, and J. T. Salzer. 2017. "On the Short-Term Grounding Zone Dynamics of Pine Island Glacier, West Antarctica, Observed With COSMO-SkyMed Interferometric Data." *Geophysical Research Letters* 44 (20): 10,410-436,444. https://doi.org/10.1002/2017GL074320.

Milly, P. C. D., J. Betancourt, M. Falkenmark, R. M. Hirsch, Z. W. Kundzewicz, D. P. Lettenmaier, R. J. Stouffer, M. D. Dettinger, and V. Krysanova. 2015. "On Critiques of 'Stationarity Is Dead: Whither Water Management?'" *Water Resources Research* 51 (9): 7785–89. https://doi.org/10.1002/2015WR017408.

Molnia, B. F. 1983. "Subarctic Glacial-Marine Sedimentation: A Model." In *Glacial-Marine Sedimentation*, 95–144. Boston, MA: Springer US. https://doi.org/10.1007/978-1-4613-3793-5_2.

Montross, S., M. Skidmore, B. Christner, D. Samyn, J. L. Tison, R. Lorrain, S. Doyle, and S. Fitzsimons. 2014. "Debris-Rich Basal Ice as a Microbial Habitat, Taylor Glacier, Antarctica." *Geomicrobiology Journal* 31 (1): 76–81. https://doi.org/10.1080/01490451.2013.811316.

Mosby, A. F. 2013. "Phytoplankton Growth Rates in the Ross Sea, Antarctica." College of William and Mary in Virginia.

Motyka, R. J., L. Hunter, K. A. Echelmeyer, and C. Connor. 2003. "Submarine Melting at the Terminus of a Temperate Tidewater Glacier, LeConte Glacier, Alaska, U.S.A." *Annals of Glaciology* 36: 57–65.

Motyka, R. J., M. Truffer, M. Fahnestock, J. Mortensen, S. Rysgaard, and I. Howat. 2011. "Submarine Melting of the 1985 Jakobshavn Isbræ Floating Tongue and the Triggering of the Current Retreat." *Journal of Geophysical Research: Earth Surface (2003–2012)* 116 (F1). https://doi.org/10.1029/2009JF001632.

Murray, J. 2001. "What Controls the Composition of Riverwater and Seawater: Equilibrium versus Kinetic Ocean." University of Washington.

Neal, C. S. 1979. "The Dynamics of the Ross Ice Shelf Revealed by Radio Echo-

Sounding." *Journal of Glaciology* 24 (90): 295–307. https://doi.org/10.3189/S0022143000014817.
Nikaido, H., and E. Y. Rosenberg. 1981. "Effect on Solute Size on Diffusion Rates through the Transmembrane Pores of the Outer Membrane of Escherichia Coli." *The Journal of General Physiology* 77 (2): 121–35. http://www.ncbi.nlm.nih.gov/pubmed/7021759.
Oppenheimer, M. 1998. "Global Warming and the Stability of the West Antarctic Ice Sheet." *Nature*. Vol. 393.
Oswald, G. K. A., and G. de Q. Robin. 1973. "Lakes Beneath the Antarctic Ice Sheet." *Nature* 245 (5423): 251–54. https://doi.org/10.1038/245251a0.
Parizek, B. R., R. B. Alley, and C. L. Hulbe. 2003. "Subglacial Thermal Balance Permits Ongoing Grounding-Line Retreat along the Siple Coast of West Antarctica." *Annals of Glaciology* 36 (September): 251–56. https://doi.org/10.3189/172756403781816167.
Parizek, B. R., K. Christianson, S. Anandakrishnan, R. Alley, R. T. Walker, R. A. Edwards, D. S. Wolfe, et al. 2013. "Dynamic (in)Stability of Thwaites Glacier, West Antarctica." *Journal of Geophysical Research: Earth Surface* 118 (2): 638–55. https://doi.org/10.1002/jgrf.20044.
Payne, A. J., P. R. Holland, A. P. Shepherd, I. C. Rutt, A. Jenkins, and I. Joughin. 2007. "Numerical Modeling of Ocean-ice Interactions under Pine Island Bay's Ice Shelf." *Journal of Geophysical Research: Oceans (1978–2012)* 112 (C10). https://doi.org/10.1029/2006JC003733.
Payne, A. J., A. Vieli, A. P. Shepherd, D. J. Wingham, and E. Rignot. 2004. "Recent Dramatic Thinning of Largest West Antarctic Ice Stream Triggered by Oceans." *Geophysical Research Letters* 31 (23). https://doi.org/10.1029/2004GL021284.
Pemberton, P., and J. Nilsson. 2016. "The Response of the Central Arctic Ocean Stratification to Freshwater Perturbations." *Journal of Geophysical Research: Oceans* 121 (1): 792–817. https://doi.org/10.1002/2015JC011003.
Phillips, D. L., and J. W. Gregg. 2001. "Uncertainty in Source Partitioning Using Stable Isotopes." *Oecologia* 127: 171–79. https://doi.org/10.1007/s004420000578.
Pillsbury, R. D., and S. S. Jacobs. 1985. "Preliminary Observations from Long-TER/Current Meter Moorings Near the Ross Ice Shelf." In *Antarctic Research Series: Oceanology of the Antarctic Continental Shelf*, 87–107. https://doi.org/10.1029/AR043p0087.
Poisson, A. 1980. "Conductivity / Salinity / Temperature Relationship of Diluted and Concentrated Standard Seawater." *IEEE Journal of Oceanic Engineering* l: 41–50.
Pollard, D., and R. M. DeConto. 2009. "Modelling West Antarctic Ice Sheet Growth and Collapse through the Past Five Million Years." *Nature* 458 (7236): 329–32. https://doi.org/10.1038/nature07809.
Popov, S. V., and V. N. Masolov. 2007. "Forty-Seven New Subglacial Lakes in the 0-110 Degrees E Sector of East Antarctica." https://www.igsoc.org/journal/53/181/j06J009.pdf.
Post, A. L., M. A. Hemer, P. E. O'Brien, D. Roberts, and M. Craven. 2007. "A History of Benthic Colonization beneath the Amery Ice Shelf, East Antarctica." *Marine*

Ecology Progress 344: 29–37. https://doi.org/10.3354/meps06966.
Powell, R. D., M. Dawber, and J. N. McInnes. 1996. "Observations of the Grounding-Line Glacier Terrninus Area at a Floating." *Annals of Glaciology* 22: 217–23.
Priscu, J. C. 1998. "A Lesson from the Bottom of the Planet." *Bioscience*.
Priscu, J. C., A. M. Achberger, J. E. Cahoon, B. C. Christner, R. L. Edwards, W. L. Jones, A. B. Michaud, et al. 2013a. "A Microbiologically Clean Strategy for Access to the Whillans Ice Stream Subglacial Environment." *Antarctic Science* 25 (5): 637–47. https://doi.org/10.1017/S0954102013000035.
Priscu, J. C., C. F. Wolf, C. D. Takacs, C. H. Fritsen, J. Laybourn-Parry, E. C. Roberts, B. Sattler, and W. B. Lyons. 1999. "Carbon Transformations in a Perennially Ice-Covered Antarctic Lake." *BioScience* 49 (12): 997–1008. https://doi.org/10.1525/bisi.1999.49.12.997.
Priscu, J. C., A. M. Achberger, J. E. Cahoon, B. C. Christner, R. L. Edwards, W. L. Jones, A. B. Michaud, et al. 2013b. "A Microbiologically Clean Strategy for Access to the Whillans Ice Stream Subglacial Environment." *Antarctic Science* 25 (05): 637–47. https://doi.org/10.1017/S0954102013000035.
Priscu, J. C., and K. P. Hand. 2012. "Microbial Habitability of Icy Worlds." *Microbe Magazine* 7 (4): 167–72. https://doi.org/10.1128/microbe.7.167.1.
Priscu, J. C., M. C. Kennicutt, R. E. Bell, S. A. Bulat, J. C. Ellis-Evans, V. V. Lukin, J.-R. Petit, R. D. Powell, M. J. Siegert, and I. Tabacco. 2005. "Exploring Subglacial Antarctic Lake Environments." *EOS* 86 (20): 193–97. http://www.montana.edu/priscu/documents/Publications/PriscuEtAl2005SubglacialLake.pdf.
Pritchard, H. D., S. R. M. Ligtenberg, H. A. Fricker, D. G. Vaughan, M. R. Van Den Broeke, and L. Padman. 2012. "Antarctic Ice-Sheet Loss Driven by Basal Melting of Ice Shelves." *Nature* 484: 502–5. https://doi.org/10.1038/nature10968.
Purcell, A. M., J. Mikucki, I. Alekhina, A. M. Achberger, C. Barbante, C. Brent, D. Ghosh, et al. 2014. "Microbial Sulfur Transformations in Sediments from Subglacial Lake Whillans." *Frontiers in Microbiology* 5 (November): 1–28. https://doi.org/10.3389/fmicb.2014.00594.
Rabouille, C, and J. F. Gaillard. 1991. "A Coupled Model Representing the Deep-sea Organic Carbon Mineralization and Oxygen Consumption in Surficial Sediments." *Journal of Geophysical Research: Oceans* 96 (C2): 2761–76. https://doi.org/10.1029/90JC02332.
Reddy, T. E., D. M. Holland, and K. R. Arrigo. 2010. "Ross Ice Shelf Cavity Circulation, Residence Time, and Melting: Results from a Model of Oceanic Chlorofluorocarbons." *Continental Shelf Research* 30 (7): 733–42. https://doi.org/10.1016/J.CSR.2010.01.007.
Redfield, A. C., B. K. Ketchum, and F. A. Richards. 1963. "The Influence of Organisms on the Composition of Sea-Water." In *The Sea: Ideas and Observations on Progress in the Study of the Seas*, edited by M.N. Hill, 26–77. New York, NY: John Wiley.
Reid, J. L. 1989. "On the Total Geostrophic Circulation of the South Atlantic Ocean: Flow Patterns, Tracers, and Transports." *Progress in Oceanography* 23 (3): 149–244. https://doi.org/10.1016/0079-6611(89)90001-3.

Retzlaff, R., and C. R. Bentley. 1993. “TiIning of Stagnation of Ice Stream C, West Antarctica, FroDl Short-Pulse Radar Studies of Buried Surface Crevasses.” *Journal of Glaciology*. Vol. 39.

Rignot, E., S. Jacobs, J. Mouginot, and B. Scheuchl. 2013. “Ice-Shelf Melting Around Antarctica.” *Science* 341: 266–70. https://doi.org/10.1126/science.1237966.

Rignot, E., J. Mouginot, M. Morlighem, H. Seroussi, and B. Scheuchl. 2014. “Widespread, Rapid Grounding Line Retreat of Pine Island, Thwaites, Smith, and Kohler Glaciers, West Antarctica, from 1992 to 2011.” *Geophysical Research Letters* 41: 3502–9. https://doi.org/10.1002/2014GL060140.

Rignot, E., and K. Steffen. 2008. “Channelized Bottom Melting and Stability of Floating Ice Shelves.” *Geophysical Research Letters* 35 (2): L02503. https://doi.org/10.1029/2007GL031765.

Rignot, E., I. Velicogna, M. R. Van Den Broeke, A. Monaghan, and J. Lenaerts. 2011. “Acceleration of the Contribution of the Greenland and Antarctic Ice Sheets to Sea Level Rise.” *Geophysical Research Letters* 38 (5): 1–5. https://doi.org/10.1029/2011GL046583.

Rintoul, S. R., L. Chown, M. Deconto, M. H. England, H. A. Fricker, V. Masson-Delmotte, T.R. Naish, M. J. Siegert, and J. Xavier. 2018. “Choosing the Future of Antarctica.” *Nature* 558. https://doi.org/10.1038/s41586-018-0173-4.

Robertson, J. D., and C. R. Bentley. 1990. “Seismic Studies on the Grid Western Half of the Ross Ice Shelf: RIGGS I and RIGGS II.” *American Geophysical Union*. https://doi.org/10.1029/AR042p0087.

Robin, G. de Q., C. W. M. Swithinbank, and B. M. E. Smith. 1970. “Radio Echo Exploration of the Antarctic Ice Sheet, 1970.” *Polar Record* 14 (89): 211. https://doi.org/10.1017/S0032247400056734.

Robinson, N. J., M. J. M. Williams, P. J. Barrett, and A. R. Pyne. 2010. “Observations of Flow and Ice-ocean Interaction beneath the McMurdo Ice Shelf, Antarctica.” *Journal of Geophysical Research: Oceans (1978–2012)* 115 (C3). https://doi.org/10.1029/2008JC005255.

Robinson, S. A., D. H. King, J. Bramley-Alves, M. J. Waterman, M. B. Ashcroft, J. Wasley, J. D. Turnbull, et al. 2018. “Rapid Change in East Antarctic Terrestrial Vegetation in Response to Regional Drying.” *Nature Climate Change* 8 (10): 879–84. https://doi.org/10.1038/s41558-018-0280-0.

Rohling, E. J. 2013. “Oxygen Isotope Composition of Seawater.” *Encyclopedia of Quaternary Science* 2: 915–22.

Rose, K. E. 1979. “Characteristics of Ice Flow in Marie Byrd Land, Antarctica.” *Journal of Glaciology* 24 (90): 63–75. https://doi.org/10.3189/S0022143000014659.

Rutishauser, A., D. D. Blankenship, M. Sharp, M. L. Skidmore, J. S. Greenbaum, C. Grima, D. M. Schroeder, J. A. Dowdeswell, and D. A. Young. 2018. “Discovery of a Hypersaline Subglacial Lake Complex beneath Devon Ice Cap, Canadian Arctic.” *Science Advances* 4 (4): eaar4353. https://doi.org/10.1126/sciadv.aar4353.

Scambos, T. A., E. Berthier, and C. A. Shuman. 2011. “The Triggering of Subglacial Lake Drainage during Rapid Glacier Drawdown: Crane Glacier, Antarctic Peninsula.” *Annals of Glaciology* 52 (59): 74–82.

https://doi.org/10.3189/172756411799096204.
Scambos, T. A., R. E. Bell, R. B. Alley, S. Anandakrishnan, D. H. Bromwich, K. Brunt, K. Christianson, et al. 2017. “How Much, How Fast?: A Science Review and Outlook for Research on the Instability of Antarctica’s Thwaites Glacier in the 21st Century.” *Global and Planetary Change* 153 (June): 16–34. https://doi.org/10.1016/j.gloplacha.2017.04.008.
Schaffer, J., R. Timmermann, J. E. Arndt, S. S. Kristensen, C. Mayer, M. Morlighem, and D. Steinhage. 2016. “A Global, High-Resolution Data Set of Ice Sheet Topography, Cavity Geometry, and Ocean Bathymetry.” *Earth Syst. Sci. Data* 8: 543–57. https://doi.org/10.5194/essd-8-543-2016.
Scherer, R. P., R. M. DeConto, D. Pollard, and R. B. Alley. 2016. “Windblown Pliocene Diatoms and East Antarctic Ice Sheet Retreat.” *Nature Communications* 7 (1): 12957. https://doi.org/10.1038/ncomms12957.
Scherer, R. P., A. Aldahan, S. Tulaczyk, G. Possnert, H. Engelhardt, and B. Kamb. 1998. “Pleistocene Collapse of the West Antarctic Ice Sheet.” *Science* 281 (5373): 82–85.
Schewe, J., J. Heinke, D. Gerten, I. Haddeland, N. W. Arnell, D. B. Clark, R. Dankers, et al. 2014. “Multimodel Assessment of Water Scarcity under Climate Change.” *Proceedings of the National Academy of Sciences of the United States of America* 111 (9): 3245–50. https://doi.org/10.1073/pnas.1222460110.
Schoof, C. 2007. “Ice Sheet Grounding Line Dynamics: Steady States, Stability, and Hysteresis.” *Journal of Geophysical Research* 112 (F3): F03S28. https://doi.org/10.1029/2006JF000664.
Scopelliti, G., A. Bellanca, D. Monien, and G. Kuhn. 2013. “Chemostratigraphy of the Early Pliocene Diatomite Interval from MIS AND-1B Core (Antarctica): Palaeoenvironment Implications.” *Global and Planetary Change* 102 (March): 20–32. https://doi.org/10.1016/j.gloplacha.2013.01.001.
Shabtaie, S., and C. R. Bentley. 1987. “West Antarctic Ice Streams Draining into the Ross Ice Shelf: Configuration and Mass Balance.” *Journal of Geophysical Research* 92 (B2): 1311. https://doi.org/10.1029/JB092iB02p01311.
Sharmila, S, and K. J. E. Walsh. 2018. “Recent Poleward Shift of Tropical Cyclone Formation Linked to Hadley Cell Expansion.” *Nature Climate Change* 8: 730–36. https://doi.org/10.1038/s41558-018-0227-5.
Sharp, M., J. Parkes, I. J. Fairchild, H. Lamb, and M. Tranter. 1999. “Widespread Bacterial Populations at Glaciers Beds and Their Relationship to Rock Weathering and Carbon Cycling,” no. 2: 107–10. https://doi.org/10.1130/0091-7613(1999)027<0107:WBPAGB>2.3.CO.
Shen, L., and Z. Chen. 2007. “Critical Review of the Impact of Tortuosity on Diffusion.” *Chemical Engineering Science* 62: 3748–55. https://doi.org/10.1016/j.ces.2007.03.041.
Shepherd, A., D. Wingham, and E. Rignot. 2004. “Warm Ocean Is Eroding West Antarctic Ice Sheet.” *Geophysical Research Letters* 31 (23). https://doi.org/10.1029/2004GL021106.
Siegert, M. J., S. Carter, I. Tabacco, S. Popov, and D. D. Blankenship. 2005. “A Revised Inventory of Antarctic Subglacial Lakes.” *Antarctic Science* 17 (3): 453–60.

https://doi.org/10.1017/S0954102005002889.
Siegfried, M. R., H. A. Fricker, S. P. Carter, and S. Tulaczyk. 2016. “Episodic Ice Velocity Fluctuations Triggered by a Subglacial Flood in West Antarctica.” *Geophysical Research Letters* 43 (6): 2640–48. https://doi.org/10.1002/2016GL067758.
Siegfried, M. R., B. Medley, K. M. Larson, H. A. Fricker, and S. Tulaczyk. 2017. “Snow Accumulation Variability on a West Antarctic Ice Stream Observed with GPS Reflectometry, 2007-2017.” *Geophysical Research Letters* 44 (15): 7808–16. https://doi.org/10.1002/2017GL074039.
Siegfried, M. R., and H. A. Fricker. 2018. “Thirteen Years of Subglacial Lake Activity in Antarctica from Multi-Mission Satellite Altimetry.” *Annals of Glaciology* 59 (76pt1): 42–55. https://doi.org/10.1017/aog.2017.36.
Simkins, L. M., S. L. Greenwood, and J. B. Anderson. 2018. “Diagnosing Ice Sheet Grounding Line Stability from Landform Morphology.” *The Cryosphere*, no. March 21. https://doi.org/10.5194/tc-2018-44.
Skidmore, M., M. Tranter, S. Tulaczyk, and B. Lanoil. 2010. “Hydrochemistry of Ice Stream Beds—Evaporitic or Microbial Effects?” *Hydrological Processes* 24 (4): 517–23. https://doi.org/10.1002/hyp.7580.
Skidmore, M. L., J. M. Foght, and M. J. Sharp. 2000a. “Microbial Life beneath a High Arctic Glacier Microbial Life beneath a High Arctic Glacier †.” *Applied and Environmental Microbiology* 66 (8): 3214–20. https://doi.org/10.1128/AEM.66.8.3214-3220.2000.Updated.
———. 2000b. “Microbial Life beneath a High Arctic Glacier.” *Applied and Environmental Microbiology* 66 (8): 3214–20. https://doi.org/10.1128/AEM.66.8.3214-3220.2000.
Smethie, W. M., and S. S. Jacobs. 2005. “Circulation and Melting under the Ross Ice Shelf: Estimates from Evolving CFC, Salinity and Temperature Fields in the Ross Sea.” *Deep-Sea Research I* 52: 959–78. https://doi.org/10.1016/j.dsr.2004.11.016.
Smith, B. E., N. E. Lord, and C. R. Bentley. 2002. “Crevasse Ages on the Northern Margin of Ice Stream C, West Antarctica.” *Annals of Glaciology*. Vol. 34. https://doi.org/10.3189/172756402781817932.
Smith, W. O., D. M. Nelson, G. R. DiTullio, and A. R. Leventer. 1996. “Temporal and Spatial Patterns in the Ross Sea: Phytoplankton Biomass, Elemental Composition, Productivity and Growth Rates.” *Journal of Geophysical Research: Oceans* 101 (C8): 18455–65. https://doi.org/10.1029/96JC01304.
Smith, W., P. Sedwick, K. Arrigo, D. Ainley, and A. Orsi. 2012. “The Ross Sea in a Sea of Change.” *Oceanography* 25 (3): 90–103. https://doi.org/10.5670/oceanog.2012.80.
Stearns, L. A., B. E. Smith, and G. S. Hamilton. 2008. “Increased Flow Speed on a Large East Antarctic Outlet Glacier Due to Subglacial Floods.” *Nature Geoscience* 1.
Stefánsson, U., and F. A. Richards. 1963. “Processes Contribuing to the Nutrient Distribution off the Columbia River and Strait of Juan de Fuca.” *Limnology and Oceanography* 8 (4): 394–410. https://doi.org/10.4319/lo.1963.8.4.0394.
Stewart, C. L. 2018. “Ice-Ocean Interactions beneath the North-Western Ross Ice Shelf,

Antarctica." University of Cambridge. https://doi.org/https://doi.org/10.17863/CAM.21483.

Studinger, M., R. E. Bell, D. D. Blankenship, C. A. Finn, R. A. Arko, D. L. Morse, and I. Joughin. 2001. "Subglacial Sediments: A Regional Geological Template for Iceflow in West Antarctica." *Geophysical Research Letters* 28 (18): 3493–96. https://doi.org/10.1029/2000GL011788.

Swithinbank, C. W. 1988. "Satellite Image Atlas of Glaciers of the World: Antarctica."

Thomas, R. H., and C. R. Bentley. 1978. "The Equilibrium State the Ross of the Eastern Half of Ice Shelf." *Journal of Glaciology*. Vol. 20.

Tol, R. S. J., M. Bohn, T. E. Downing, M. Guillerminet, E. Hizsnyik, R. Kasperson, K. Lonsdale, et al. 2006. "Adaptation to Five Metres of Sea Level Rise." *Journal of Risk Research* 9 (5): 467–82. https://doi.org/10.1080/13669870600717632.

Tranter, M. 2005. "Perturbation of Hydrochemical Conditions in Natural Microcosms Entombed within Antarctic Ice." *Geographical* 12 (6): 273–74.

Tranter, M., M. J. Sharp, H. R. Lamb, G. H. Brown, B. P. Hubbard, and I. C. Willis. 2002. "Geochemical Weathering at the Bed of Haut Glacier d'Arolla, Switzerland - A New Model." *Hydrological Processes* 16 (5): 959–93. https://doi.org/10.1002/hyp.309.

Trenberth, K. E. 2011. "Changes in Precipitation with Climate Change." *Climate Research* 47: 123–38. https://doi.org/10.3354/cr00953.

Tulaczyk, S., J. A. Mikucki, M. R. Siegfried, J. C. Priscu, C. G. Barcheck, L. H. Beem, A. Behar, et al. 2014. "WISSARD at Subglacial Lake Whillans, West Antarctica: Scientific Operations and Initial Observations." *Annals of Glaciology* 55 (65): 51–58. https://doi.org/10.3189/2014AoG65A009.

Tulaczyk, S., J. A. Mikucki, M. R. Siegfried, J. C. Priscu, C. G. Barcheck, L. H. Beem, A. Behar, et al. 2014. "WISSARD at Subglacial Lake Whillans, West Antarctica: Scientific Operations and Initial Observations." *Annals of Glaciology* 55 (65): 51–58. https://doi.org/10.3189/2014AoG65A009.

Turner, K.W., B. B. Wolfe, T. W. D. Edwards, T. C. Lantz, R. I. Hall, and G. Larocque. 2014. "Controls on Water Balance of Shallow Thermokarst Lakes and Their Relations with Catchment Characteristics: A Multi-Year, Landscape-Scale Assessment Based on Water Isotope Tracers and Remote Sensing in Old Crow Flats, Yukon (Canada)." *Global Change Biology* 20 (5): 1585–1603. https://doi.org/10.1111/gcb.12465.

Vaughan, D. G., A. Rivera, J. Woodward, H. F. J. Corr, J. Wendt, R. Zamora, D. G. Vaughan, et al. 2007. "Topographic and Hydrological Controls on Subglacial Lake Ellsworth." *Geophys. Res. Lett* 34: 18501. https://doi.org/10.1029/2007GL030769.

Vick-Majors, T. J., A. B. Michaud, M. L. Skidmore, C. Turetta, B. C. Christner, K. Christianson, A. C. Mitchell, M. Amanda, J. A. Mikucki, and J. C. Priscu. n.d. "Subglacial Carbon and Nutrient Fluxes to the Marine Cavity under the Ross Ice Shelf," 1–25.

Vick-Majors, T. J., A. C Mitchell, A. M Achberger, B. C Christner, J. E. Dore, A. B. Michaud, J. A. Mikucki, A. M. Purcell, M. L. Skidmore, and J. C. Priscu. 2016. "Physiological Ecology of Microorganisms in Subglacial Lake Whillans." *Frontiers*

in Microbiology 7 (October): 1–16. https://doi.org/10.3389/fmicb.2016.01705.
Vick-Majors, T. J. 2016. "Biogeochemical Processes in Antarctic Aquatic Environments: Linkages and Limitations." Montana State University.
Vick-Majors, T. J., A. Achberger, P. Santibáñez, J. E. Dore, T. Hodson, A. B. Michaud, B. C. Christner, et al. 2016. "Biogeochemistry and Microbial Diversity in the Marine Cavity beneath the McMurdo Ice Shelf, Antarctica." *Limnology and Oceanography* 61 (2): 572–86. https://doi.org/10.1002/lno.10234.
Vogel, S. W. 2004. "The Basal Regime of the West-Antarctic Ice Sheet Interaction of Subglacial Geology with Ice Dynamics." *Arctic*. University of California, Santa Cruz. https://doi.org/3127401.
Vogel, S. W., S. Tulaczyk, B. Kamb, H. Engelhardt, F. D. Carsey, A. E. Behar, A. L. Lane, and I. Joughin. 2005. "Subglacial Conditions during and after Stoppage of an Antarctic Ice Stream: Is Reactivation Imminent?" *Geophysical Research Letters* 32 (14). https://doi.org/10.1029/2005GL022563.
Wadham, J. L., M. Tranter, M. Skidmore, A. J. Hodson, J. Priscu, W. B. Lyons, M. Sharp, P. Wynn, and M. Jackson. 2010. "Biogeochemical Weathering under Ice: Size Matters." *Global Biogeochemical Cycles* 24 (3). https://doi.org/10.1029/2009GB003688.
Williams, R. T., and E. S. Robinson. 1979. "Ocean Tide and Waves Beneath the Ross Ice Shelf." *New Series*. Vol. 203. https://www.jstor.org/stable/pdf/1747129.pdf?refreqid=excelsior%3A62c827ee6a124b24bcf2fdd6988eb598.
Wingham, D. J., M. J. Siegert, A. Shepherd, and A. S. Muir. 2006. "Rapid Discharge Connects Antarctic Subglacial Lakes." *Nature* 440 (7087): 1033–36. https://doi.org/10.1038/nature04660.
Wright, A., and M. Siegert. 2012. "A Fourth Inventory of Antarctic Subglacial Lakes." *Antarctic Science* 24 (6): 659–64. https://doi.org/10.1017/S095410201200048X.
Wyk de Vries, M. van, R. G. Bingham, and A. S. Hein. 2017. "A New Volcanic Province: An Inventory of Subglacial Volcanoes in West Antarctica." *Geological Society, London, Special Publications*, no. 1: SP461.7. https://doi.org/10.1144/SP461.7.
Yuan-Hui, L., and S. Gregory. 1974. "Diffusion of Ions in Sea Water and in Deep-Sea Sediments." *Geochimica et Cosmochimica Acta* 38 (5): 703–14. https://doi.org/10.1016/0016-7037(74)90145-8.

CHAPTER TWO

SIGNATURES OF SUBGLACIAL WATER IN SHALLOW SEDIMENTS OF THE WHILLANS GROUNDING ZONE AND OVERLYING WATER COLUMN

Contribution of Authors and Co-authors

Author: Kimberly A. Roush

Contributions: Processed sediment core, porewaters and analyzed data, generated figures and tables and wrote thesis.

Co-author: John Priscu

Contributions: Provided funding, oversight, samples, conceived the study, and aided in thesis preparation.

Co-author: Mark Skidmore

Contributions: Provided oversight for geochemical and isotope analysis.

Co-author: Wei Li

Contributions: Processed sediment core.

Co-author: Alex Michaud

Contributions: provided framework for procedure and analysis; performed oxygen microsensor analysis and interpretation.

Co-author: WISSARD Science Team

Contributions: Collected sediment core; helped in all phases of field work

Manuscript Information

Kimberly A. Roush, John Priscu, Mark Skidmore, Alex Michaud and the WISSARD Science Team

Status of Manuscript:
__X__ Prepared for submission to a peer-reviewed journal
____ Officially submitted to a peer-reviewed journal
____ Accepted by a peer-reviewed journal
____ Published in a peer-reviewed journal

Introduction

The WGZ is an important environment for determining whether there is subglacial freshwater influence on the Siple Coast because it is a location where channelized water empties into the Ross Ice Shelf (RIS) cavity (Siegfried et al. 2016). Sediments and porewater at the WGZ are particularly important because they: 1) reveal unique geochemical characteristics that have not been previously analyzed; 2) can provide information about the source of water (marine, subglacial freshwater or basal ice melt) and potential source mineralogy and diagenesis based on the porewater geochemistry; and 3) can provide information about diurnal tides and/or episodic subglacial flood events that could impact RIS cavity, Ross Sea and Southern Ocean stratification.

Research in subglacial environments suggests the potential for an assemblage of microbes that are able to survive in subglacial conditions (Priscu 1998; Skidmore et al. 2000; Priscu et al. 2005; Lanoil et al. 2009; Christner et al. 2014; Montross et al. 2014). While the Ross Sea is one of the most studied marine environments in the Antarctic region (Smith et al. 2012), no physical studies had been completed along the Siple Coast GZ before sampling by the WISSARD team in 2015 (Christner et al. 2014). Accessing subglacial systems cleanly (Priscu et al. 2013b) has provided researchers the opportunity to understand the interaction between basal geology, comminuted till and the microbial life that inhabits these environments, and to characterize sub-ice shelf basal melt and subglacial water discharge across the grounding zone, both of which impact the stability of the RIS and the greater WAIS (Gordon et al. 2000; Carter and Fricker 2012).

Recently, radio-echo sounding measurements were used to identify two hypersaline subglacial lakes near the ice divide of the Devon Ice Cap (DIC) in the Canadian Arctic (Rutishauser et al. 2018). Local evaporite-rich sediments and ice temperature profiling to 300 m (-18.5^{o}C) support the hypothesis that the lakes beneath the DIC have a significantly depressed freezing point temperature. Given that microbial life has been found to exist in high salinity conditions exhibited by the McMurdo Dry Valleys (Mikucki et al. 2004), it is suggested that these isolated lakes might contain microbial life and furthermore, serve as an analogue to what conditions and microbes may exist on Mars or Europa (Priscu and Hand 2012).

In contrast, freshwater subglacial systems such as the Haut Glacier d'Arolla in Switzerland are known to be dominated by high concentrations of Ca^{2+}, Mg^{2+}, SO_4^{2-} and HCO_3^-, which can help model linkages between sulfide oxidation and, carbonate and silicate dissolution (Sharp et al. 1999). The abundance of calcium, a dominant cation in alpine subglacial waters and typical in terrestrially sourced waters, is due to the rapid dissolution kinetics of carbonate (Anderson et al. 1997; Murray 2001).

Sampled in the 2000-2001 season (Kamb 2001; Catania 2004; Vogel et al. 2005), the Kamb Ice Stream (KIS) and Bindschlader Ice Stream (BIS) (Vogel 2004) were found to have geochemistry characterized by higher concentrations of ions than subglacial fluvial streams in the Swiss Alps, Greenland, Norway or Canada (Skidmore et al. 2010). The mineralogy of the glacial flour and labile organic matter were found to determine the diversity of microbes present in the system (Skidmore et al. 2000; Tranter et al. 2005a, 2005b; Lanoil et al. 2009; Skidmore et al. 2010). The concentrations of Cl^- and Na^+ are ~0.2 to 0.4% and 1.4 to 7.4% of seawater, compared to <0.01% for most glacial run-off, including subglacial fluvial streams in Norway and Canada. KIS and BIS porewater is most similar to concentrations found in the cold, semi-arid regions of Canada, or within the Artic Canadian permafrost, where silicate and sulfide weathering are thought to give rise to the aqueous geochemistry (Skidmore et al., 2010). The KIS and BIS ice-stream porewater type is characterized by Na^+-$SO_4{}^2$-Ca^{2+}-Mg^{2+}-$HCO_3{}^-$, while most sub-glacial geochemistry is characterized by Ca^{2+}-$HCO_3{}^-$-$SO_4{}^{2-}$-Mg^{2+} (Skidmore et al. 2010).

In comparison, the crustal derived non-seawater component of Subglacial Lake Whillans (SLW) is dominated by K^+ and Na^+, likely from silicate weathering (Michaud et al. 2016). It is proposed that residence time and the formation of secondary silicates are probably the key discriminating variables in producing the different Si concentrations relative to the major ions. The major marine ions of interest at the WGZ include: Cl^-, Na^+, $SO_4{}^{2-}$, Mg^{2+}, K^+, Ca^{2+} and Br^-.

Background

Physical Characteristics of the Sediment Core

High latitude coastal sediments are typically dominated by ice-rafted debris (IRD), terrigenous material (formed on land and chemical and/or physically degraded prior to transport) and biogenic debris (dominated by amorphous silica introduced by diatoms). The terrigenous fraction is primarily dominated by clays, in mineral (ranging from gibbsite- to brucite-endmember clays) and size composition (< 2 μm). Porosity is largely controlled by grain size and mineralogy, where smaller grain sizes are characteristic of higher porosities and larger grain sizes are characteristic of lower porosities. Sediments near the continental marine transition typically have a porosity of 0.7 to 0.9; following compaction porosity decreases to 0.4 to 0.6 within a few tens of centimeters or meters below the sediment water interface (Lerman 1978) In addition to sediment porosity changes over time and with depth throughout the sediment profile, Menzies et al. (2018) discusses the geomorphology of how different till deposits are created in subglacial environments associated with the GZ.

Water Isotopes

The hypothesis, *sediment porewater geochemistry at the GZ is influenced by subglacial flow, was addressed using* stable isotopes of porewater ($\delta^{18}O$ and δD) at the SLW GZ in reference to the data previously collected at SLW (Christner et al. 2014). Due to the global and local parameters that influence oxygen and hydrogen isotopes, it is important to emphasize that SLW is predominantly a freshwater system that drains/fills on a decadal cycle with measured water column conductivity of 720 μS cm^{-1} and a water column temperature of -0.49°C, while porewaters have a conductivity of 860 μS cm^{-1} (Christner et al. 2014). The WGZ sediment core, in contrast, is marine dominated with an average porewater conductivity of ~56,000 μS cm^{-1}, temperatures of -1.7 to -1.89°C and salinities of 34.45 to 34.61 (Vick-Majors et al. 2016).

Evaporation and condensation of water display a similar pattern, but different magnitude, in hydrogen isotopes as they do in oxygen isotopes. The different magnitudes are due to corresponding differences in vapor pressure that exist between H_20 and HDO in one case and $H_2{}^{16}O$ and $H_2{}^{18}O$ in the other (Hoefs 2015). Hydrogen and oxygen isotopes are correlated by the relationship between $\delta D = 8\delta^{18}O + 10$, which describes the interdependence of H- and O-isotope ratios in meteoric waters on a global scale. Neither the numerical coefficient 8 or the constant, 10, also known as the deuterium excess, d, are constant in nature. Both can vary depending on the conditions of evaporation, vapor transport and precipitation and can therefore offer insight into climatic processes (Hoefs 2015)

The variation in stable water isotopes at specific locations, the temperature of condensation of precipitation and the degree of rainout of the air mass are used to constrain the isotopic signature. Factors that control isotopic composition of precipitation before and after recharge allows the use of oxygen and hydrogen isotopes as tracers of source water and meteoric processes. These factors include altitude, latitude, distance from coast and the amount of rainfall (Kendall et al. 2004) (Figure 2.1).

$$\delta_x = \left(\frac{R_{sample}}{R_{standard}} - 1\right) * 1000‰$$

The equation above defines the isotopic composition, where δ_x (parts per thousand, per mil, ‰) is the isotope ratio in a sample is expressed in reference to the isotope ratio in a common standard. *R* is the ratio of the heavy isotope to the light isotope.

Oxygen is comprised of two major stable isotopes: ^{16}O (99.76% of water molecules) and ^{18}O (0.20% of water molecules). The ^{18}O:^{16}O in the sample is analyzed in reference to the ^{18}O:^{16}O in VSMOW (Vienna Standard Mean Ocean Water). In the precipitation process, heavier isotopic species, ^{18}O and ^{2}H, will rain out first because they have a lower saturation vapor pressure than ^{16}O and ^{1}H (Craig and Gordon 1965). A positive $\delta^{18}O$ value indicates enrichment in the heavy isotope, relative to the standard, and conversely, a negative $\delta^{18}O$ indicates depletion of the heavy isotope (Rohling 2013). Precipitation in cold polar regions is depleted in ^{18}O as it all precipitates out at lower latitudes. While ^{16}O always dominates, the amount of ^{18}O relative to ^{16}O changes. While glacially-derived sources tend to be isotopically *light,* marine-derived sources are typically isotopically heavy (comparatively enriched in ^{18}O). Salinity and the $\delta^{18}O$ of seawater are closely correlated (Epstein and Mayeda, 1953).

Phase transitions between vapor, liquid, and ice through evaporation/precipitation and boiling/condensation in the Earth's atmosphere, at the surface and in the upper part of the crust cause the most variation in hydrogen and oxygen isotopes. Under conditions of evaporation and condensation, hydrogen and oxygen isotopes show similar fractionation patterns. As a result, hydrogen and oxygen isotope distributions are correlated by the Global Meteoric Water Line, calculated by Craig, represented by:

$$\delta D = 8\ \delta^{18}O + 10$$

Local Mean Water Lines (LMWLs) in arid environments plot with a higher D-excess because of evaporation. LMWLs in humid environments plot higher on the $\delta^{18}O$ axis (x-axis) because of the phase change which favors liquid precipitation (Hoefs 2015).

Deuterium , the heavy isotope of H, fractionates less than the heavy isotope of O on evaporation, leading to an excess of D relative to ^{18}O in precipitation (Turner et al. 2014). Deuterium excess ($d = \delta D - 8\ \delta^{18}O$) is particularly useful in determining the age and origin of water vapor. In oceanic water vapor, d is determined by surface temperature, humidity, and wind speed (Merlivat and Jouzel 1979). Negative d values suggest that evaporation fractionation has occurred. Negative d values in Antarctic ice cores have been interpreted as indicators of higher relative humidity in the oceanic source area providing moisture for Antarctic precipitation (Jouzel et al. 1982).

The GMWL or MWL (Figure 2.1) shows values of $\delta^{18}O$ and δD that are not characterized by signs of evaporation after precipitation and are linearly related by the line. High correlation coefficients ($r^2 = 1$) show that oxygen and hydrogen stable isotopes are closely related; as a result, isotopic ratios and fractionations of the two elements are usually discussed together (Kendall et al. 2004). The LMWL shows a smaller slope and y-intercept. Water that has evaporated or has mixed with evaporated water typically plots below the meteoric water line (Craig and Gordon 1965).

While waters in most rivers at lower latitudes are altered by two major sources (recent precipitation that results in surface runoff and groundwater), glaciated or sub-ice sheet watersheds are different (Kendall et al. 2015). Variations in stream isotopic abundances provide information on contributions of snow pack, glacial melt, and/or direct precipitation to runoff. Stable isotopes have been used to delineate and quantify sources of water to the closed basin lakes of the McMurdo Dry Valleys (Antarctica) in addition to establishing hydrologic histories of the lakes (Gooseff et al. 2006).

Table 2. 1 The following locations show different $\delta^{18}O$ and δD for a variety of samples, ranging from fresh to hypersaline and glacial samples from varying latitudes, distances from the coast and duration and extent of ice cover.

Location	**Sample Type**	**$\delta^{18}O$ (‰)**	**δD (‰)**	**Citation**
SLW	Fresh water with relict marine influence	-38 (lake water) to -36.5 (porewater)	-301 (lake water) to -287	(Michaud et al. 2016)
Ross Sea	AASW (Antarctic Surface Water)	-0.67		(S. S. Jacobs 2002)
Mean Global Precipitation		-4	-22	(Craig and Gordon 1965)

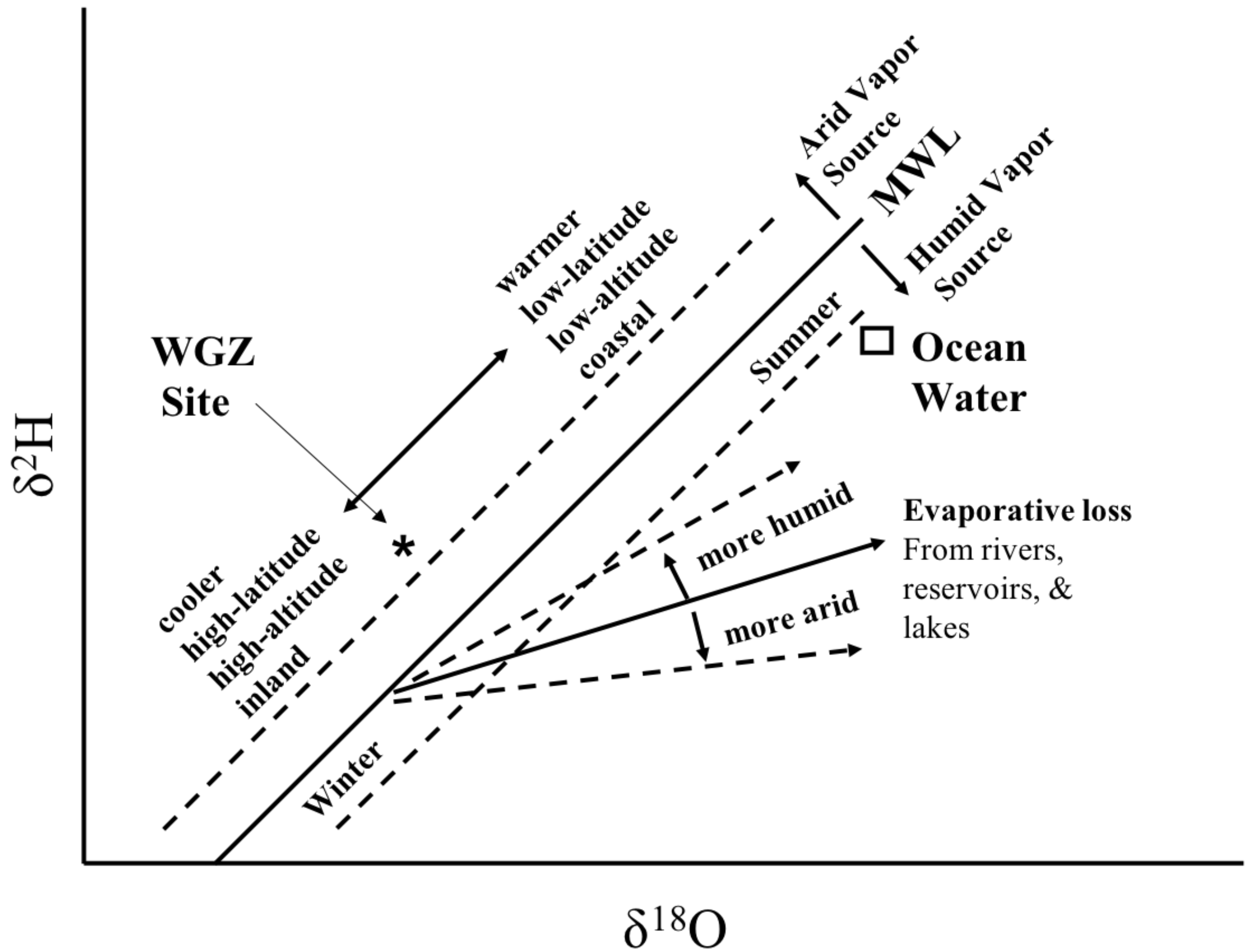

Figure 2.1 δD and δ^{18}O values vary depending on water type, vapor source, altitude, latitude and distance inland (adapted from Hoefs 2015). The asterisk designates the relative location of WGZ waters.

Dissolved Ions

My study focused on the major ions chloride and sodium. Chloride and sodium are conservative ions and, owing to their relatively low reactivity, can remain in specific seawater types for long periods of time (98 x 10^6 years for chloride and 80 x 10^6 years for sodium)(Emerson and Hedges 2008). They make up the first two greatest ion concentrations, respectively 55.3% and 30.7% (SOEST, 2015), of the seven ion species that dominate seawater and are often used to define distinct water masses in the world's oceans. Sulfate and magnesium, at 7.8% and 3.7%, have the third and fourth greatest concentrations of the major seawater ions. Sulfate is a non-conservative ion, with a comparatively short residence time (10 x 10^6 years) (Emerson and Hedges 2008) and can be affected by biological and non-biological processes. In contrast, magnesium has a residence time of 16 x 10^6 years and is not classified as being conservative (Emerson and Hedges 2008).

Methods

Sample Collection and Core Processing

Sampling at SLW and the WGZ is unique because it marks the advent of a drilling and sampling technique established to access water samples hundreds of meters beneath the surface of the ice sheet (Priscu et al. 2013). In this study I use organic and inorganic geochemical measurements of water chemistry to assess the influences of subglacial sources from within the West Antarctic Ice Sheet.

Water column samples and sediment cores WGZ-1 GC3 (70-cm core) and WGZ-1 GC-9 (25-cm core) were collected on January 15, 2015 at the WGZ (84.33543°S, 163.6119°W). The ~10m water column lay under ~680m of ice and was located ~8 km downstream from the marine side of the grounding line of the Whillans Ice Stream (Figure 1.1). The site was ~650 km from the northern edge of the Ross Ice Shelf (Slawek Tulaczyk et al. 2014). Water column samples and sediment cores were retrieved through a ~0.6-m diameter borehole that was created with a microbially clean, hot water drill, then transported frozen to Crary Laboratory at McMurdo Station and eventually to Montana State University for final analysis.

A borehole water treatment system (Priscu et al. 2013) was used to eliminate particles > 0.2 μm in diameter, and reduce the concentration of microbial cells present in the borehole water. Before drilling and sampling, snow feeding the treatment system, inline water at two ports, and borehole water (for hot water drilling) were sampled to be evaluated for stable water isotopes. Inline port samples could have varied because of UV treatment or because of the difference in snow shoveled on different sampling days. The less depleted snow isotope values reflect the source of collection from the ice sheet surface. Borehole isotope samples were the most depleted and could have reflected fractionation due to heating for hot water drilling.

Water Column. Eight discrete hydrocasts using a 10-L Niskin bottle collected seawater between 9 January and 15 January 2015 at 5m from a ~10-m water column and were stored at 4°C until analysis (Vick-Majors et al., in review). Water column samples were decanted into acid-washed low density polyethylene (LDPE) bottles (dissolved N), acid washed fluorinated high-density polyethylene (HDPE) bottles (Thermo Scientific, Nalgene, Waltham, MA) or acid washed and combusted glass bottles (ions, particulate and dissolved organic matter) as was done for Subglacial Lake Whillans (SLW) (Christner et al. 2014).

Sediment Porewater Extraction. Following collection, sediment cores were stored at -20°C for transport to MSU-Bozeman where they were stored until they were processed. The 70-cm sediment core was cut frozen into two sections for sampling. The upper 22-cm sediment core section (2 to 24 cm) was band saw cut frozen in a -5°C class 100 cold room. This section was then placed at ~12°C for ~10 h, which allowed it to thaw completely. The upper 2-cm and lower 1.5-cm of the core section were removed owing to possible contamination that occurred during cutting and handling (Figure 2.2). The remaining 22-cm core was sliced into 2 cm sections (pucks), subsampled with a cookie-cutter type ring and aliquoted with sterile syringes for porosity (5 ml) and other analyses not associated with my thesis. Contamination along the outer circumference of the core was eliminated by removing the outer ~3 mm with the cookie-cutter type ring. Approximately 30 mL of excess overflow pore water was collected in a clean petri dish below the sediment core thawing at ~12°C. The bottom of the sediment core sleeve was not stoppered.

a.

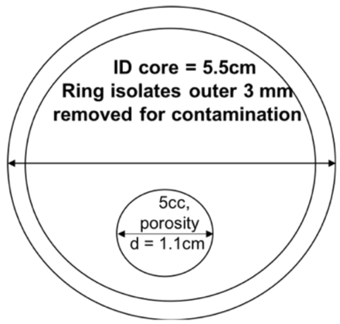

b.

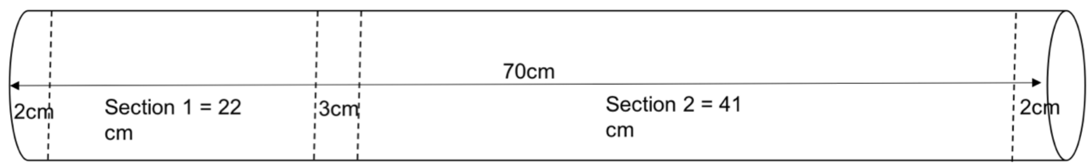

Figure 2.2 a) Aerial cut view of how the 2-cm sediment puck was aliquoted for porosity (5 cc syringe). b) Shows where core was cut frozen into sections and where sediment was removed

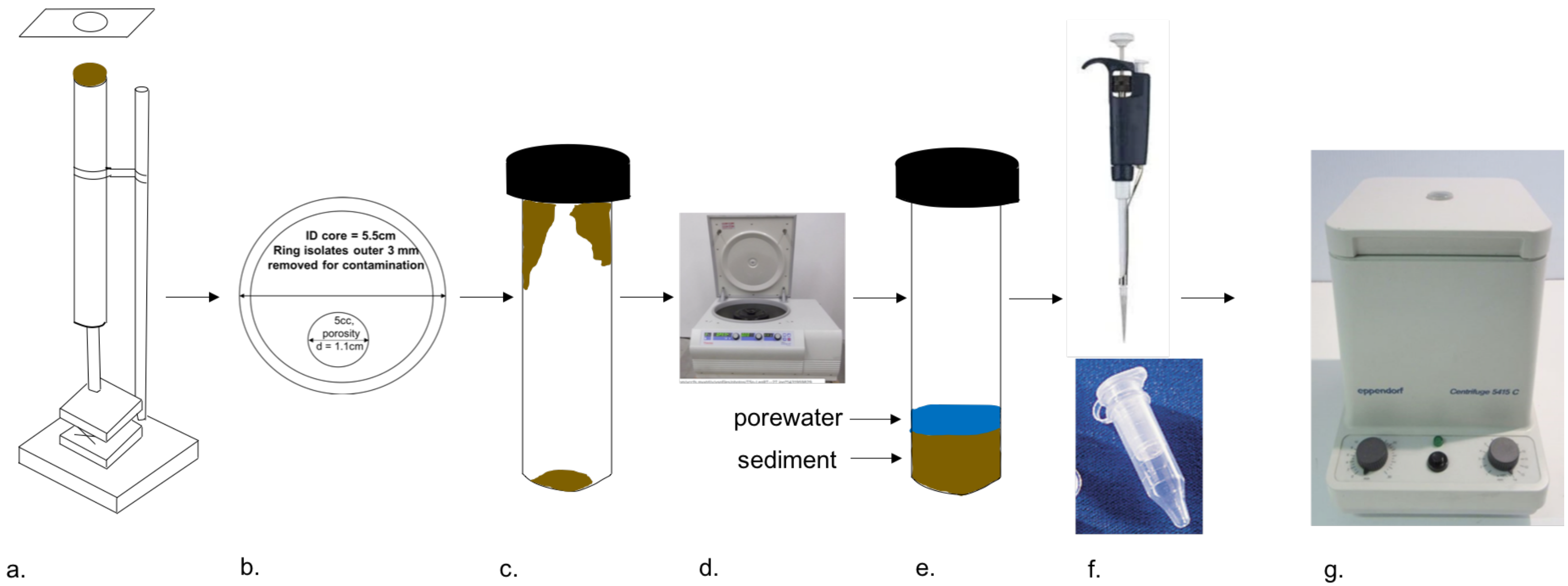

Figure 2. 3 The process above shows the steps of processing the sediment core, from slicing the sediment core to spin filtering porewater.

Sediments were placed in acid washed and milli-Q rinsed 30-mL high strength borosilicate glass vials and placed on ice for 1 to 2 hours (Figure 2.3c). Glass vials containing sediment and porewater were centrifuged in a Sorvall Legend Machlok temperature regulated centrifuge at 4°C and 7,000xg for 10 minutes (Figure 2.3d). The sediment and porewater mixture separated into a porewater and a sediment layer (Figure 2.3e).extract porewater. The porewater fraction was then pipetted into 500 μL low protein binding snap top vials (Figure 2.3f) containing a 0.2 um internal filter membrane (NA #82031-356) and spun for 3 minutes at 10,000xg on an Eppendorf Centrifuge 5415D to remove any residual sediment (Figure 2.3g). The final porewater supernatant from each section was aliquoted and stored separately for dissolved organic carbon, total dissolved nitrogen, $\delta^{18}O$, δD, electrical conductivity, nutrients (ammonia, nitrate and phosphate), and major ions (cations: lithium, sodium, ammonium, potassium, calcium, magnesium; anions: fluoride, acetate, formate, chloride, nitrite, bromide, nitrate, sulfate, phosphate). The deeper core section (41 cm spanning 27 to 68 cm) was thawed for ~8 hours in a ~12°C room and sampled on May 22, 2017. The core was processed according to the aforementioned description used to process the shallow (2 to 24 cm) core section. No overflow water was present as the sediment core we applied a shorter thaw interval prior to slicing the sediment core.

Porosity and Particle Density

A 1 ml (Section 2) or 2 ml (Section 1) sediment plug was extracted using a sterile cut 5 ml syringe and weighed immediately to determine porosity. One sediment plug from each 2 cm sediment puck was placed in a pre-weighed tin boat, combusted for 5 hours at 475°C, cooled in a desiccator, and re-weighed. The water lost, porosity (volume/volume), bulk density and particle density were determined using results from this procedure as shown below. Particle density is adjusted for salt loss by multiplying 0.025 times the mass of water lost and subtracting this from the dry sediment mass.

$$Water\ Lost, g = (Wet\ sediments, g) - (Dry\ sediments, g)$$

$$Porosity\ (\frac{v}{v}) = \frac{(\frac{Water\ Mass, g}{Seawater\ density,\ g\ mL^{-1}})}{(Sediment\ volume, mL)}$$

$$Bulk\ density = \frac{(Dry\ sediment\ mass, g)}{(Sediment\ volume, mL)}$$

$$Particle\ density = \frac{(Dry\ sediment\ mass, g)}{(Volume\ of\ sediment\ solids, mL)}$$

$$Particle\ density, adjusted\ for\ salt\ loss$$

$$= \frac{(Dry\ sediment\ mass, g) - (water\ mass\ lost, g * 0.025)}{(Sediment\ volume, mL) * (1 - porosity)}$$

Porewater Conductivity and Salinity

Following filtering and centrifugation (Figure 2.3f, g), 100 μL of supernatant porewater for conductivity analysis was aliquoted from each sediment puck section into a 200 μL Polymerase Chain Reaction (PCR) tube and stored at 4ºC until further analysis. At the time of analysis, the 100 μL sample was diluted at 1:150 by bringing 0.1 mL of sample up to 15 mL (v/v) with MQ water in clean 20 mL serum vials. Specific conductivity was evaluated with a Hach 3300 conductivity meter, temperature corrected to 25 ºC.

Salinity (‰) was determined using equations described by Poisson (1980) as shown below. Poisson's equation was used because there was a limited amount of sample and dilutions were applied. The Poisson equation corrects for the nonlinearity of seawater conductivity with dilution.

Grain size

WGZ GC-3 sediments from one sample depth, including sediments from 0 to 1.5 cm below the sediment water interface, were analyzed for grain size distribution. Sediments were wet sieved, using stacked 2000 μm and 250 μm sieves, into 250 mL beakers. Two grain size fractions (2000 to >250 μm; ≤250 μm) in solution with water were placed in 50 mL Falcon tubes and brought to the Environmental Analysis Lab (EAL) lab at MSU where they were analyzed for grain size distribution. A Malvern Particle Analyzer was used to determine the grain size distribution of sediments that made up the two size fractions.

Grain Composition

Mineral composition was determined on three sample depths (3, 21, and 32 cm depth) by using the SCINTAG X1 X-Ray Powder Diffraction Spectrometer at the Imaging and Chemical Analysis Laboratory (ICAL) at Montana State University. Samples were dried and sieved with a 0.2 µm sieve prior to analysis. Patterns from 3, 21 and 32 cm depth were analyzed and matched with peaks in the mineralogy peak library at ICAL.

Geochemistry

Water Column. Samples for major ion analysis were taken from hydro casts 1 through 8. Each sample was diluted at 1:150 (v/v) (100 μL sample water brought up to in 15 mL with MQ water) in a 15 mL Falcon tube. Falcon tubes containing the sample solution were vortexed for homogenization. Approximately 4 mL from the prepared 1:150 diluted solution for each cast was processed on a Metrohm Ion Chromatograph (IC). The IC was outfitted with a C6 cation column and an AnSupp5 anion column.

Sediment Porewater. Following centrifugation (Figure 2.3g), a 100 μL porewater supernatant aliquot was transferred to 200 μL Polymerase Chain Reaction (PCR) tube and stored at 4ºC until further analysis. Samples were then diluted 1:150 (100 μL porewater brought to 15 mL total with MQ water). The diluted samples were processed on a Metrohm Ion Chromatograph outfitted with a C6 cation column and an AnSupp5 anion column. For future processing, when working with such small volumes, it is recommended that samples for ions be stored frozen (-20°C) in screw-top vials (similar to those used for isotopes) and to minimize the empty headspace by using the smallest volume vial a sample will fit in.

Diffusion. Vertical gradients of solutes were determined between the porewater concentrations at 0.03 m and the cast (n=8) average sampled at 5 m in the water column. Diffusion flux was as J (g m^{-2} $year^{-1}$) = $\phi * D_s * (\frac{\partial C}{\partial z})$ where ϕ is porosity (v/v) or the fluid filled space, D_s is the bulk sediment diffusion coefficient (m^2 $year^{-1}$) and $(\frac{\partial C}{\partial z})$ is in g m^{-4}. For the purpose of addressing diffusive flux with the data collected, it is assumed that the concentration at 5m is the same as at the water/sediment interface.

The three equations used to determine diffusion flux (tortuosity, bulk sediment diffusion coefficient and diffusive flux) are described below. Tortuosity (τ^2) was determined using $\tau^2 = 1 - A*(\ln(\varphi))$, where A = 2.02 for fine grained clay sediments (Shen and Chen 2007) and the average porosity (φ, unitless where $\frac{volume\ pore\ space, mL}{total\ sediment + pore\ space\ volume, mL}$) is 0.425. Tortuosity is the path of molecular species in the fluid filled pore space in fine-grained unlithified sediments (Shen and Chen 2007; Boudreau 1996). Tortuosity is physically defined as the ratio of the actual distance Δl traveled by the species per unit length Δx of the medium (Shen and Chen 2007).

The bulk sediment diffusion coefficient, D_s (m^2 s^{-1}), can be determined using tortuosity, τ^2, where $D_s = \frac{D_o}{\tau^2}$. The diffusion coefficient, D_o (m^2 s^{-1}), used for chloride (Li and Gregory 1974) and sulfate (Iversen and Jørgensen 1993) were 1.01 x 10^{-5} cm^2 s^{-1} and 0.56 x 10^{-5} cm^2 s^{-1} , respectively. The bulk sediment diffusion coefficient, D_s, was determined according to $D_s = \frac{D_o}{\tau^2}$, where D_o is the diffusion coefficient of the species in question in the fluid filled pore space (Yuan-Hui and Gregory 1974). Bulk sediment diffusion coefficients, D_s, for sulfate and chloride were determined and applied to sediment flux diffusion (Yuan-Hui and Gregory 1974; Iversen and Jørgensen 1993).

Dropstones. Dropstones throughout the sediment core with a long axis greater than 2 cm were measured using calipers.

Isotopes

Water Column. Water (200 µL) from casts 1 through 8 was aliquoted into a 350 µL glass shell insert (Fischer Supelco #24716) and placed in a glass screw top vial (Fischer #03-391-18). Samples were injected with a 5 µL SGE Analytical Science syringe (Fischer #001982) and processed on a Cavity-ringdown Spectrometer (CRDS) L1102-*i* water vapor isotope analyzer from Picarro Inc. (Sunnyvale, CA, USA). The CRDS L1102-*i* measures the $\delta^{18}O$ and $\delta^{2}H$ of water from light absorbance at specific wavelengths at a precision of 0.025‰ and 0.1‰, respectively. Two standards (USGS46, https://isotopes.usgs.gov/lab/referencematerials/USGS46.pdf; USGS48; https://isotopes.usgs.gov/lab/referencematerials/USGS48.pdf) were used to calibrate the instrument. Stable hydrogen and oxygen isotopic compositions are expressed as delta values relative to VSMOW (Vienna Standard Mean Ocean Water). USGS46 has a $\delta^{2}H$ of -235.8‰ and $\delta^{18}O$ of -29.8‰, while USGS48 has a $\delta^{2}H$ of -2.0‰ and a $\delta^{18}O$ of -2.224‰.

A two-component mixing model of $\delta^{18}O$ (H_2O) was used to determine the percentage of glacier melt water and seawater in the WGZ GC3 sediment core porewater (Phillips and Gregg 2001), using SLW column water with an average (3 casts) $\delta^{18}O$ of -38.0‰ (Christner et al. 2014) and the Ice Shelf Water $\delta^{18}O$ of -0.63‰ (Jacobs 2002).

Sediment Porewater. Following centrifugation of the sediment and porewater (Figure 2.2d), the porewater supernatant was pipetted into 0.2 μm, 500 μL VWR Centrifugal modified nylon filter, low protein binding snap top vials (#82031-356) and further (Figure 2.3e), spun for 3 minutes at 10,000xg on an Eppendorf Centrifuge 5415D (Figure 2.3g). Porewater (200 μL) from this final filtration step was pipetted into 200 μL PCR tubes, sealed with parafilm, and stored at 4ºC until processing. Vials were filled as full as possible to minimize isotopic fractionation with atmospheric headspace. Stable isotopes in the samples were analyzed as described above for water column hydrocast samples.

Results

Porosity and Particle Density

Porosity varied from 0.3 to 0.588 throughout the extent of the sediment core yielding an average porosity of 0.425 (Figure 2.4). Neglecting the single sample at 25 cm, porosity is generally constant until it reaches 0.51 at 62 cm.

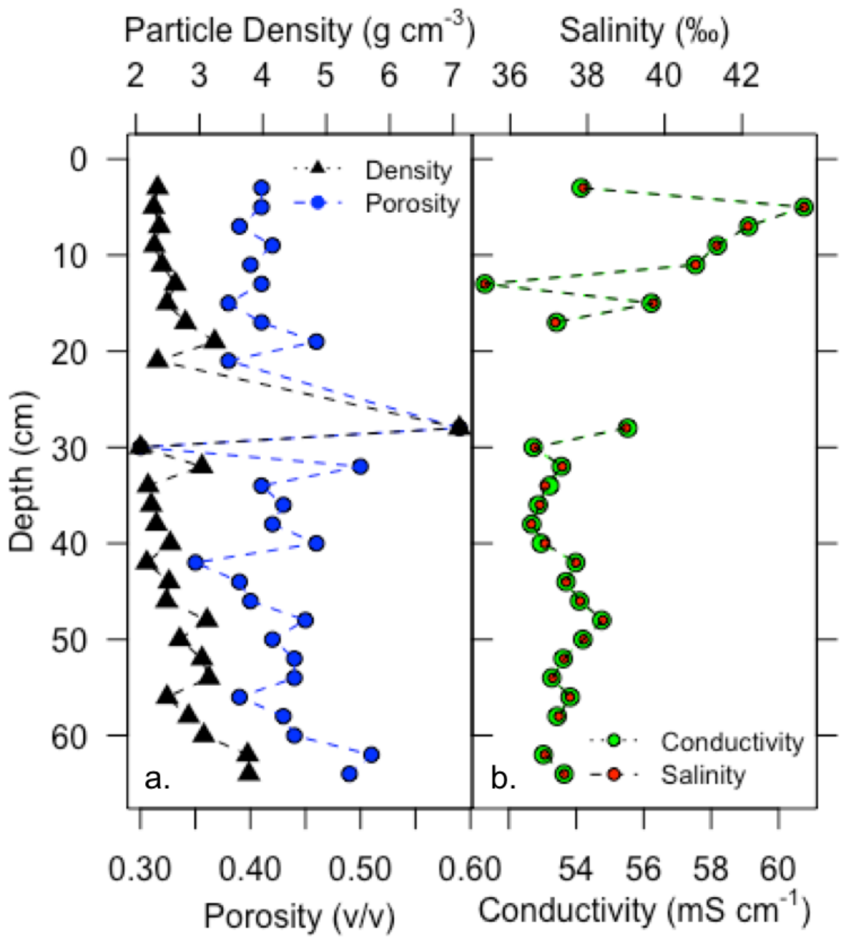

Figure 2. 4 a. Particle density and porosity increase with depth. b. Conductivity and salinity are more variable in the upper core segment and stabilize in the lower core segment.

Porewater Conductivity and Salinity

Salt corrected particle density varies from 2.1 to 3.8 g mL^{-1} throughout the extent of the sediment core (Figure 2.4) with an overall average particle density of 2.7 g mL^{-1}. The section from 3 to 17 cm depth has an average particle density of 2.52 g mL^{-1} and the section from 28 to 62 cm has an average particle density of 2.75 g mL^{-1}. The deep section is 8.4% more dense than the shallow section.

Porewater conductivity varied between 51.3 and 60.7 mS cm^{-1} throughout the GC3 core with a whole core average of 54.4 mS cm^{-1}. The shallow (2-24 cm) part of the core had an average porewater conductivity of 56.3 mS cm^{-1}, whereas the deeper (27-68 cm) part of the core had an average porewater conductivity of 53.6 mS cm^{-1}. On average, the shallow part of the core had a 4.8% higher specific conductivity than the shallow part of the core. Overall, the prevailing vertical trend shows that conductivity decreased with depth, however the upper section appears to have been compromised, while the lower section looks more constant.

Salinity mirrors conductivity because it is based on conductivity data (Poisson 1980). The salinity of the entire core varied between 35.4 and 43.6‰ with an average of 38.1‰. The shallow (2 to 24 cm) part of the core has an average of 39.8‰ and the deep (27 to 68 cm) part of the core has an average of 37.4‰.

Grain Size

Bimodal grain size distribution is present in sediments size fractions ≤ 250 µm (green) and sediments ≤ 2000 µm (blue) in the upper 2 cm of the core (Figure 2.5). The ≤ 250 µm size fraction (green) shows a bimodal distribution with the peaks in percent volume density of between 0.3 and 1.0 µm (maximum 1.3%) and 4.0 and 100.0 µm (maximum 4.4%).

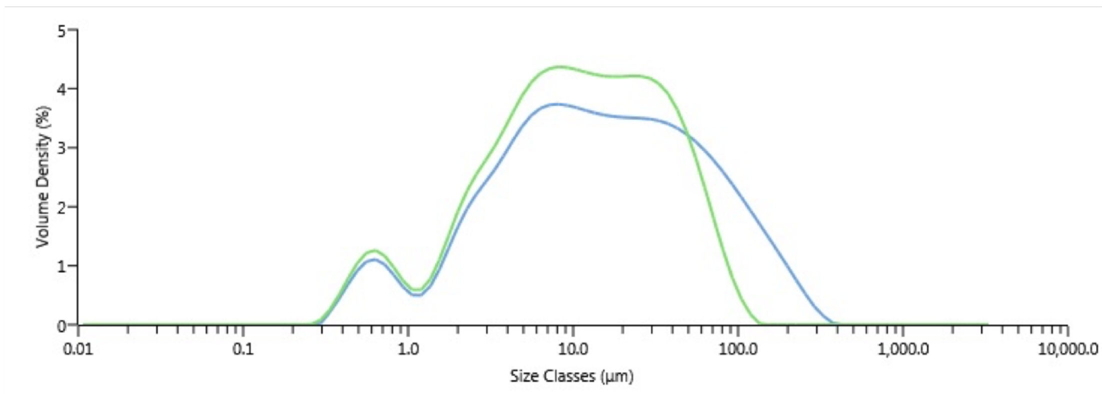

Figure 2.5 The green line shows the bimodal size distribution of sediments from the upper 2 cm of WGZ that was captured with a 250 µm sieve. The blue line shows the size distribution of sediments sieved with a 2000 µm sieve. The y-axis shows volume density (percent) at the x-axis shows size class (µm), or grain size.

Grain Composition

The XRD plot (Figure 2.6) shows combined peaks which indicate the presence of quartz, berlinite and sodium-plagioclase. Plots from 3, 21 and 32 cm depth were analyzed and matched with peaks in the mineralogy peak library. The image (Figure 2.6) at 3 cm shows the sample had quartz, Ca-plagioclase and a phyllosilicate (either muscovite or biotite). At 21 cm (not shown), the sample appeared to have quartz, biotite and plagioclase.

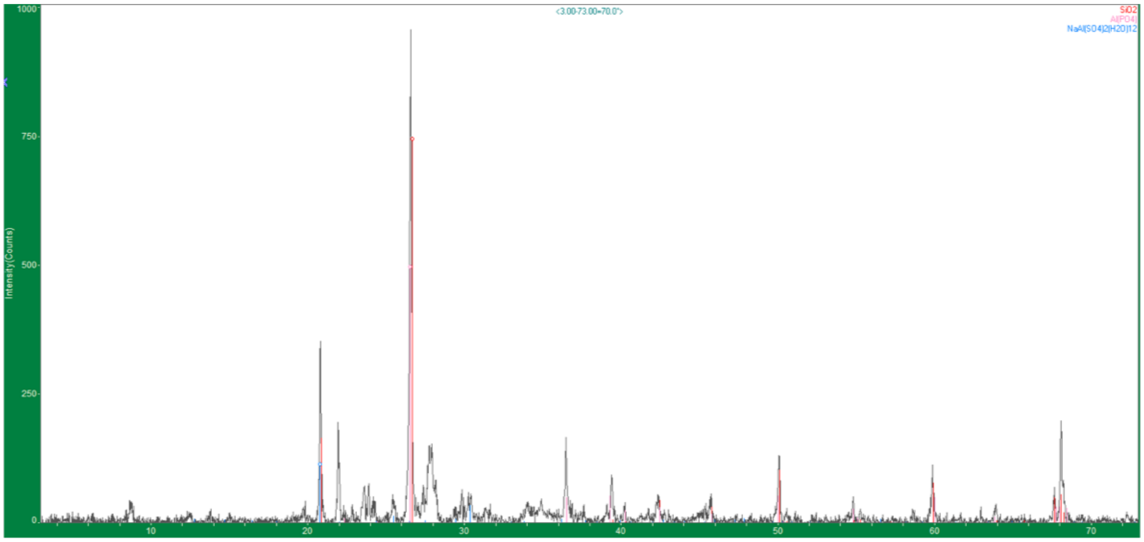

Figure 2.6 XRD chromatograph shows combined peaks from which indicate the presence of quartz, berlinite and sodium-plagioclase. The y-axis shows intensity (counts) and the x-axis shows time (minutes).

Geochemistry

Water Column. The hydrologic flow of sub-ice shelf estuaries is known to be regulated by episodes of high volume, high velocity subglacial flows (Siegfried et al. 2016). These high volume flows could create different geochemical signatures.

Eight hydrocasts were obtained from a mid-water column depth of 5 m (i.e., 5 m below the ice water interface in a 10 m deep water column) from January 10 to January 15, 2015. These samples were collected across a spectrum of tidal cycles (Figure 2.7), which owing to the irregular and intermittently spaced sampling intervals constrained by borehole accessibility, made it difficult to infer specific patterns from the data. Average concentrations for each isotope and ion are displayed on Figure 2.7, but again, the ice shelf cavity is dominated by diurnal tides (Robinson et al. 2010) so conclusions on distinct patterns are difficult to assess. Since seawater essentially has a constant composition of major ions, the major ions mirror each other as tide height increases (and seawater dominates the system) and as tide height decreases (and subglacial freshwater water increases in concentration).

Column water from the WGZ shows a higher percentage of sodium and magnesium than open ocean seawater; WGZ column water shows lower percentages of chloride, sulfate, calcium and potassium compared to open ocean seawater (Table 2.2). Global open seawater chloride concentration is 546 mmol L^{-1}, which is 2.4% below the eight cast chloride average of 559 mmol L^{-1} from the GZ water column. Global surface seawater sodium concentration is 469 mmol L^{-1}, which is 4.9% below the eight cast sodium concentration average of 492 mmol L^{-1} from the GZ water column. Global surface seawater has a sulfate concentrations of 28 mmol L^{-1} (Canfield and Farquhar 2009). As with Cl^- and Na^+, the water column has an eight-cast sulfate average that is lower than this average (26.0 mmol L^{-1}).

Open ocean seawater and WGZ column water ion ratios are compared in Table 2.3. The Na^+/ K^+, Na^+/ Ca^{2+}, and SO_4^{2-}/Cl^- ratios are greater in open ocean water than the WGZ column water; the Mg^{2+}/ Ca^{2+} ratio is the same in open ocean water as it is in the WGZ water column; and the Na^+/ Cl^- ratio is less in open ocean water than it is in the WGZ water column.

Table 2.2 The six major seawater and WGZ column water ion concentrations are shown below. *Average is based on Casts 2 through 8.

Ion	Seawater Concentration (mmol L^{-1})	Percent of Total Ion Composition	WGZ Average* Column Water Concentration (mmol L^{-1})	Percent of Total Ion Composition
Cl^-	546	55.3	537	47.5
Na^+	469	30.7	487	43.1
Mg^{2+}	53	3.69	58	5.1
SO_4^{2-}	28	7.8	26	2.3
Ca^{2+}	10.3	1.2	11.3	1.0
K^+	10.2	1.1	10.7	0.9

Table 1.3 Ion ratios of standard open seawater and WGZ column water (based on average of Casts 2 through 8) at 5 m are shown below.

Ion Ratio	Standard Seawater	WGZ Column Water	WGZ Porewater
Na^+/ K^+	46.0	45.7 ± 6.4	46.0 ± 1.2
Mg^{2+}/ Ca^{2+}	5.1	5.1 ± 0.2	4.6 ± 0.2
Na^+/ Ca^{2+}	46.0	43.0 ± 5.7	41.7 ± 1.6
SO_4^{2-}/Cl^-	0.051	0.049 ± 0.007	0.050 ± 0.002
Na^+/ Cl^-	0.86	0.91 ± 0.12	0.94 ± 0.01

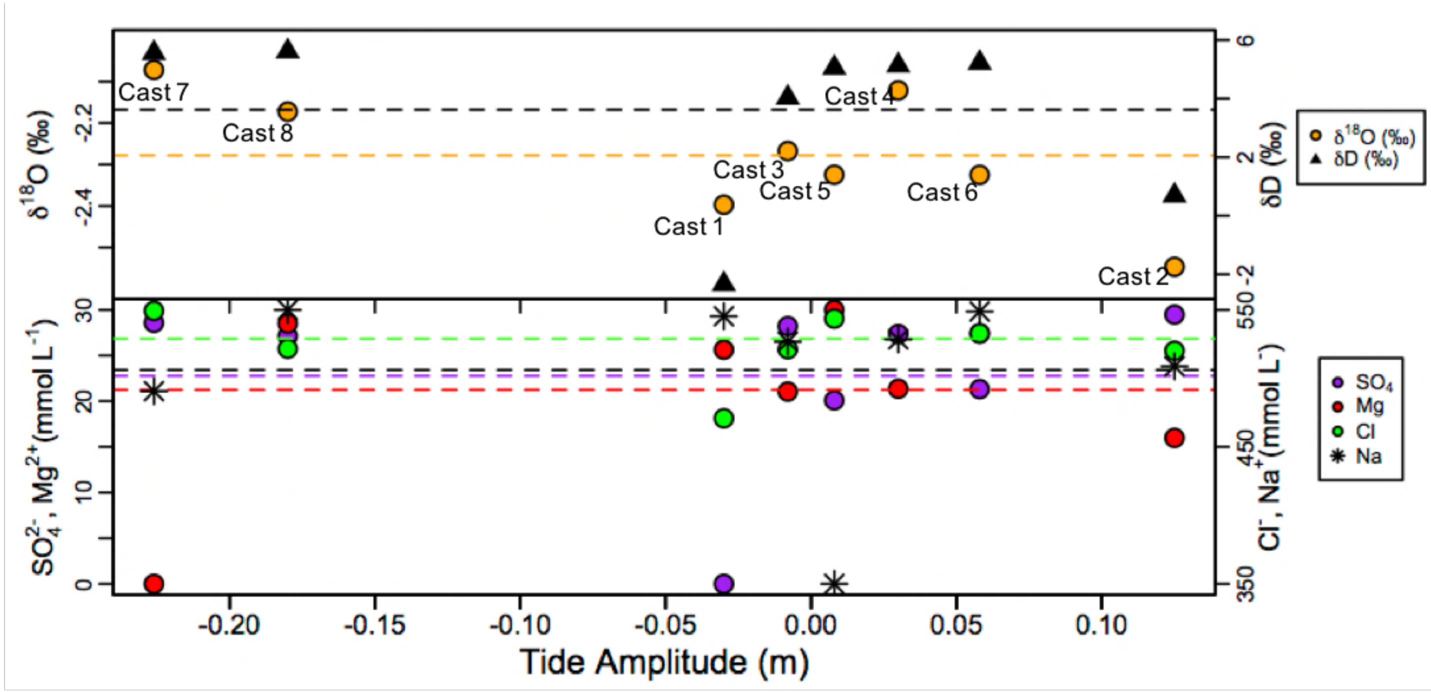

Figure 2.7 Major ion and water stable isotope values across the tidal cycle. Dashed lines indicate averages for each isotope or ion analyzed. Individual samples from January 9 through January 15, 2015 are represented by a dot or asterisk. Eight casts from 5 m, each representing a different part of the tidal cycle are presented.

Sediment Porewater. Chloride concentrations in WGZ range from 517.2 to 672.7 mmol L^{-1}, and have an average ± s.d. of 559.2 ± 38.4 mmol L^{-1} and are more variable above 21 cm (Figure 2.7). Sodium ranges from 478.1 to 618.6 mmol L^{-1} (Figure 2.7) and has an overall sediment porewater average ± s.d. of 522.6 ± 31.3 mmol L^{-1}. Sodium drops to 478 mmol L^{-1} at 13 cm. Sodium has a shallow (3 - 17 cm) core average ± s.d. of 547.4 ± 46.4 mmol L^{-1} and a deep (28 - 64 cm) core average ± s.d. of 510.9 ± 8.7 mmol L^{-1}. As with the other data, values above 21 cm are more variable than those in the deeper sediments.

Sulfate concentrations in the GC3 sediment pore water varied from 26.5 to 34.3 mmol L^{-1} with a whole core average ± s.d. of 29.4 ± 1.5 mmol L^{-1} (Appendix, Table 4.2). The shallow depths (2 to 22 cm) of GC3 had an average ± s.d. of 30.6 ± 2.3 mmol L^{-1} while the deeper part of the core (28 to 68 cm) had an average ± s.d. of 28.8 ± 0.3 mmol L^{-1}. Sulfate concentration shows a decrease at 13 cm (26.5 mmol L^{-1}).

The Na^+/ K^+ ratio in standard seawater (Table 2.3) reveals that the WGZ porewater is 0.7% higher than the WGZ column water ratio. The Mg^{2+}/ Ca^{2+} ratio in standard seawater and the WGZ water column are 10.9% higher than the WGZ Porewater. The SO_4^{2-}/Cl^- ratio is 4.1% higher in standard seawater than it is in the WGZ water column. The Na^+/ Cl^- ratio in WGZ porewater is 9.3% higher than standard seawater and 3.3% higher than the WGZ water column ratios.

Diffusion. Sediment-water interface diffusion flux (J) calculations indicate higher flux for chloride than for sulfate, which were the only ions that showed clear gradients from the surface of the sediment to the water column (Table 2.4).

Table 2.4 Diffusion flux (J, g m^{-2} yr^{-1}) calculations between surficial sediments and the water column at the WGZ indicate a higher rate of diffusion flux for chloride than for sulfate, where the gradient was determined using porewater concentrations between porewater at 0.03 m and the cast (n=8) average sampled at 5 m in the water column. The term Δz is the distance across which flux is determined and D_s is the sediment diffusion coefficient, m^2 s^{-1}).

Ion	**ϕ, Porosity (v/v)**	**ΔConcentration (g m^{-3})**	**Δz (m)**	**D_s (sediment diffusion coefficient, m^2 s^{-1})**	**J, diffusion flux (g m^{-2} $year^{-1}$)**
SO_4^{2-}	0.425	922.13	0.03	2.14E-10	88.20
Cl^-	0.425	739.89	0.03	3.84E-10	126.93

Dropstones. Dropstones with one axis greater than 2 cm are displayed in the sediment core profile (Figure 2.8g). Dropstones in WGZGC3 ranged from 2 to 5 cm along the major axis. The largest dropstones were identified at 30 and 60 cm depth

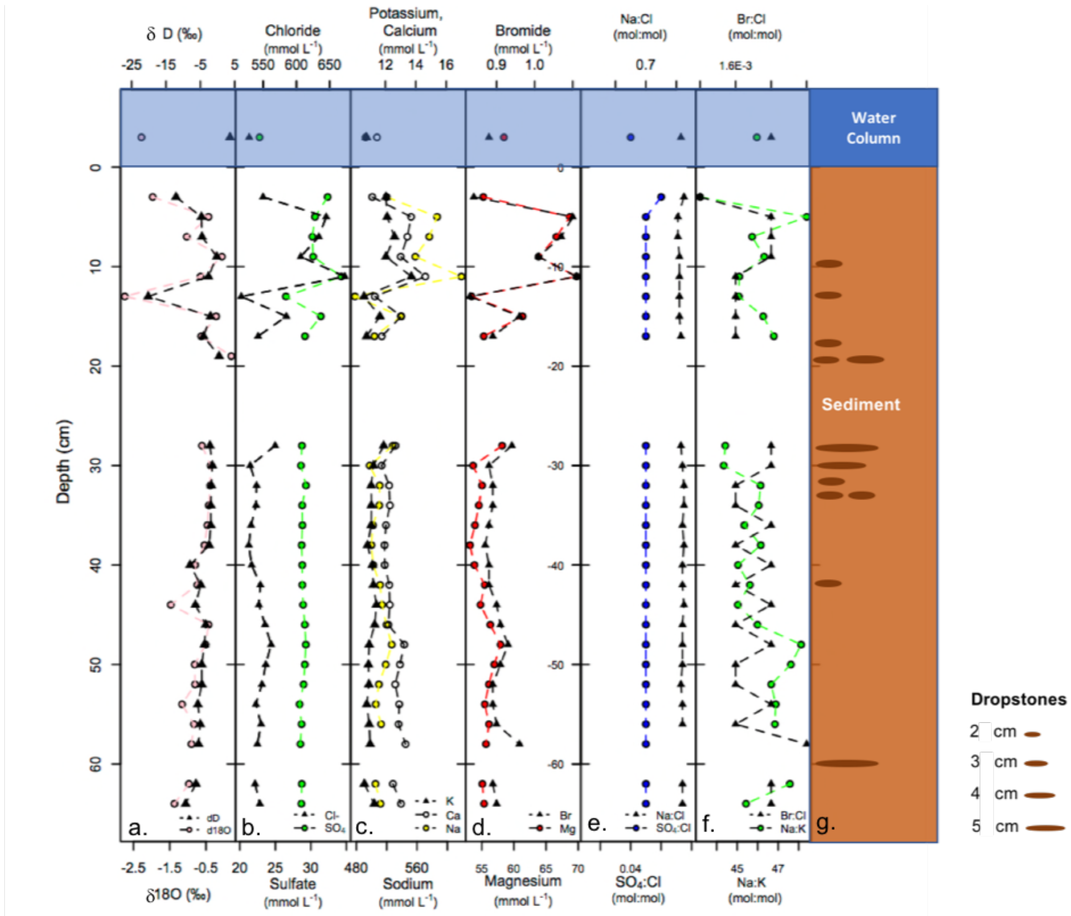

Figure 2.8 Depth profiles of stable isotopes of water and ion profiles in sediment porewater and the mid-depth of the overlying water column at the WGZ. The point in theater column represents the average of 8 casts sampled at 5 m in the 10 m water column from 9 to 16January2015. Dropstones (brown ellipses) with one axis greater than 2 cm are shown in panel g.

Isotopes

Water Column. Prior to sample analysis, the water treatment sterilization system was verified. Water from inline sample ports averaged -32.3‰ and -34.3‰ $\delta^{18}O$ on two sample days (6Jan15; 8Jan15), snow averaged -30.2‰ (7Jan15), and borehole water averaged -36.69‰ (9Jan15) (n=2). For δD, inline sample port averages were -232.8‰ and -245.9‰, snow averaged -203.2‰, and borehole water averaged -265.08‰ (n=2) for the days mentioned above.

Figure 2.7 and Figure 2.10 show the 5 m hydro casts 1 through 8 of stable isotopes sampled at different times associated with different tidal height. Cast 1 appears to show signs of borehole drill contamination. Removing Cast 2, $\delta^{18}O$ concentrations from casts 2 through 8 have a combined average ± s.d. of -2.28 ± 0.16‰. Low tide casts 7 and 8 have a cast average ± s.d. of -2.12 ± 0.07‰. High tide casts 2, 3, 4, 5, and 6 have a cast average ± s.d. of -2.31 ± 0.15‰. For δD, Casts 1 through 8 show an average ± s.d. of 3.62 ± 2.90‰. Excluding cast 1, which shows evidence of contamination, casts 2 through 8 show an average ± s.d. of 4.47 ± 1.75‰ for δD. Low tide casts 7 and 8 have a cast average of 5.58 ± 0.04‰, while high tide casts 2 through 6 have a cast average of 4.03 ± 1.93‰. Due to the depleted signal (more negative values), data for $\delta^{18}O$ shows that it is influenced by glacially fed source.

Using the whole core porewater averages, the two-component mixing model of $\delta^{18}O$ (H_2O) used to determine the percentage of glacier melt water and seawater in the

WGZ GC3 sediment core porewater (Phillips and Gregg 2001) found that the GC3 sediment porewater is composed of 99.6% seawater and 0.4% glacial melt.

Sediment Porewater. $\delta^{18}O$ and δD show similar trends throughout the 70 cm sediment porewater profile (Figures 2.8, Figure 2.9). At 3m depth, $\delta^{18}O$ is -1.93‰, then becomes more depleted in $\delta^{18}O$ at 13 cm at -2.74‰ and again at 44 cm depth (-1.47‰). δD shows a trend similar to $\delta^{18}O$ as δD is -12.1‰ at 3 cm, -20.19‰ at 13 cm, -8.01‰ at 40 cm and -6.45‰ at 44 cm.

The GMWL (Global Meteoric Water Line) is $\delta D = 8\ \delta^{18}O + 10$, while the (Local Meteoric Water Line) LMWL is $\delta D = 6.6\ \delta^{18}O + 0.3$. Deep-subglacial ice upstream of SLW yields a $\delta^{18}O$ of -39.0‰ (Michaud et al. 2016), the SLW water column has a $\delta^{18}O$ of -38.0‰ and the porewater has a $\delta^{18}O$ of -37.5‰ (Christner et al. 2014).

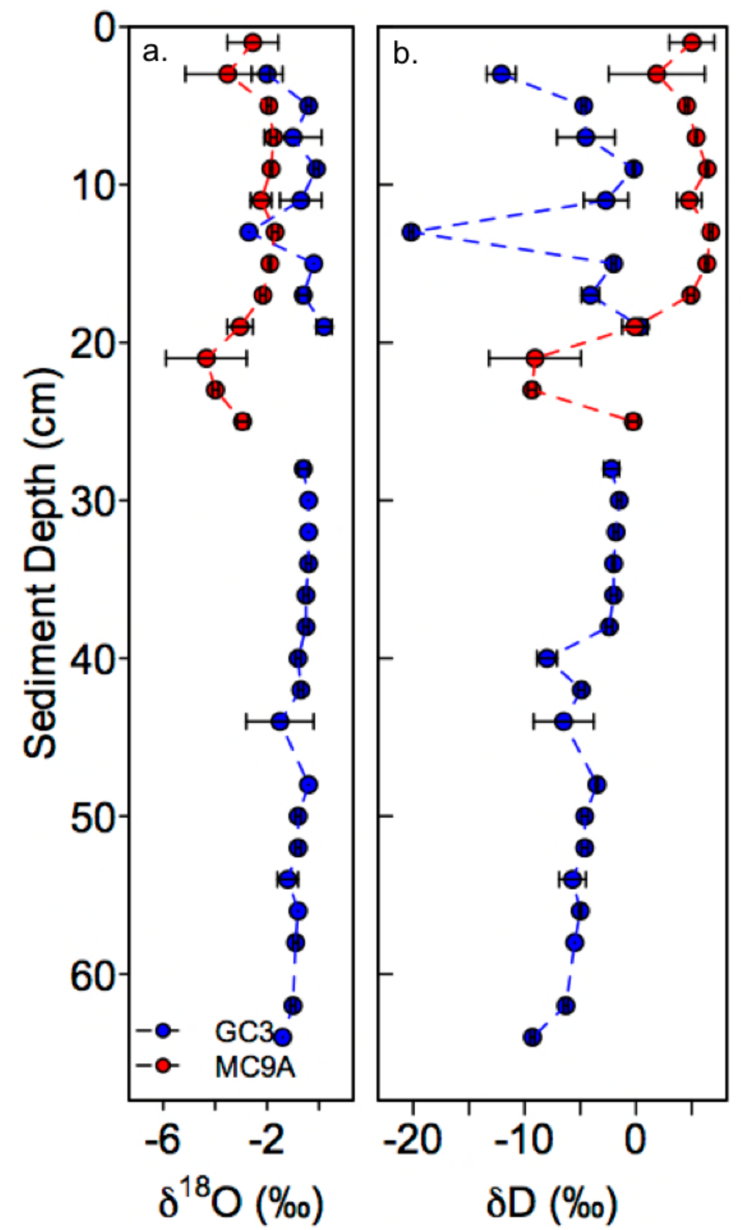

Figure 2.9 (a) Sediment depth profiles of $\delta^{18}O$ and (b) δD from WGZ GC3 and MC9A. Error bars represent standard error (n=3).

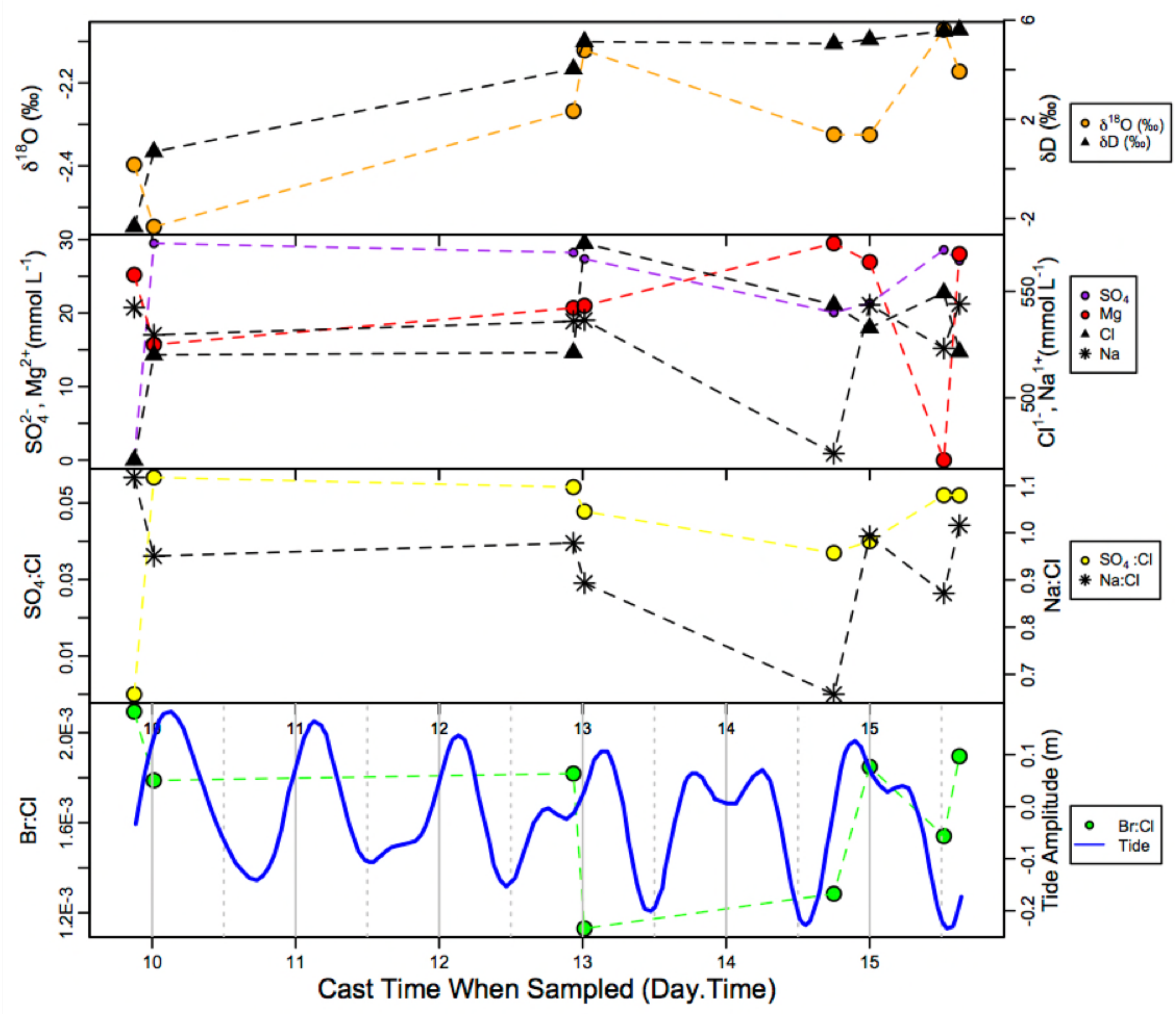

Figure 2.10 Stable isotopes and ion concentrations are on the y-axis and time (from 10Jan2015 to 15Jan2015 and the time of day) is on the x-axis. The blue line in the bottom panel shows tidal amplitude (m) at the borehole where samples were taken. Casts 1 through 8 (represented by points) were taken 5 m below the bottom of the ice. The vertical solid grey lines represent midnight and the short dash grey line represent noon of each day. All casts were sampled at 5 m depth at different times from 9Jan2015 to 16Jan2015. The first sample appears to show more indication of freshwater influence or potential basal ice melt.

Discussion

Porosity and Particle Density

WGZ sediments have an average ± s.d. porosity (v/v) of 0.43 ± 0.05 porosity and show an overall increase in porosity with depth. A series of similar grounding zone wedges, with an average porosity of 0.45, were identified beyond the Ross Ice Shelf, in the Ross Sea (Anandakrishnan et al. 2007). Wedge samples from the Ross Sea indicate that they are composed of diamicton, which can be distinguished from "water washed sub-ice-shelf sediments" (Kamb et al. 2013). Typical clay sized marine sediments in deep sea, open water environments have a porosity of about 0.8 to 0.9 (80% to 90% water content) (McElroy 2007).

With an average particle bulk density of 2.7 g cm^{-3}, WGZ sediments are characterized by a bulk density similar to that of terrestrial tills evaluated in northeast England (Clarke 2008). These tills have bulk densities that range from 2.06 to 2.18 g cm^{-3}. Characterized as glacio-terrestrial deposits, these English tills formed subglacially as lodgement till, deformation till or were deposited from within the ice of a retreating glacier in the form of melt-out or flow till (Clarke 2008).

Porewater Conductivity and Salinity

Porewater conductivity varies from an average of 56.3 mS cm^{-1} in the shallow core section (2 to 24 cm) to an average of 53.6 mS cm^{-1} in the deep core section (27 to 68 cm). The shallow core section (2 to 25 cm) exhibits 4.8% higher average concentrations than the deep core section (28 to 68 cm). This shows that the WGZ GC3 sediment core is predominantly marine with a greater seawater influence in the shallow section (2 to 24 cm) compared to the deeper core section (27 to 68 cm), or that conductivity results from the upper section were compromised.

Vick-Majors et al. (2016) profiled salinity, temperature, current velocity and current direction to characterize water layers from the surface of the MIS to 900 m depth. From the surface to 95 m depth, the Antarctic Surface Water is characterized by warmer, less saline water represented by Antarctic Surface Water (AASW). The Intermediate Shelf Water (ISW), from 95 to 315 m depth, is characterized by a colder layer (-1.90°C to -1.93°C) of intermediate salinity from and the water deeper than 315 m, the modified High Salinity Shelf Water (mHSSW), is characterized by more moderate temperatures (-1.88°C to -1.90°C) and higher salinities (34.66-34.76).

My data shows that the average porewater in WGZ GC3 had 11% greater salinity than the average of the first 95 m of the water column beneath the MIS. Perhaps multiple transgressions, or rises in global seawater, has concentrated salts in the upper 22 cm compared to the deeper section of the sediment core, which could be more influenced by a freshwater source. Another possibility is that conductivity results from the upper section were compromised. There is variation between sediment porewater and water column conductivity from different parts of the Ross Ice Shelf cavity. Without further investigation of sediment porewater and the water column in the Ross Ice Shelf cavity a simple conclusion remains elusive.

Conductivity and salinity are hypothesized to vary as a function of basal ice melt influence, and tidal height in the water column. In low-latitude estuaries, seawater has a greater influence at high tide and freshwater generally has a greater influence in the water column at low tides. However, this pattern is not clearly evident from the eight casts collected in the WGZ water column (Figure 2.10) due to the inconsistent sampling interval. Since the hydrologic flow of high latitude estuaries under the ice shelf are known to be regulated by episodes of high volume, high velocity flows, sub-shelf waters probably experience stages of intense mixing of seawater ions followed by a re-stratification of layers.

While there were a limited number of samples available to characterize the sub-ice shelf estuary region on the Siple Coast, well-studied estuaries (Cloern et al. 2017) at lower latitudes serve as proxies to help characterize physical and geochemical parameters that exist at the WGZ. Physical dynamics, including the structure of the salinity gradient, estuarine circulation, transport time scales, and stratification, are determined by the variability of freshwater inflow. While salinity has been used as a frame of reference for understanding spatial structure since the beginning of estuary science (Stefánsson and Richards 1963), it can aide in understanding how physical and geochemical parameters interact with each other under the Ross Ice Shelf.

Grain Size

The majority of the sediment core was dominated by grain size fractions between 0.2 and 400 μm (Figure 2.5). Dropstones greater than 2 cm appeared to be randomly distributed throughout the sediment core. The proximity to the coast and the lack of observable features evident to the unaided eye suggests that sediments are not impacted by the effects of bioturbation (Burdige 2006). Sediments displayed a homogenous stratigraphic depositional sequence that were void of deformation and/or structures that could be caused by burrowing, bioturbation, or bio-irrigation, however further investigation is discussed in association with porosity (Burdige 2006; Hemer et al. 2007).

Grain Composition

XRD suggests that mineralogy from the three sampled depths is dominated by quartz, Ca-plagioclase and a phyllosilicate. These mineral assemblage suggests a clay dominated sediment as was observed at SLW (Michaud et al. 2016).

<u>Geochemistry</u>

<u>Water Column.</u> The variability in water column ion concentration shown in Figure 2.11 suggests that they could be associated with the diurnal tide influence, but samples were not collected at consistent intervals from which a definitive conclusion could be made. Sampling at consistent time intervals over longer intervals, such as the 13.66-day tidal phase shift cycle (Robinson et al. 2010), would help to better constrain the variability of ion concentration in the seawater cavity with respect to tides. Further sampling is needed to show (Figure 2.7, Figure 2.10) that the concentration over the eight hydrocasts collected at 5 m in the WGZ water column can be correlated with ebb and neap tides.

Figure 2.11 shows the distribution of the percentage of $Na^+ + K^+$, Ca^{2+} and Mg^{2+} on the ternary diagram. Expanded plots of WGZ-GC3 porewater (green cross), SLW porewater (black circle) and WGZ water from the water column (red triangle) show that WGZ porewater and WGZ column water are most similar in their geochemical ion distribution. WGZ porewaters show an average of 88.4% $Na^+ + K^+$, 9.5% Ca^{2+} and 2.1% Mg^{2+}, while the eight cast water column average at the WGZ shows 87.7% $Na^+ + K^+$, 10.3% Ca^{2+} and 2.0% Mg^{2+}. Porewater from SLW shows a higher concentration of sodium plus potassium at 92.6%, a higher concentration of magnesium at 3.8% and a lower concentration of calcium at 3.6%. The WGZ porewater and water column is ~2.6 to 2.9 times more concentrated in calcium than sediment porewater at SLW. The average magnesium concentration in SLW porewater is 1.8 to 1.9 times greater than the average magnesium concentration in WGZ porewater or column water.

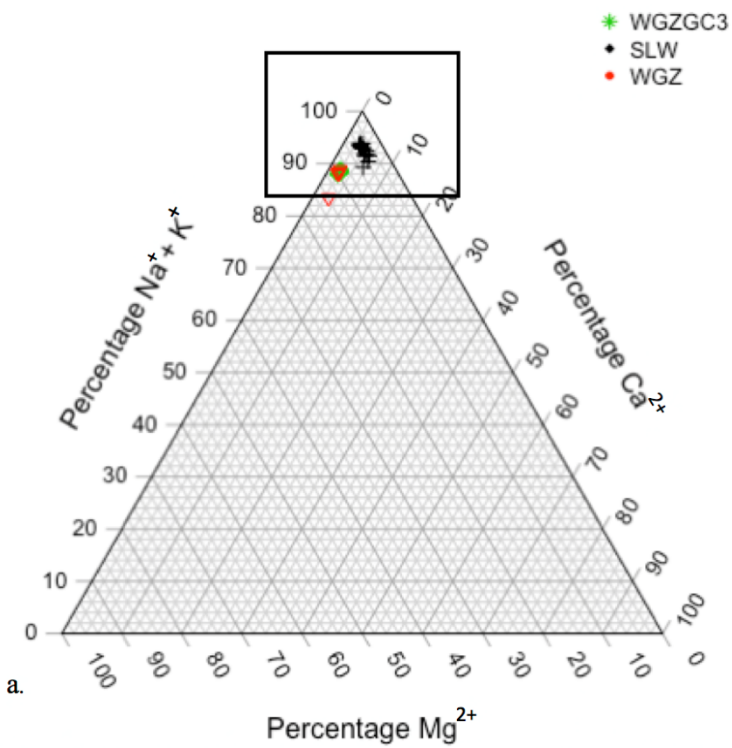

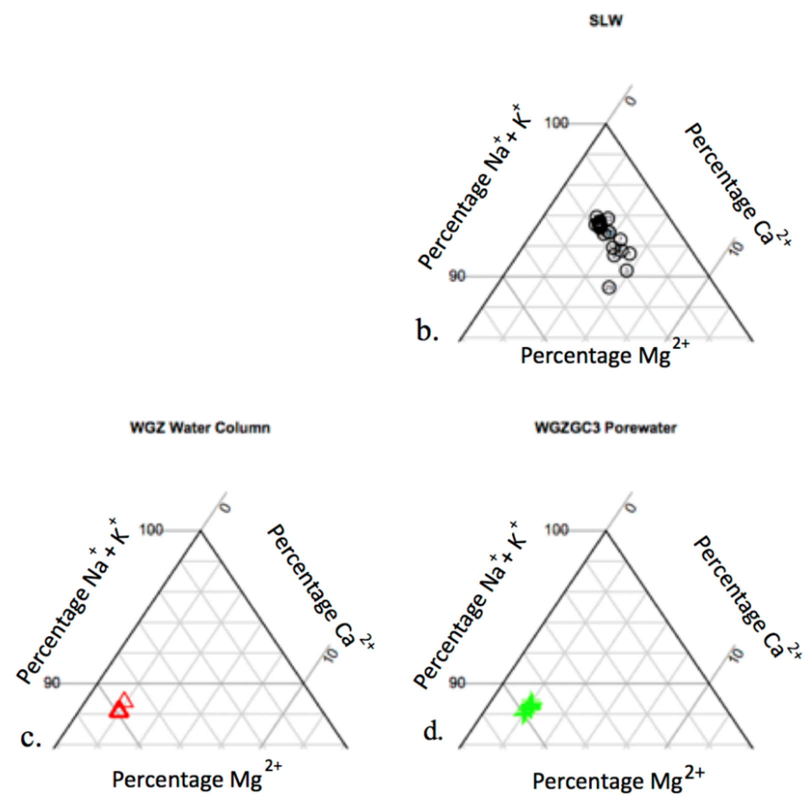

Figure 2.11 a) Shows a ternary geochemical plot with the combined percentage of Na^{+}+K^{+}, Ca^{2+} and Mg^{2+} on three separate axes. The black box shows the frame for the zoomed in frame of b) SLW, c) WGZ Water Column and d) WGZ GC3.

The WGZ column water was sampled immediately following the drilling and reaming of the borehole. As a result, Cast 1 could contain a greater influence of drill water or basal ice melt, both of which would indicate a freshwater signal (Figure 2.7; Figure 2.10). Cast 1 shows a distinct difference in geochemical concentration compared to Casts 2-8. Cast 1 shows lower concentrations of chloride and sulfate but does not appear to show a decreased concentration in sodium and magnesium.

Sediment Porewater. Porewater ion geochemistry at the WGZ (Figure 2.8) shows decreases in major marine ion concentrations, most abruptly at 13, but also at 40 cm. These are thought to be locations where greater subglacial influence permeates the core, thus decreasing the concentration of dominant marine ions. Evidence of geochemical signals sourced by freshwater sources is present at 13 cm and at 40 cm.

Scambos (2017) hypothesized that the WGZ porewater and sediment data are hydrologically influenced by subglacial discharge, sourced by an upstream hydrologic network. Previously analyzed features thought to influence the Whillans Ice Stream (WIS) include the: Kamb Ice Stream (KIS), Bindschladler Ice Stream (BIS), SLW and the Ross Ice Shelf (RIS) (Clough and Hansen 1979).

In SLW, the dominant cation from column and sediment porewater is sodium. The seawater component of total solute in SLW sediment pore water increases from 57% in the column water to 77% at 37 cm. Total solution concentrations are ~13 meq L^{-1} and ~67 meq L^{-1}, respectively (Michaud et al. 2016). Subglacial waters beneath Casey Station, on the East Antarctic Ice Sheet, also show evidence of geochemical influence where waters are 34% seawater solute and total solute concentration is 3.5 meq L^{-1} (Goodwin 1988). Goodwin (Goodwin 1988) suggested that the type and concentrations of chemical species found in the jökulhlaup waters in East Antarctica indicate that the source of enrichment is the weathering of geological materials**.** Although Casey Station is located on the other side of Antarctica, this was one of the earliest instances in which subglacial geochemistry was analyzed.

Only about 3% of the solute is of marine origin (Skidmore et al. 2010) indicating that the subglacial environments beneath the Bindschladler and Kamb Ice Streams are not heavily influenced by seawater. In contrast, SLW pore water chloride, sulfate and sodium display the linear profiles that increase in concentration with depth (Michaud et al. 2016). An estimate of seawater contribution to SLW water was made using Cl^{-}:Br^{-} ratios. It has been suggested that the seawater signature is the result of ancestral marine transgressions where widespread seawater inundation and marine sediment deposition occurred on the Siple Coast (Scherer et al. 1998; Studinger et al. 2001).

Historically, the ratio between alkali (Na^{+} + K^{+}) and alkaline-earth (Ca^{2+} + Mg^{2+}) content has been applied as an indicator of the subglacial terrain and the processes controlling the solute enrichment of associated waters (Emerson and Hedges 2008). In March 1985, a 6 month long jökulhlaup event at Casey Station, Law Dome, Antarctica took place, marking the first documented observation of a subglacial outburst of water in Antarctica (Goodwin 1988; Lewis et al. 2006). This was a unique event as it was the first documented evidence of hydrologically charged water being released on the continent of Antarctica (Goodwin 1988). During the winter of 1985, the (Na^{+} + K^{+})/(Ca^{2+} + Mg^{2+}) in the jökulhlaup (Sample JA) was 26.88 meq L^{-1} while the value (Sample JB) was 24.61 meq L^{-1} in the spring of 1985 (Goodwin 1988). Jökulhlaup Samples JA and JB were found to be 12 times higher than values for the Cape Folger glacier ice (south of Casey Station on Siple Coast) and jökulhlaup waters were characterized by high concentrations of total solute load with a dominant enrichment in alkalis (Goodwin 1988). The ratio value increase has been attributed to the advanced monovalent/divalent separation of cationic species where ion exchange allows the water to exchange divalent ions (Ca^{2+}, Mg^{2+}) for monovalent ions (Na^+, K^+) with clay minerals, thus increasing the Na^+ and K^+ content of the melt water (Goodwin 1988).

Long water residence times in porewater permit the dissolution of minerals and production of greater amounts of crustal-derived Na^+ and K^+ to subglacial waters (Wadham et al. 2010). Given that SLW contains a higher concentration of Na^+ and K^+ than the WGZ, it is likely that the grounding zone would reflect higher concentrations of these ions as a potential result of subglacial flow.

Understanding sub-ice shelf and ice stream flow enables researchers to better understand and quantify the episodic and long-term flow patterns and how they could impact ice-sheet stability. Although daily and seasonal flow patterns have not been identified in subglacial flow on the Ross Sea, episodic drainage cycles have been described (Carter and Fricker 2012; Siegfried et al. 2016). Given the location of the WGZ to the outflow stream from SLW (Siegfried et al. 2016), subglacial freshwater can influence the Ross Ice Sheet marine cavity through direct advective input or via diffusion from the marine sediment to the water column.

Diffusion. Given a porosity of 0.425 (v/v) in WGZ GC3, diffusive flux was calculated for sulfate and chloride with sediment diffusion coefficients of 2.14 x 10^{-10} m^2 s^{-1} and 3.84 x 10^{-10} m^2 s^{-1}, respectively (Table 2.4). This resulted in a diffusion flux for sulfate and chloride of 88. 20 g m^{-2} yr^{-1} and 126.93 g m^{-2} yr^{-1}, respectively. In nanofossil ooze-chalks from the Indian Ocean seafloor with a porosity of only 25% and water content of 11%, Manheim and Waterman (1974) determined a diffusion coefficient of 3.4 x 10^{-10} m^2 s^{-1} for seafloor surficial sediments and 2.9 x 10^{-10} m^2 s^{-1} for sediments at 486 m deep.

Isotopes

Water Column. Endmember water isotope sources (δD, $\delta^{18}O$) can be used to determine the source water variation in porewater geochemistry throughout the extent of the sediment column porewater profile. Advection, diffusion and mixing of water masses from different source areas strongly affects the baseline $\delta^{18}O$ composition. Since there is no evaporation or precipitation in the subsurface, $\delta^{18}O$ can be used as a conservative tracer for transport and mixing of water masses in the subsurface ocean.

The two-component mixing model of $\delta^{18}O$ (H_2O) showed models do not determine that the percentage of glacier melt water and seawater in the WGZ GC3 sediment core porewater (Phillips and Gregg 2001) was composed of 99.6% seawater and 0.4% glacial melt. The model results shows that, for the whole core averages of δD and $\delta^{18}O$, there is subglacial freshwater influence at the WGZ. Although a two-component model provides a general idea of source analysis, if Ross Ice Shelf basal ice was available, a three-component model would create a more realistic system model.

Sediment Porewater. Subglacial water from freshwater sources show a more depleted isotopic signature compared to seawater. More depleted signatures are associated with subglacial sources of freshwater sourced by glacial meltwater. Condensation preferentially removes the heavier isotope (O^{18} or H^3) and makes the δD or $\delta^{18}O$ more negative. During evaporation, ^{16}O is released preferentially, creating a positive $\delta^{18}O$ or δD signature. δD shows signs of depletion at -20.19‰ at 13 cm, -8.01‰ at 40 cm, and -5.74‰ at 54 cm. Substantial differences exist in stable water isotopes between the WGZ (Figure 2.11a) and SLW (Figure 2.11b). Deuterium for GC3 has an average ± s.d. of -5.6 ± 6.6‰ (coefficient of variation, CV = -118.2%) while MC9A has an average ± s.d. of 4.5 ± 2.3‰ (CV= 49.9%). To determine whether, porewater from both sediment cores is sourced by the *same two underlying populations that have the same mean,* a t-test is applied. Using a paired t-test, there is 0.34% probability that both data sets came from the same source that have the same mean. A homoscedastic t-test yields a 0.05% probability that both data sets came from the same source that have the same mean.

Oxygen-18 also shows substantial differences between porewater from the two sediment cores. GC3 has an average ± s.d. of -0.84 ±0.95‰, and a CV of -113.7% while MC9A has an average ± s.d of -2.2 ± 0.6‰ and a CV of -28.5%. Using a paired t-test, there is 0.6% probability that both data sets came from the same source that have the same mean. A homoscedastic t-test yields a 0.2% probability that both data sets came from the same source that have the same mean.

Potential sources of error due to variation between porewater from both cores could be due to subsurface spatial heterogeneity, variation in sampling technique (gravity versus multi-coring), porewater extraction (rhizon versus slice and centrifugation method), thaw wait time prior to extraction, the impact due to the distribution of dropstones and potential repeated sediment sampling in the same borehole.

The equation for the WGZ porewater LMWL regression line is $\delta D = 6.5\ \delta^{18}O + 0.3$ (r^2=1) and the equation for the SLW porewater LMWL regression line is by $\delta D = 7.7\ \delta^{18}O - 8.5$ (r^2=1; Figure 2.12). The high correlation coefficient for the GMWL, $\delta D = 8\ \delta^{18}O + 10$ ($r^2 = 1$), shows that oxygen and hydrogen stable isotopes are closely related; as a result, isotopic ratios and fractionations of the two elements are usually discussed together (Kendall et al. 2004).

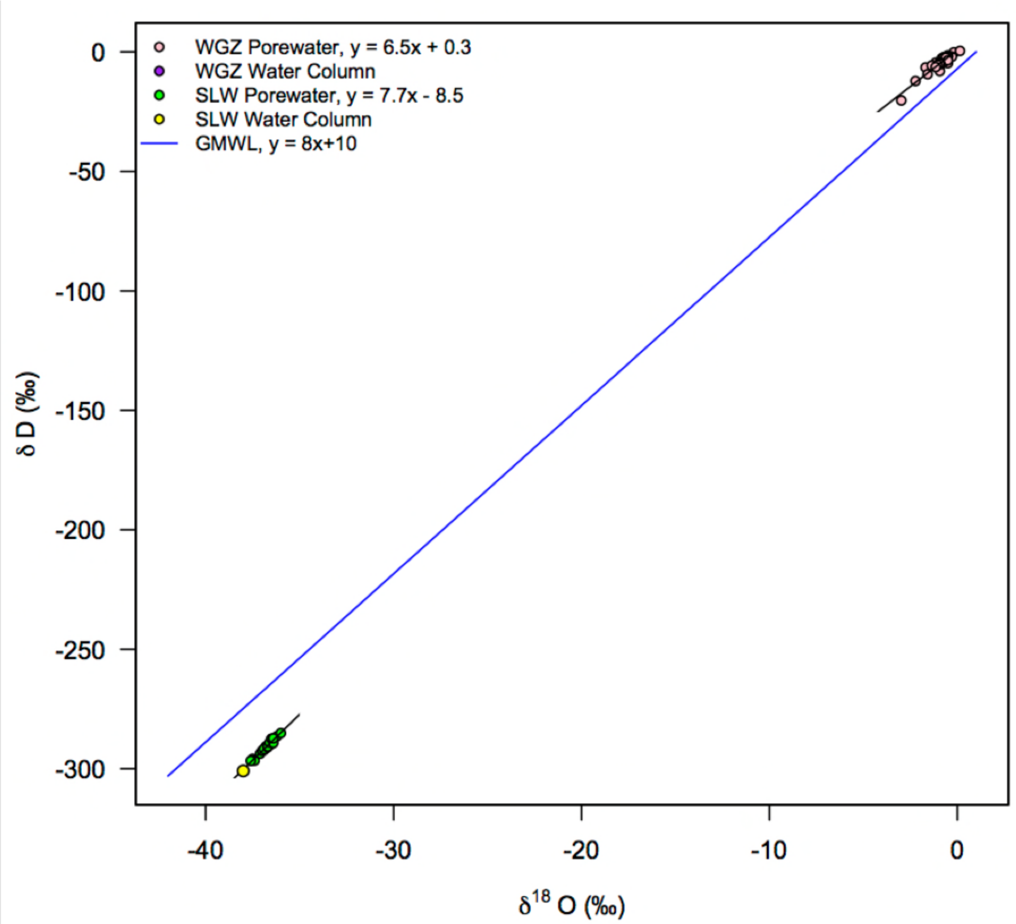

Figure 2.12 Figure 2.15 shows the Ground Meteoric Water Line (GMWL), $\delta D = 8\ \delta^{18}O + 10$, compared to the WGZ porewater (pink dots clustered at upper right) and SLW porewater (green dots clustered at lower left) Local Meteoric Water Lines (LMWL) represented by the regression lines for WGZ and SLW porewater. The GMWL (blue line), $\delta D = 8\ \delta^{18}O + 10$, compared to the WGZ (clustered at upper right) and SLW (clustered at lower left) LMWL represented by the regression lines for WGZ and SLW porewater. The WGZ LMWL is $\delta D = 6.5\ \delta^{18}O + 0.3$ and the SLW LMWL is $\delta D = 7.7\ \delta^{18}O - 8.5$. The high correlation coefficient ($r^2 = 1$) shows that oxygen and hydrogen stable isotopes are closely related; as a result, isotopic ratios and fractionations of the two elements are usually discussed together (Kendall et al., 2004).

Conclusion

Hypothesis 1: Based on the variation that is observed throughout the extent of the 70 cm sediment porewater, I accept H1 *Porewater geochemical data shows that the source of porewater is subglacially-influenced*, with a caveat. Although there is geochemical and isotopic evidence of subglacially influenced, freshwater melt from the WAIS at 13 and 40 cm, two sample depths across 70 cm in a single sediment core is not sufficient to definitively ascribe the variation being sourced by freshwater.

Hypothesis 2, *Sediments and porewaters are enriched in geochemical concentrations with respect to the overlying water column*, is supported by the data but requires clarification. The concentration of the ions chloride and sulfate show the greatest evidence of diffusion across the sediment-porewater boundary into the water column. Although this trend is not consistent across all of the ions, the hypothesis can be accepted for sulfate and chloride, but deserves further analysis at a location closer to the actual grounding zone.

Bibliography

Anandakrishnan, S., Catania, G. A., Alley, R. B., & Horgan, H. J. (2007). Discovery of Till Deposition at the Grounding Line of Whillans Ice Stream. *Science*, *315*, 1835–1838. https://doi.org/10.1126/science.1138393

Anderson, S. P., Drever, J. I., & Humphrey, N. F. (1997). Chemical weathering in glacial environments. *Geology*, *25*(5), 399–402. https://doi.org/10.1130/0091-7613(1997)025<0399:CWIGE>2.3.CO

Boudreau, B. (1996). The diffusive tortuosity of fine-grained unlithified sediments. *Geochimica et Cosmochimica Acta*, *60*(16), 3139–3142. https://doi.org/10.1016/0016-7037(96)00158-5

Boyd, E. S., Lange, R. K., Mitchell, A. C., Havig, J. R., Hamilton, T. L., Lafrenière, M. J., … Skidmore, M. (2011). Diversity, abundance, and potential activity of nitrifying and nitrate-reducing microbial assemblages in a subglacial ecosystem. *Applied and Environmental Microbiology*, *77*(14), 4778–4787. https://doi.org/10.1128/AEM.00376-11

Burdige, D. (2006). *Geochemistry of Marine Sediments*. Princeton, N.J.: Princeton University Press.

Canfield, D. E., & Farquhar, J. (2009). Animal evolution, bioturbation, and the sulfate concentration of the oceans. *PNAS*, *106*(20), 8123–8127. Retrieved from www.pnas.org/cgi/content/full/

Carter, S., & Fricker, H. (2012). The supply of subglacial meltwater to the grounding line of the Siple Coast, West Antarctica. *Annals of Glaciology*, *53*(60), 267–280. https://doi.org/10.3189/2012AoG60A119

Catania, G. (2004). *Dynamic History of the Kamb Ice Stream, West Antarctica: Controls on streaming behavior and ice stream shutdown*. University of Washington.

Christner, B. C., Priscu, J. C., Achberger, A. M., Barbante, C., Carter, S. P., Christianson, K., … Purcell, A. (2014). A microbial ecosystem beneath the West Antarctic ice sheet. *Nature*, *512*(7514), 310–313. https://doi.org/10.1038/nature13667

Clarke, B. (2008). Physical characteristics of subglacial tills. *Géotechniques*, *58*(1), 67–76. https://doi.org/10.1680/geot.2008.58.1.67]67

Cloern, J. E., Jassby, A. D., Schraga, T. S., Nejad, E., & Martin, C. (2017). Ecosystem variability along the estuarine salinity gradient: Examples from long-term study of San Francisco Bay. *Limnology and Oceanography*, *62*(S1), S272–S291. https://doi.org/10.1002/lno.10537

Clough, J. W., & Hansen, B. L. (1979). The Ross Ice Shelf Project. *Science*, *203*(4379), 433–434.

Craig, H., & Gordon, L. (1965). *Deuterium and oxygen 18 variations in the ocean and the marine atmosphere*. *Stable Isotopes in Oceanographic Studies and Paleotemperatures*.

Emerson, S., & Hedges, J. (2008). *Chemical Oceanography and the Marine Carbon Cycle*. New York.

Epstein, S., & Mayeda, T. (1953). Variation of O^{18} content of waters from natural sources. *Geochimica et Cosmochimica Acta*, *4*(5), 213–224. https://doi.org/10.1016/0016-7037(53)90051-9

Gaidos, E., Lanoil, B., Thorsteinsson, T., Graham, A., Skidmore, M., Han, S., … Popp, B. (2004). A Viable Microbial Community in a Subglacial Volcanic Crater Lake, Iceland. *Astrobiology*, *4*(3), 327–344. https://doi.org/10.1089/ast.2004.4.327

Goodwin, I. D. (1988). The nature and origin of a jokulhlaup near Casey Station, Antarctica. *Journal of Glaciology*, *34*(116), 95–101. https://doi.org/10.1017/S0022143000009114

Gooseff, M. N., Lyons, W. B., McKnight, D. M., Vaughn, B. H., Fountain, A. G., & Dowling, C. (2006). A Stable Isotopic Investigation of a Polar Desert Hydrologic System, McMurdo Dry Valleys, Antarctica. *Arctic, Antarctic, and Alpine Research*, *38*(1), 60–71. https://doi.org/10.1657/1523-0430(2006)038[0060:ASIIOA]2.0.CO;2

Gordon, D. A., Priscu, J., & Giovannoni, S. (2000). Origin and Phylogeny of Microbes Living in Permanent Antarctic Lake Ice. *Microbial Ecology*, *39*(3), 197–202. https://doi.org/10.1007/s002480000016

Hemer, M. A., Post, A. L., O'Brien, P. E., & Craven, M. (2007). Sedimentological signatures of the sub-Amery Ice Shelf circulation. *Antarctic Science*, *19*(4), 497–506. https://doi.org/10.1017/S0954102007000697

Hoefs, J. (2015). *Stable Isotope Geochemistry*. https://doi.org/10.1007/978-3-319-19716-6

Iversen, N., & Jørgensen, B. B. (1993). Diffusion coefficients of sulfate and methane in marine sediments: Influence of porosity. *Geochimica et Cosmochimica Acta*, *57*(3), 571–578. https://doi.org/10.1016/0016-7037(93)90368-7

Jacobs, S. S. (2002). Freshening of the Ross Sea During the Late 20th Century. *Science*, *297*(5580), 386–389. https://doi.org/10.1126/science.1069574

Jouzel, J., Merlivat, L., & Lorius, C. (1982). Deuterium excess in an East Antarctic ice core suggests higher relative humidity at the oceanic surface during the last glacial maximum. *Nature*, *299*(5885), 688–691. https://doi.org/10.1038/299688a0

Kamb, B. (2001). Basal Zone of the West Antarctic Ice Streams and its Role in Lubrication of Their Rapid Motion. In *The West Antarctic Ice Sheet: Behavior and Environment* (pp. 157–199). American Geophysical Union (AGU). https://doi.org/10.1029/AR077p0157

Kendall, B., Creaser, R. A., Reinhard, C. T., Lyons, T. W., & Anbar, A. D. (2015). Transient episodes of mild environmental oxygenation and oxidative continental weathering during the late Archean. *Science Advances*, *1*(10), 1–7. https://doi.org/10.1126/sciadv.1500777

Kendall, C., Caldwell, E., & Snyder, D. (2004). Resources on Isotopes. Retrieved August 20, 2004, from https://wwwrcamnl.wr.usgs.gov/isoig/period/o_iig.html

Lanoil, B., Skidmore, M., Priscu, J. C., Han, S., Foo, W., Vogel, S. W., … Engelhardt, H. (2009). Bacteria beneath the West Antarctic Ice Sheet. *Environmental Microbiology*, *11*(3), 609–615. https://doi.org/10.1111/j.1462-2920.2008.01831.x

Lerman, A. (1978). CHEMICAL EXCHANGE ACROSS SEDIMENT-WATER INTERFACE. *Annual Review of Earth and Planetary Sciences*, *6*, 281–303.

Retrieved from www.annualreviews.org
Lewis, A. R., Marchant, D. R., Kowalewski, D. E., Baldwin, S. L., & Webb, L. E. (2006). The age and origin of the Labyrinth, western Dry Valleys, Antarctica: Evidence for extensive middle Miocene subglacial floods and freshwater discharge to the Southern Ocean. *Geology*, (7), 513–516. https://doi.org/10.1130/G22145.1
Manheim, F. T., & Waterman, L. S. (1974). *32. Diffusimetry (Diffusion Constant Estimation) on Sediment Cores*. Retrieved from http://deepseadrilling.org/22/volume/dsdp22_32.pdf
McElroy, M. B. (2007). *Ocean Biogeochemical Dynamics*. *Physics Today* (Vol. 60). Princeton, N.J.: Princeton University Press. https://doi.org/10.1063/1.2754608
Menzies, J., van der Meer, J. W., & Shilts, W. W. (2018). Subglacial Processes and Sediments. In *Past Glacial Environments* (pp. 105–158). Amsterdam: Elsevier.
Merlivat, L., & Jouzel, J. (1979). Global climatic interpretation of the deuterium-oxygen 18 relationship for precipitation. *Journal of Geophysical Research*, *84*(C8), 5029. https://doi.org/10.1029/JC084iC08p05029
Michaud, A. B., Skidmore, M. L., Mitchell, A. C., Vick-Majors, T. J., Barbante, C., Turetta, C., … Priscu, J. C. (2016). Solute sources and geochemical processes in Subglacial Lake Whillans, West Antarctica. *Geology*, *44*(5), 347–350. https://doi.org/10.1130/G37639.1
Michaud, A. B., Skidmore, M. L., Mitchell, A. C., Vick-Majors, T. J., Barbante, C., Turetta, C., … Priscu, J. C. (2016). Solute sources and geochemical processes in Subglacial Lake Whillans, West Antarctica. *GEOLOGY*, *44*(5). https://doi.org/10.1130/G37639.1
Mikucki, J. A., Foreman, C. M., Sattler, B., Berry Lyons, W., & Priscu, J. C. (2004). Geomicrobiology of blood falls: An iron-rich saline discharge at the terminus of the Taylor Glacier, Antarctica. *Aquatic Geochemistry*, *10*(3–4), 199–220. https://doi.org/10.1007/s10498-004-2259-x
Montross, S., Skidmore, M., Christner, B., Samyn, D., Tison, J. L., Lorrain, R., … Fitzsimons, S. (2014). Debris-Rich Basal Ice as a Microbial Habitat, Taylor Glacier, Antarctica. *Geomicrobiology Journal*, *31*(1), 76–81. https://doi.org/10.1080/01490451.2013.811316
Murray, J. (2001). What Controls the Composition of Riverwater and Seawater: Equilibrium versus Kinetic Ocean. University of Washington.
Phillips, D. L., & Gregg, J. W. (2001). Uncertainty in source partitioning using stable isotopes. *Oecologia*, *127*, 171–179. https://doi.org/10.1007/s004420000578
Poisson, A. (1980). Conductivity / Salinity / Temperature Relationship of Diluted and Concentrated Standard Seawater. *IEEE Journal of Oceanic Engineering*, *l*, 41–50.
Post, A. L., Hemer, M. A., O'Brien, P. E., Roberts, D., & Craven, M. (2007). A history of benthic colonization beneath the Amery Ice Shelf, East Antarctica. *Marine Ecology Progress*, *344*, 29–37. https://doi.org/10.3354/meps06966
Priscu, J. C. (1998). A Lesson from the bottom of the planet. *Bioscience*.
Priscu, J. C., Achberger, A. M., Cahoon, J. E., Christner, B. C., Edwards, R. L., Jones, W. L., … Vick-Majors, T. J. (2013a). A microbiologically clean strategy for access to the Whillans Ice Stream subglacial environment. *Antarctic Science*, *25*(05), 637–

647. https://doi.org/10.1017/S0954102013000035

Priscu, J. C., Achberger, A. M., Cahoon, J. E., Christner, B. C., Edwards, R. L., Jones, W. L., … Vick-Majors, T. J. (2013b). A microbiologically clean strategy for access to the Whillans Ice Stream subglacial environment. *Antarctic Science*, *25*(5), 637–647. https://doi.org/10.1017/S0954102013000035

Priscu, J. C., & Hand, K. P. (2012). Microbial Habitability of Icy Worlds. *Microbe Magazine*, *7*(4), 167–172. https://doi.org/10.1128/microbe.7.167.1

Priscu, J. C., Kennicutt, M. C., Bell, R. E., Bulat, S. A., Ellis-Evans, J. C., Lukin, V. V., … Tabacco, I. (2005). Exploring Subglacial Antarctic Lake Environments. *EOS*, *86*(20), 193–197. Retrieved from http://www.montana.edu/priscu/documents/Publications/PriscuEtAl2005SubglacialLake.pdf

Priscu, J. C., Wolf, C. F., Takacs, C. D., Fritsen, C. H., Laybourn-Parry, J., Roberts, E. C., … Lyons, W. B. (1999). Carbon Transformations in a Perennially Ice-Covered Antarctic Lake. *BioScience*, *49*(12), 997–1008. https://doi.org/10.1525/bisi.1999.49.12.997

Robinson, N. J., Williams, M. J. M., Barrett, P. J., & Pyne, A. R. (2010). Observations of flow and ice-ocean interaction beneath the McMurdo Ice Shelf, Antarctica. *Journal of Geophysical Research: Oceans (1978–2012)*, *115*(C3). https://doi.org/10.1029/2008JC005255

Rohling, E. J. (2013). Oxygen Isotope Composition of Seawater. *Encyclopedia of Quaternary Science*, *2*, 915–922.

Rutishauser, A., Blankenship, D. D., Sharp, M., Skidmore, M. L., Greenbaum, J. S., Grima, C., … Young, D. A. (2018). Discovery of a hypersaline subglacial lake complex beneath Devon Ice Cap, Canadian Arctic. *Science Advances*, *4*(4), eaar4353. https://doi.org/10.1126/sciadv.aar4353

Scambos, T. A., Bell, R. E., Alley, R. B., Anandakrishnan, S., Bromwich, D. H., Brunt, K., … Yager, P. L. (2017). How much, how fast?: A science review and outlook for research on the instability of Antarctica's Thwaites Glacier in the 21st century. *Global and Planetary Change*, *153*, 16–34. https://doi.org/10.1016/j.gloplacha.2017.04.008

Scherer, R. P., Aldahan, A., Tulaczyk, S., Possnert, G., Engelhardt, H., & Kamb, B. (1998). Pleistocene Collapse of the West Antarctic Ice Sheet. *Science*, *281*(5373), 82–85.

Sharp, M., Parkes, J., Fairchild, I. J., Lamb, H., & Tranter, M. (1999). Widespread bacterial populations at glaciers beds and their relationship to rock weathering and carbon cycling, (2), 107–110. https://doi.org/10.1130/0091-7613(1999)027<0107:WBPAGB>2.3.CO

Shen, L., & Chen, Z. (2007). Critical review of the impact of tortuosity on diffusion. *Chemical Engineering Science*, *62*, 3748–3755. https://doi.org/10.1016/j.ces.2007.03.041

Siegfried, M. R., Fricker, H. A., Carter, S. P., & Tulaczyk, S. (2016). Episodic ice velocity fluctuations triggered by a subglacial flood in West Antarctica. *Geophysical Research Letters*, *43*(6), 2640–2648. https://doi.org/10.1002/2016GL067758

Skidmore, M. L., Foght, J. M., & Sharp, M. J. (2000a). Microbial life beneath a high arctic glacier. *Applied and Environmental Microbiology*, *66*(8), 3214–3220. https://doi.org/10.1128/AEM.66.8.3214-3220.2000

Skidmore, M. L., Foght, J. M., & Sharp, M. J. (2000b). Microbial Life beneath a High Arctic Glacier Microbial Life beneath a High Arctic Glacier †. *Applied and Environmental Microbiology*, *66*(8), 3214–3220. https://doi.org/10.1128/AEM.66.8.3214-3220.2000.Updated

Skidmore, M., Tranter, M., Tulaczyk, S., & Lanoil, B. (2010). Hydrochemistry of ice stream beds—evaporitic or microbial effects? *Hydrological Processes*, *24*(4), 517–523. https://doi.org/10.1002/hyp.7580

Smith, W., Sedwick, P., Arrigo, K., Ainley, D., & Orsi, A. (2012). The Ross Sea in a Sea of Change. *Oceanography*, *25*(3), 90–103. https://doi.org/10.5670/oceanog.2012.80

Stefánsson, U., & Richards, F. A. (1963). Processes contribuing to the nutrient distribution off the Columbia River and Strait of Juan de Fuca. *Limnology and Oceanography*, *8*(4), 394–410. https://doi.org/10.4319/lo.1963.8.4.0394

Studinger, M., Bell, R. E., Blankenship, D. D., Finn, C. A., Arko, R. A., Morse, D. L., & Joughin, I. (2001). Subglacial sediments: A regional geological template for iceflow in West Antarctica. *Geophysical Research Letters*, *28*(18), 3493–3496. https://doi.org/10.1029/2000GL011788

Tranter, M. (2005). Perturbation of Hydrochemical Conditions in Natural Microcosms Entombed within Antarctic Ice. *Geographical*, *12*(6), 273–274.

Tranter, M., Sharp, M. J., Lamb, H. R., Brown, G. H., Hubbard, B. P., & Willis, I. C. (2002). Geochemical weathering at the bed of Haut glacier d'Arolla, Switzerland - A new model. *Hydrological Processes*, *16*(5), 959–993. https://doi.org/10.1002/hyp.309

Tulaczyk, S., Mikucki, J. A., Siegfried, M. R., Priscu, J. C., Barcheck, C. G., Beem, L. H., … Sci, T. (2014). WISSARD at Subglacial Lake Whillans, West Antarctica: scientific operations and initial observations. *Annals of Glaciology*, *55*(65), 51–58. https://doi.org/10.3189/2014AoG65A009

Turner, K. W., Wolfe, B. B., Edwards, T. W. D., Lantz, T. C., Hall, R. I., & Larocque, G. (2014). Controls on water balance of shallow thermokarst lakes and their relations with catchment characteristics: a multi-year, landscape-scale assessment based on water isotope tracers and remote sensing in Old Crow Flats, Yukon (Canada). *Global Change Biology*, *20*(5), 1585–1603. https://doi.org/10.1111/gcb.12465

Vick-Majors, T. J., Achberger, A., Santibáñez, P., Dore, J. E., Hodson, T., Michaud, A. B., … Priscu, J. C. (2016). Biogeochemistry and microbial diversity in the marine cavity beneath the McMurdo Ice Shelf, Antarctica. *Limnology and Oceanography*, *61*(2), 572–586. https://doi.org/10.1002/lno.10234

Vick-Majors, T. J., Michaud, A. B., Skidmore, M. L., Turetta, C., Christner, B. C., Christianson, K., … Priscu, J. C. (n.d.). Subglacial carbon and nutrient fluxes to the marine cavity under the Ross Ice Shelf, 1–25.

Vogel, S. W. (2004). *The basal regime of the West-Antarctic ice sheet interaction of subglacial geology with ice dynamics*. *Arctic*. University of California, Santa Cruz. https://doi.org/3127401

Vogel, S. W., Tulaczyk, S., Kamb, B., Engelhardt, H., Carsey, F. D., Behar, A. E., … Joughin, I. (2005). Subglacial conditions during and after stoppage of an Antarctic Ice Stream: Is reactivation imminent? *Geophysical Research Letters*, *32*(14). https://doi.org/10.1029/2005GL022563

Wadham, J. L., Tranter, M., Skidmore, M., Hodson, A. J., Priscu, J., Lyons, W. B., … Jackson, M. (2010). Biogeochemical weathering under ice: Size matters. *Global Biogeochemical Cycles*, *24*(3). https://doi.org/10.1029/2009GB003688

Yuan-Hui, L., & Gregory, S. (1974). Diffusion of ions in sea water and in deep-sea sediments. *Geochimica et Cosmochimica Acta*, *38*(5), 703–714. https://doi.org/10.1016/0016-7037(74)90145-8

CHAPTER THREE

SEDIMENT POREWATER ORGANIC MATTER CONTENT

Contribution of Authors and Co-authors

Author: Kimberly A. Roush

Contributions: Processed sediment core, porewaters and analyzed data, generated figures and tables and wrote thesis.

Co-author: John Priscu

Contributions: Provided funding, oversight, samples, conceived the study, and aided in thesis preparation.

Co-author: John Dore

Contributions: Provided oversight for nutrient analysis and interpretation.

Co-author: Wei Li

Contributions: Processed sediment core.

Co-author: Tristy Vick-Majors

Contributions: Provided framework and oversight for organic matter analysis.

Co-author: WISSARD science and drilling team

Contributions: Drilling ice, acquiring sediment core and providing logistics.

Manuscript Information

Kimberly A. Roush, John Priscu, John Dore, Wei Li, Tristy Vick-Majors and the WISSARD Science Team

Status of Manuscript:
__X__ Prepared for submission to a peer-reviewed journal
____ Officially submitted to a peer-reviewed journal
____ Accepted by a peer-reviewed journal
____ Published in a peer-reviewed journal

Introduction

The Ross Ice Shelf Project (RISP, 1977-1978) was the first to profile oceanographic characteristics and analyze biological activity beneath the Ross Ice Sheet (RIS). Located at site J9, the station was located about 400 km from the edge of the RIS (Clough and Hansen 1979). A diversity of organisms, including bacteria, algae and microzooplankton were identified throughout the water column (Azam et al. 1979). Microbial heterotrophic activity under the RIS was shown to be 10^3 to 10^4 times lower than in the Ross Sea. Sediment sampling at the J9 site was noteworthy as it was first time benthic sediment from the Ross Sea was cored.

The Ross Ice Shelf Project (RISP) identified other sources of organic material that could serve as a source of advected organic matter at the WGZ (Azam et al. 1979). Samples collected at J9 with RISP provide context for local planktonic and benthic organisms in the southern part of the Ross Sea. After drilling through 360 m of the RIS and sampling the 237 m water column underlying the Ross Ice Shelf, a diversity of bacteria, eukaryotic phytoplankton (including pennate and centric diatoms, dinoflagellates, and silicoflagellates), algae (including 37 taxa that comprise 30% of Antarctic flora (Gambi et al. 2000), protozoans (including radiolarians and tintinnids), metazoans (including crustaceous zooplankton) were identified (Azam et al. 1979). Overall, the water column (8.7×10^6 to 1.2×10^7 bacteria per liter) and sediment (10^7 to 10^8 bacteria per gram, dry weight) contained sparse populations of bacteria (Azam et al. 1979).

Data collected on five tracks (1994; 1995-1996) aboard the *R.V.I.B. Nathaniel B. Palmer* revealed the extreme variability in space and depth (Mean Surface POC range = 14.4 to 37.3 mmol L^{-1}; Integrated POC concentration range = 0.8 to 2.72 mol m^{-2}) of organic matter concentrations as a result of extensive phytoplankton blooms during the austral summer (Mosby 2013; Asper 2003). Waters in the northern portion of the Ross Sea are characterized by a lower concentration of POC (Smith et al. 1996) and is thought to be due to the presence of a longer ice cover than the southern Ross Sea. The southern Ross Sea has a different food web and also exhibits substantial spatial variation in organic matter, which appear to be correlated with the length of time the region is ice free (Arrigo et al. 1999).

Vick-Majors and others (2016b) evaluated the water column beneath the McMurdo Ice Shelf (MIS) and reported DOC values of 42.1 µM and 31.8 µM at 30-m and 850-m water column depth (total water column depth was 872 m from the ice-water interface to the seafloor).

While Alder and others stated that there is essentially no organic matter derived from the continent in the Southern Ocean (Alder et al. 2016), the DOC concentration was 221 µmol L^{-1} in the SLW column water (Christner et al. 2014; Vick-Majors et al. 2016a). Christner and others hypothesized that DOC could be laterally advected from open water polynyas more than 1000 km away and/or transported as a result of subglacial flow from biotic (heterotrophy and chemoautotrophy) and abiotic (weathering of aluminosilicates) sources (Christner et al. 2014). Advected phytoplankton carbon and in situ chemolithoautotrophic production provide important sources of organic matter and other reduced compounds to partially support ecosystem processes in the dark waters of the RIS cavity (Vick-Majors et al. 2016a; 2016b).

Previous research suggests that rates of chemosynthesis exceed rates of heterotrophic production at freshwater SLW (Christner et al. 2014; Mikucki et al. 2016; Vick-Majors 2016). Rates of dark C^{14}-bicarbonate incorporation directly above the sediments were approximately three times higher (100 ng C l^{-1} d^{-1}) (Mikucki et al. 2016) than rates in the water column (about 1 m above the sediment-water interface). Dark carbon fixation rates in the SLW water column are comparable to rates reported from the North Atlantic Ocean (75 ng C l^{-1} d^{-1}) (Herndl et al. 2005). Phylogenetic analysis of samples from SLW water and sediments showed a diverse community dominated by taxa related to chemolithoautotrophs that use reduced N, Fe and S species in energy generating pathways. The SLW water column contained more species than the surficial sediment (0-2 cm), containing 3931 compared to 2424 groups or OTUs (Achberger et al. 2016).

Redox data at SLW also suggests a distinct transition from the water column to the sediments (Mikucki et al. 2016). While dissolved oxygen was 71.9 μmol l^{-1} in the column water at SLW (sediment oxygen was not analyzed), dissolved oxygen at the water sediment interface on the continental coast of the Patton Escarpment was 140 μmol l^{-1}(Rabouille and Gaillard 1991). In general, [^{14}C] bicarbonate incorporation, redox data and 16S DNA data support the conclusion that a greater diversity of species are present in the water column than in the sediment porewater (Achberger et al. 2016; Mikucki et al. 2016).

Table 3. 1 Primary production rates for environments relevant to biogeochemistry at the WGZ. *Daily rates (RISP R9, 4.2 mg C m^{-2} d^{-1} ; Arctic, 1.0 mg C m^{-2} d^{-}) reported by Horrigan were converted to (g C m^{-2} yr^{-1}) (Horrigan 2012).

Location	Primary Productivity (g C m^{-2} yr^{-1})	Primary Production (chemo- or photo-)	Citation
RISP J9 [C^{14}] bicarbonate incorporation	1.533	Chemoautotrophic	(Horrigan 2012)
Ross Sea sector, Southern Ocean [C^{14}] bicarbonate incorporation	69	Phototrophic	(Arrigo et al. 2008a)
Ross Sea Continental Shelf [C^{14}] bicarbonate incorporation	179	Phototrophic	(Arrigo et al. 2008b)
Arctic	0.365	Chemotrophic	(Horrigan, 2012)
SLW – water column (average dark [^{14}C] bicarbonate incorporation)	3.29E9 g C L^{-1} d^{-1}	Chemoautotrophic	(Vick-Majors et al. 2016)
SLW – water directly overlying sediments [^{14}C] bicarbonate incorporation	1.0E-7 g C L^{-1} d^{-1}	Chemoautotrophic	(Mikucki et al. 2016)

Table 3. 2 DOC concentration of SLW compared to the Ross Sea open water concentration.

Location	**Concentration (µmol C L^{-1})**	**Citation**
SLW water column	221	(Vick-Majors et al. in review; Christner et al. 2014)
WGZ water column	74.9	(Vick-Majors et al. in review)
WGZ pore water	1,600	(current research)
Ross Sea open water	41.5	(Vick-Majors et al. 2018; Hansell et al. 1998)
Ross Sea water column	44.2	(Carlson et al. 1998)
Antarctic Ice Sheet	12.5	(Hood et al. 2015)
WISSARD MIS	42.1/31.8*	(Vick-Majors et al. 2016b)

*Represents samples taken at 30-m/850-m below ice water interface.

Table 3. 3 C:N ratios of DOM in SLW were determined for the water column, surface sediment porewater and the flux ratio from the sediment to the porewater (Vick-Majors et al. 2016).

Source	Water Column	Surface Sediment Porewater	Flux Ratio
SLW	95.2	14.5	10.0

Methods

Sediment Particulate Organic Carbon (PC) and Particulate Organic Nitrogen (PN)

A 2.0 cm resolution profile was created for the 70 cm sediment core. From each 2 cm puck, a 2.0 g sample of sediment was sieved with water using sequential 250 µm and 2000 um sieves yielding the following size fractions: 250 to 2000 µm and <250 µm. Different procedures were applied to the two different size fractions. Sediment from the 250 to 2000 µm sediment fraction was placed in a 50 mL Falcon tube with ~20 mL of rinse water (w/v = 0.10 g mL^{-1}). The Falcon tube was centrifuged for 10 minutes at 10,000 xg to separate the sediment from the rinse water. The pH and the conductivity of the rinse water (supernatant) were measured, the supernatant was decanted and 1.0 mL of 3N HCl was added to the wet sediment to remove DIC. Following the acidification step, three to five Milli-Q washes were done to bring the pH of the rinse water to ~5 and remove the salts. The rinsed, acidified and neutralized sediment samples for the <250 µm fraction were then placed in pre-weighed tins and dried for 24 hours at 105ºC. Detailed preparation is outlined in Appendix. Sediments for the 250 to 2000 µm fraction were transferred to clean, washed 20 mL scintillation vials with 1.0 of 3 N HCl and swirled. Scintillation vials with sediments and HCl were placed on a hot plate. A 250 mL beaker was place on the hot plate with 150 mL water and maintained at 60°C water temperature for ~1.5 to 2 hours or until the HCl evaporated and the inorganic carbon was removed.

Samples of fractions <250 µm and 250 to 2000 µm for PC:PN were analyzed with a ThermoFinnigan Elemental analyzer. Replicates were run for the < 250 µm size fraction (Appendix).

A standard curve ranging from 0.2 to 1.0 mg acetanilide (71.09% carbon, 10.36% nitrogen) was generated, bracketing the range of carbon and nitrogen in the samples. Peak areas were corrected for tin cup blank averages. A soil reference standard (3.5% carbon and 0.37% nitrogen) was used to check sample percent recovery nitrogen (109.7% N) and percent recovery carbon (101.0% C).

<u>Porewater Dissolved Organic Carbon (DOC) and Total Dissolved Nitrogen (TDN)</u>

The upper 22-cm sediment core section was band saw cut frozen in a -5°C cold room (Figure 2.2) and thawed for ~10 hours in a ~12°C room before slicing the sediment core into pucks (Figure 2.3) and concentrating the sediments via centrifugation on a Sorvall Legend Machlok at 4°C. Supernatant from replicate 30.0 mL HS borosilicate screw-top vials was placed into 0.2 μm, 500 μL VWR Centrifugal filter modified nylon, low protein binding snap top vials (product number #82031-356) and spun for an additional 3 minutes at 10,000 xg on the VWR 24:16 centrifuge (product number 37001-300) to remove any remaining particulate matter. The deep core section (41 cm) was band saw cut frozen and the same procedure was used to separate sediments and porewater.

Porewater samples for DOC and TDN were aliquoted into milliQ rinsed, acid washed and combusted (> 4 hours at 475ºC) 20 mL glass serum vials with polytetrafluoroethylene (PTFE) lined caps and stored at 4 ºC until analysis. DOC and TDN concentrations were determined using a Shimadzu TOC-VCSH TOC analyzer.

All glassware used for the DOC and TDN analyses was soaked overnight in NoChromix acid solution (GODAX Laboratories), followed by six rinses with nanopure water (18.2 MΩ) and 8 h of baking at 500^{0}C. A standard curve ranging from 0.3 to 15 ppm of potassium hydrogen phthalate ($C_8H_5KO_4$) in nanopure water (0.3, 0.5, 1.0, 1.25, 1.5, 1.75, 2.0, 2.5, 3, 5, 7, 10 and 15 ppm) was made and run in conjunction with a DSR CRM (Deep Sea Reference Consensus Reference Material) water (41-45 µM DOC) kindly supplied by the Hansell Lab from the University of Miami. According to Shimadzu, the range of detection for total carbon is 4 µg L^{-1} to 30,000 µg L^{-1} and for total dissolved nitrogen is 5 µg L^{-1} to 30,000 µg L^{-1} .

Results

Sediment Particulate Organic Carbon and Particulate Organic Nitrogen

My sediment fractionation procedure yielded two size fractions: <250 µm and 250 to 2,000 µm. PC and PN and PC:PN ratios from both size fractions were determined every two centimeters throughout the sediment core. For GC3 sediments <250µm (Figure 3.1), PC concentration values range from 52.5 µmol C g^{-1} to 239 µmol C g^{-1} dry sediment with an average of 177.7 ± 43.4 μmol C g^{-1}. PN concentration values range from 1.5 to 21.9 μmol N g^{-1} dry sediment with an average of 15.3 ± 4.6 μmol N g^{-1} dry sediment.

Sediment between 250 μm and 2,000 μm (Figure 3.2) ranged from 42.1 to 141.8 μmol C g^{-1} dry sediment with an average ± s.d. of 77.3 ± 34.5 μmol C g^{-1}. Sediment between 250 μm and 2,000 μm (2 mm) ranged from 1.5 to 5.6 μmol N g^{-1} dry sediment with an average ± s.d. of 3.3 ± 1.4 μmol N g^{-1}. Molar ratios vary from a minimum to maximum of 11.0 to 30.7 with a whole core (2 to 65 cm) average of 23.0 ± 7.8.

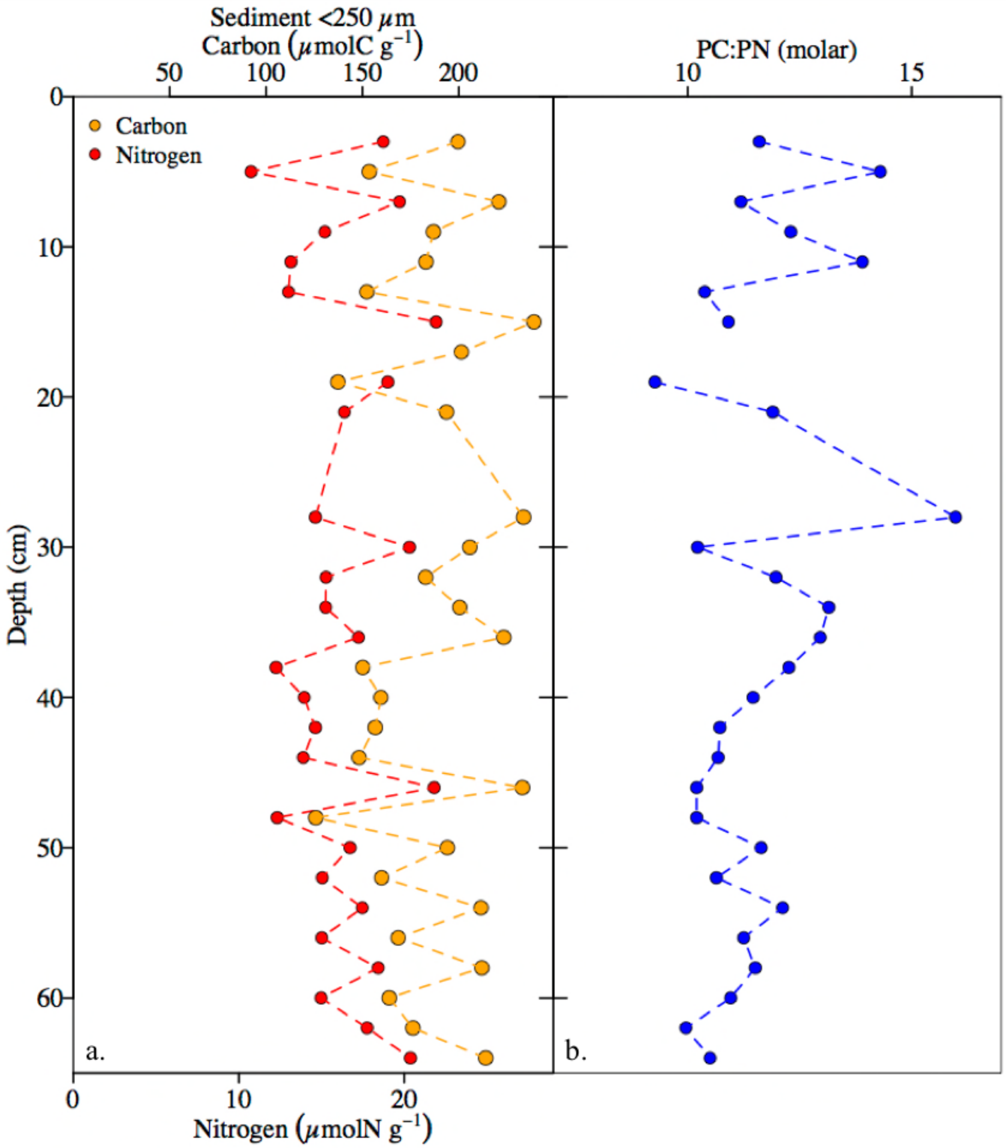

Figure 3.1 a) Particulate carbon, particulate nitrogen and c) PC:PN for sediment <250 µm in particle size. The Nitrogen sample from 17 cm was removed for unreasonably low concentration.

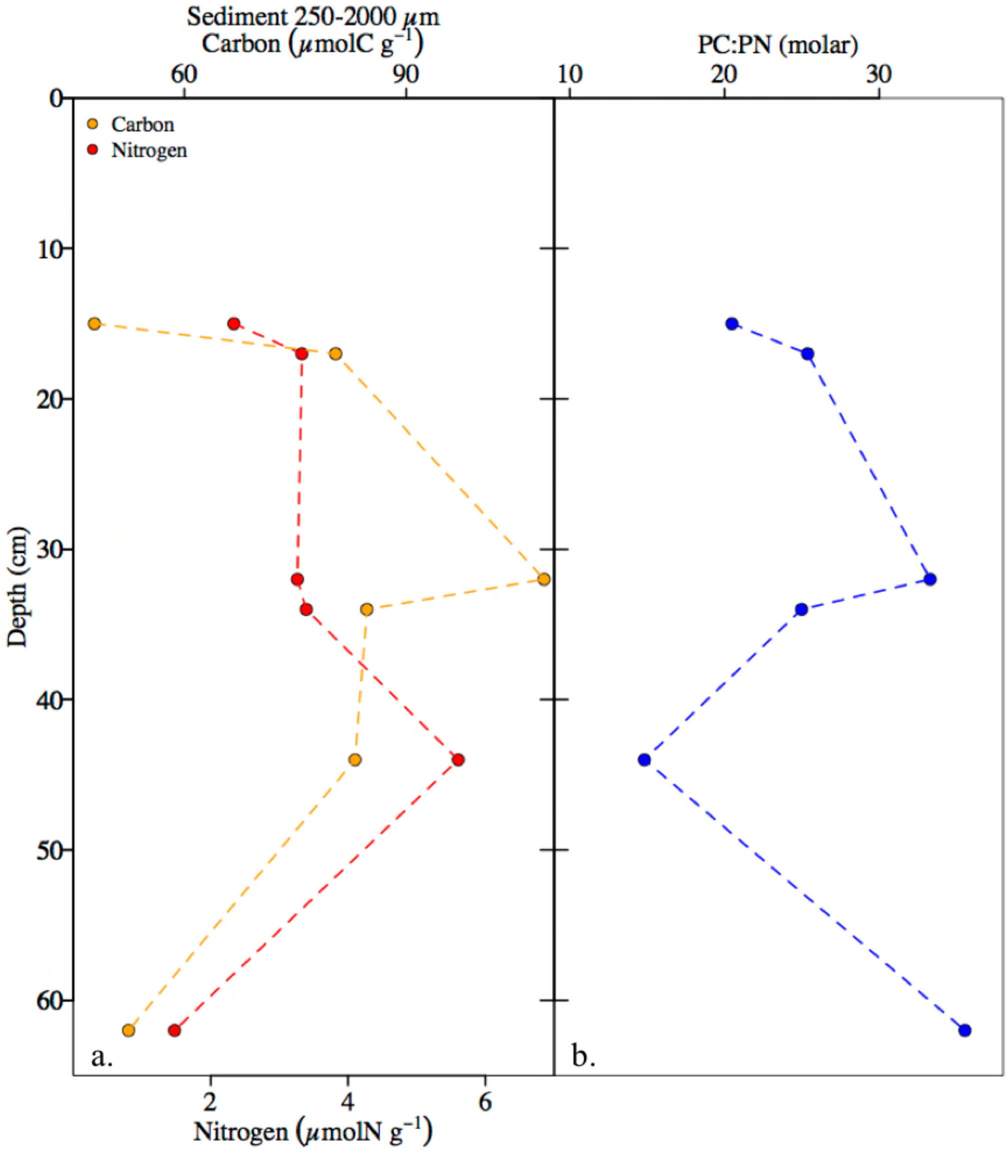

Figure 3.2 The figure shows a) PC (μmol g^{-1}), PN (μmol g^{-1}), and b) PC:PN (molar) for sediments from 250 to 2000 μm.

Porewater Dissolved Organic Carbon and Total Dissolved Nitrogen

My analysis identified that porewater DOC ranges from 520 µmol L^{-1} at 11 cm to 2600 µmol L^{-1} at 48 cm. The shallow section (2-24 cm) averaged 1,000 µmol DOC L^{-1}, the deep section (27-68 cm) had an average of 1,900 µmol DOC L^{-1} and the average DOC over the whole core was 1,600 µmol DOC L^{-1}.

Porewater TDN ranged from 33 µmol TDN L^{-1} at 19 cm to 75 µmol TDN L^{-1} at 50 cm. The shallow section averaged 44 µmol TDN L^{-1}, whereas the deep section averaged of 48 µmol TDN L^{-1} and the whole core averaged 46 µmol TDN L^{-1}.

Table 3.4 Concentrations of DOC in the WGZ porewater compared to other Antarctic environments.

Location	**Concentration (µmol C L^{-1})**	**Citation**
SLW water column	221	(Vick-Majors et al. in review; Christner et al. 2014)
SLW sediment porewater	667	(Vick-Majors, unpublished data)
WGZ water column	74.9	(Vick-Majors et al., in review)
WGZ sediment porewater	1615	(current research)
Ross Sea open water	41.5 – 41.9	(Vick-Majors et al. 2018; Hansell et al. 1998)
Ross Sea water column	44.2	(Carlson and Hansell 2003)
Antarctic Ice Sheet	12.5	(Hood et al. 2015)
WISSARD MIS	42.1/31.8*	(Vick-Majors et al. 2016b)

*Represents samples taken at 30-m/850-m below ice water interface.

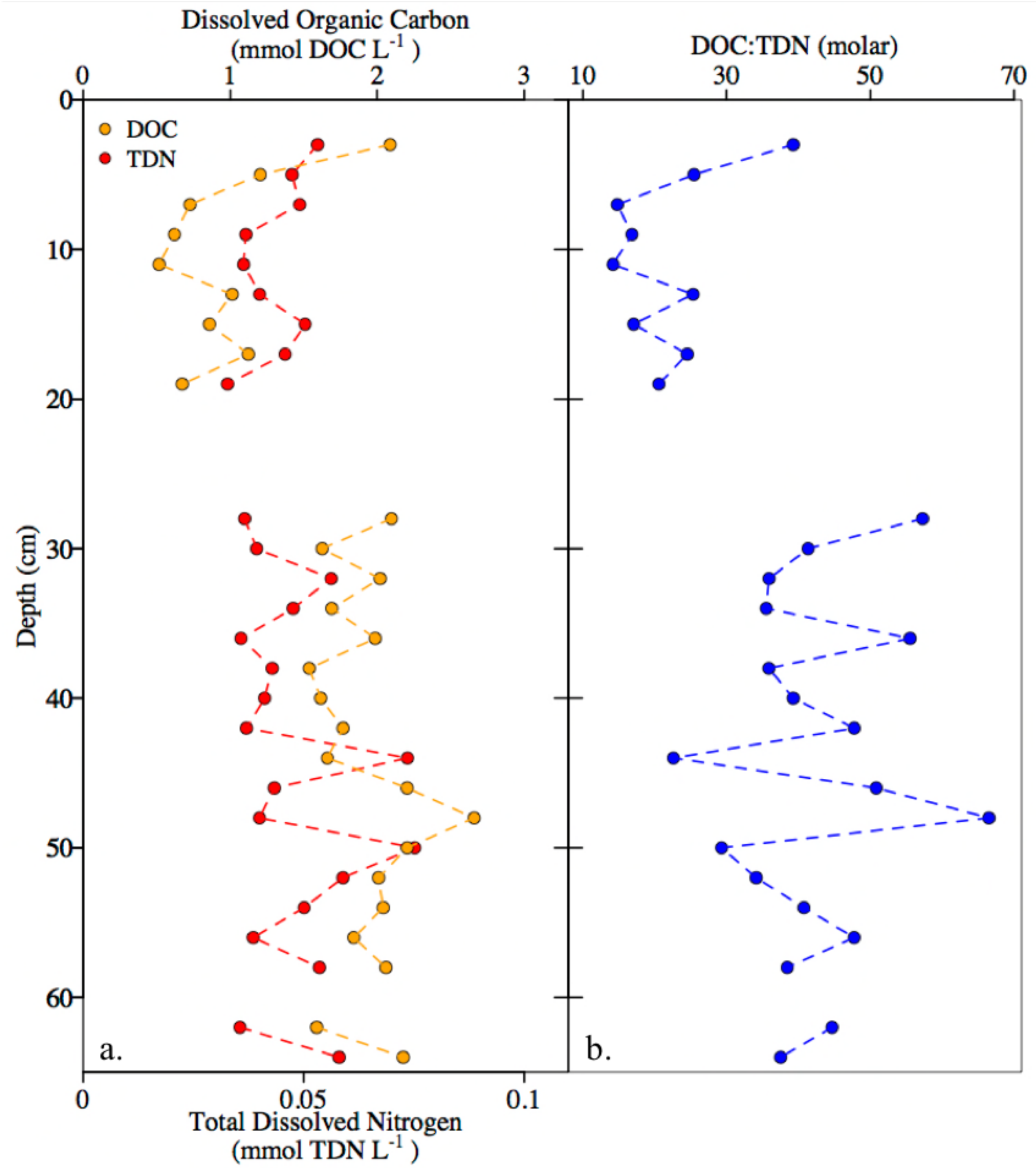

Figure 3.3 a) WGZ GC3 porewater TDN, DOC, and b) C:N are shown.

Discussion

Sediment Particulate Organic Carbon and Particulate Organic Nitrogen

Sediments <250 µm have a total core PC:PN average of 11.5 ± 0.5 (molar). The largest size fraction of sediments (250 to 2000 µm) has a PC:PN molar ratio of 25.8 ± 7.8. The Redfield Ratio is the stoichiometric ratio at which phytoplankton are typically in balanced growth. The average particulate C:N molar ratio of microbial biomass in the oceans is 6.6 (Redfield et al. 1963). Elemental analysis of global stoichiometric C:N:P ratios sampled mostly from 5 to 20 m depth and at latitudes between -90°S to -60°S and 10° to 35°N suggest that there continues to be a strong correlation between C and N for global evaluations, but systematic regional differences show variations that stray from the standard 106:16:6 Redfield Ratio of C:N:P (Martiny et al. 2013; Martiny et al. 2014).

Sediments with a particulate organic matter molar ratio greater than 6.6 are considered depleted in nitrogen, while sediments with a ratio less than 6.6 are considered to be nitrogen sufficient relative to balanced microbial growth. Although the WGZ is located under 800 m of ice and is not photosynthetically active, the Redfield Ratio provides a crude proxy for comparison. It is important to note that Redfield based his ratio on phytoplankton, not heterotrophic bacteria (C:N:P:Fe = 100:24:6:1) (Egli 2015). This indicates that all of the sediment size fractions may be N-deficient with respect to bacterial growth. The < 250 µm fraction is 1.5 times more nitrogen deficient that the stoichiometric Redfield Ratio (Molar C:N = 6.6) and the 250 – 2,000 µm fraction is 3.5 times more nitrogen deficient. Figure 3.4 shows that sediment samples above the red dashed line are depleted in particulate nitrogen relative to carbon, while samples below the red dashed line would be enriched in nitrogen relative to the Redfield Ratio.

SLW sediment has a molar PC concentration of 384.2 ± 37.0 μmol C g^{-1} dry weight (based on upper 2 cm of sediment), a molar PN concentration of 21.5 ± 1.7 μmol N g^{-1} dry weight and an average molar PC:PN ratio of 65.4 ± 0.3 (Christner et al. 2014). Sediment from the WGZ GC3 core has an average PC concentration of 184.6 ± 18.6 μmol C g^{-1} dry weight, an average PN of 15.7 ± 1.8 μmol N g^{-1} dry weight and an average PC:PN ratio (molar) of 11.5 ± 0.5. This suggests that SLW sediments are enriched with 52% more PC, 27% more PN and a molar PC:PN ratio with 82% more in SLW sediments than WGZ sediments. With a molar PC:PN ratio of 65.4 ± 0.3, SLW sediments are more depleted in nitrogen than WGZ sediments (11.8). SLW sediment contained a particulate carbon-particulate nitrogen molar ratio of 17.9, implying N-deficiency.

The WGZ water column (n=2) has a PC concentration of 23.0 ± 5.4 μmol L^{-1}, a PN concentration of 0.6 ± 0.1 μmol L^{-1}, and an average PC:PN (molar) ratio of 37.2 ± 2.3 (Vick-Majors, unpublished data). The SLW water column has a PC concentration of 78.5 ± 7.4 μmol C L^{-1}, a PN concentration of 1.2 ± 0.4 μmol N L^{-1} and an average PC:PN (molar) ratio of 65.4 ± 0.3 (Christner et al. 2014). The SLW water column shows evidence of N-deficiency according to the Redfield Ratio.

It is possible that soil particulate carbon and particulate nitrogen could be dissolved and serve as a source of particulates or DOM in the sediment porewater, but it is not likely that PC and PN would diffuse to the water column unless sediments are located in a higher energy system where there is greater turbidity in the water column.

Porewater Dissolved Organic Carbon and Total Dissolved Nitrogen

Sediments will be assumed to: not contain fauna and be dominated by vertically oriented molecular diffusion as a means of solute transport. Vertical diffusion is limited by the size of the solute particle (Nikaido and Rosenberg 1981). Given the porosity (0.45) and assuming constant gradients, diffusion could facilitate the geochemical transfer of solute sized carbon from benthic sediment porewater to the water column. Any reduction in porosity will diminish diffusive flux.

My analysis found that WGZ porewater DOC from the GC3 sediment column was, on average, 1.60 mmol DOC L^{-1}, with a minimum of 0.52 mmol DOC L^{-1} at 11 cm and a maximum of 2.60 mmol DOC L^{-1} at 48 cm. The shallow section (2 to 24 cm) had an average of 1.00 mmol DOC L^{-1}, the deep section has an average of 1.90 mmol DOC L^{-1} and the whole core had an average 1.60 mmol DOC L^{-1}. The deep section contained 47.3% more DOC than the shallow section. Overall porewater DOC:TDN data suggests that most samples are depleted in TDN relative to the Redfield Ratio as most porewater sample points are above the Redfield Ratio represented by the dashed red line (Figure 3.5).

The WGZ column water contains 0.75 mmol DOC L^{-1} (Vick-Majors et al., in review). The Ross Sea water column was reported to have a concentration of 0.44 mmol DOC L^{-1}(Hansell and Carlson 1998). When WGZ porewater (1.60 mmol DOC L^{-1}) is compared to the column water of SLW (0.22 ± 0.06 mmol DOC L^{-1}), WGZ porewater shows 86.2% more DOC than SLW column water.

Due to the relatively high concentration of dissolved organic carbon in SLW column water (0.22 ± 0.06 mmol DOC L^{-1}) compared to the DOC in WGZ waters, I suggest that subglacial waters from SLW, basal melt and other subglacial organic sources that could have originally decomposed, been lithified in the rock record and/or frozen into the ice serve as a potential source of dissolved organic carbon at the WGZ (Vick-Majors et al., in review). DOC in the SLW water column averaged about five times greater than average values for the deep ocean and similar to the maximum range estimate for Subglacial Lake Vostok (0.09 – 0.16 mmol L^{-1}) (Christner et al. 2014). SLW surface sediment porewater concentrations of DOM were found to exceed those of the water column (Christner et al. 2014). The presence of acetate and formate in the WGZ water column at concentrations 1.3 and 1.2 μM L^{-1}, respectively, indicates that 0.11% and 0.1% (where average porewater DOC at the WGZ was 1.6 mmol L^{-1}) of the water was comprised of acetate and formate. This suggests that at least a small fraction of the DOC was labile. The DOC in SLW is thought to originate from ancient marine sediments, chemoautotrophic production or a combination of the two (Christner et al. 2014).

WGZ GC3 porewater TDN ranges from 0.03 mmol TDN L^{-1} at 19 cm to 0.08 mmol TDN L^{-1} at 50 cm (Figure 3.3). The deep core section has 4% more average TDN than the shallow core section. TDN was 0.04 mmol L^{-1} in the overlying water column.

Soluble reactive phosphorous levels in SLW were similar to the total inorganic nitrogen pool (dissolved N:P molar ratio of 1.1), suggesting a biologically nitrogen-deficient system, relative to phosphorus. Additionally, ammonia is an energy source for chemolithoautotrophic ammonia-oxidizing bacteria and archaea (Christner et al. 2014).

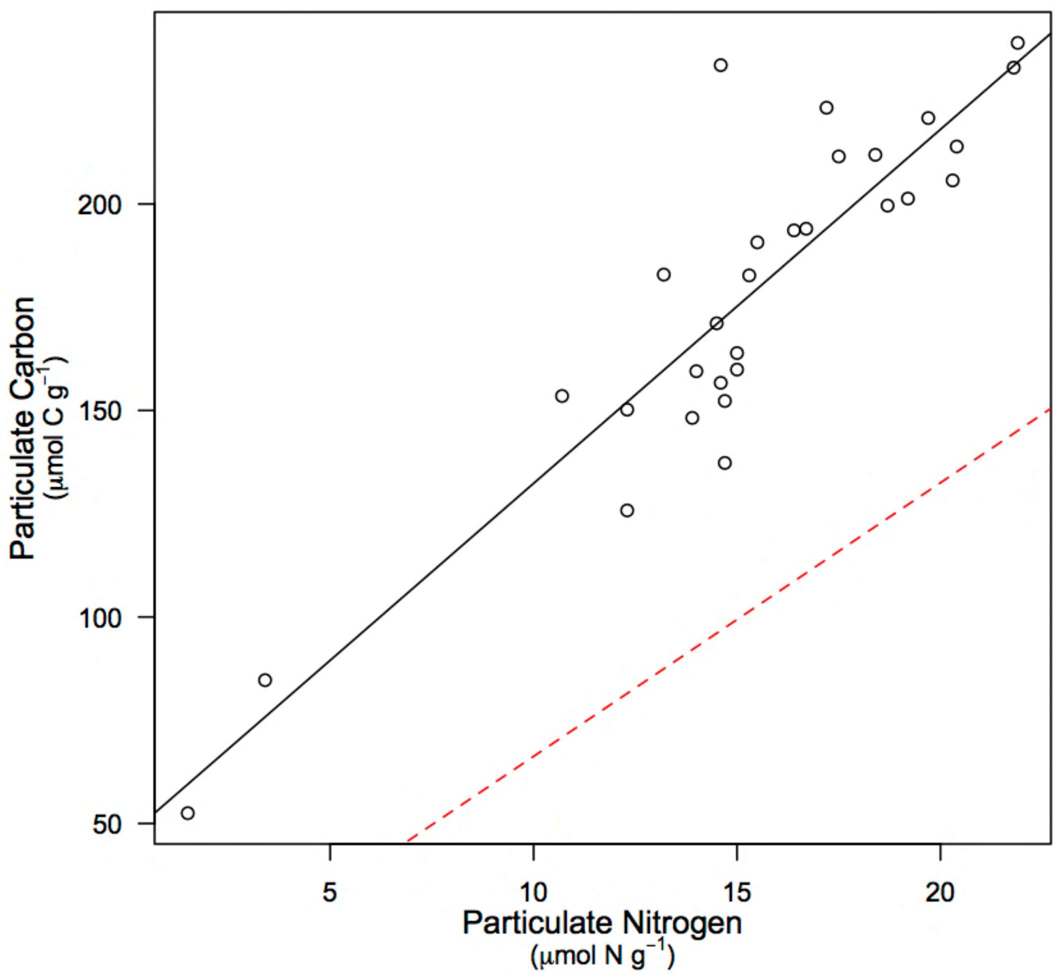

Figure 3.4. The black line is the regression line of GC3 porewater samples and the dashed red line represents the Redfield Ratio line, where y = 6.682x. Samples above the dashed red line are depleted in nitrogen relative to carbon. All of sediment samples from the ≤ 250 µm size fraction are depleted in nitrogen relative to the Redfield Ratio.

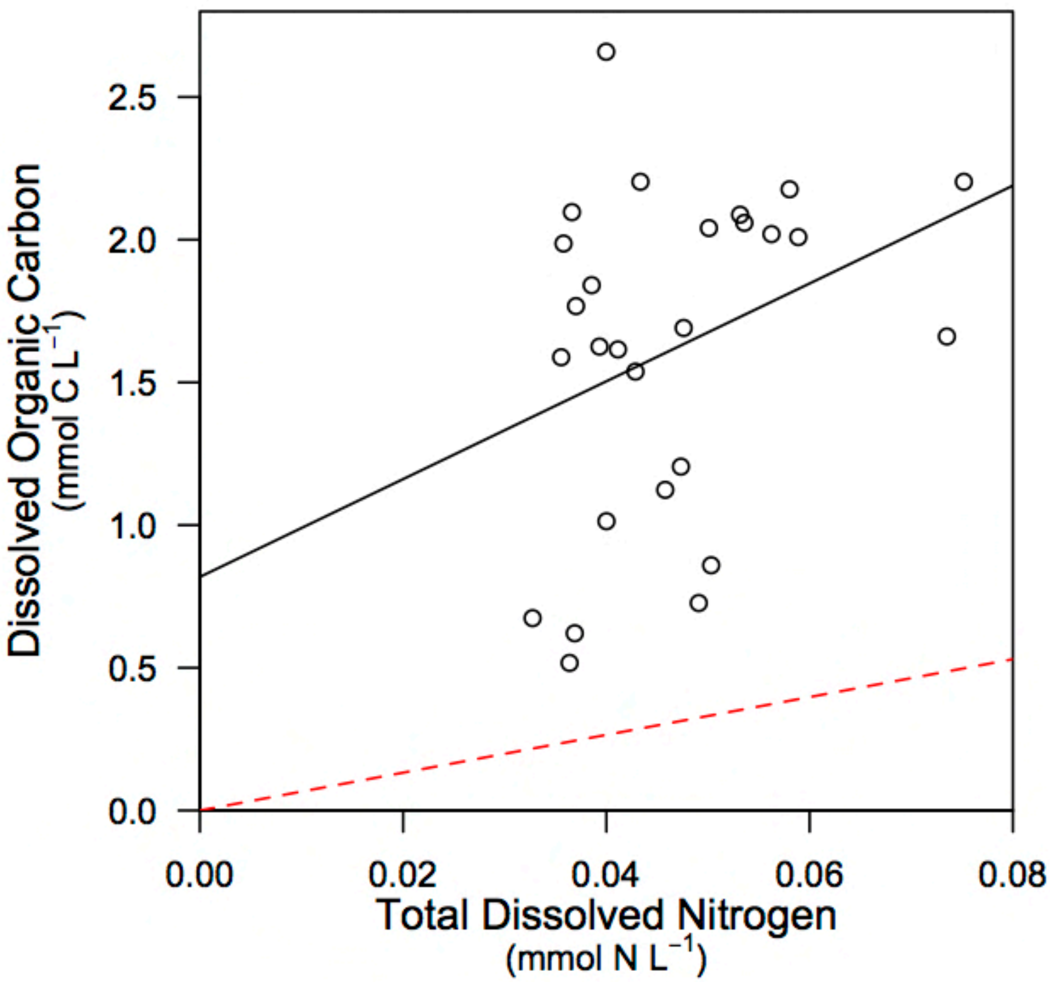

Figure 3.5. The relationship between DOC and TDN in the porewater samples from the WGZ relative to the Redfield Ratio (dashed red line) is shown here. All porewater samples are depleted in total dissolved nitrogen relative to dissolved organic carbon since they plot above the Redfield Ratio line, y = 6.625x.

<u>Conclusions</u>

The majority of sediments from the GC3 sediment core show that most samples, regardless of size fraction, are depleted in nitrogen. The smaller particle size fraction, <250 um, has an average molar PC:PN ratio of 9.8 while the larger particle size fraction, between 250 um and 2 mm, has an average molar PC:PN ratio of 23, indicating that the larger size fraction is more nitrogen-depleted than the smaller size fraction.

The overall PC:PN molar ratio of the WGZ sediments was 11.5 ± 1.5. The average molar PC:PN ratio of cast 1 and 2 in the water column was 37.2 ± 2.3 (Vick-Majors et al. unpublished), indicating that the WGZ water column was more depleted in nitrogen relative to sediments in GC3. The molar PC:PN ratio in the surficial SLW sediment layer and water column were 17.9 and 65.4, respectively (Christner et al. 2014). This suggests that the subglacial SLW sediments were more depleted in particulate nitrogen than sediments at the WGZ.

The Ross Sea Mesoscale Experiment (RoME) sampled 43 different hydrological stations in three different areas in the Ross Sea water column (Mangoni et al. 2017). Ecological measurements yielded a POC:PON molar ratios of 5.7 to 7.0 (Mangoni et al. 2017), which is close to the Redfield Ratio. In comparison, molar ratios from the SLW and WGZ water columns were 65.4 and 37.2, respectively. This suggests they are more recalcitrant than the Ross Sea data.

Sediment porewater DOC at the WGZ was 1,600 μM DOC L^{-1}, while the overlying column water was 74.9 μM C L^{-1} (Vick-Majors et al. in review). Consequently, sediment DOC should be a source to the WGZ water column via upward diffusion. Given the higher concentrations of TDN in the sediment porewater water column (43.7 μmol L^{-1}) relative to the water column (33.1μmol L^{-1}), the sediments should also be a source of TDN to the WGZ water column via upward diffusion. Data suggests that potential sources of dissolved organic matter appear come from upstream subglacial sources and from sediment porewater by diffusion.

Future Directions

For future processing, it is recommended that samples for ions be stored frozen (-20°C) in screw-top vials (similar to those used for isotopes). Although phytoplankton community and trophic structure in the Ross Sea in response to increases in water temperature was addressed by Mangoni and others (2017), there remain questions about how nutrients, organic matter and geochemistry vary seasonally with the annual increase in phytoplankton production under the ice shelf. Assuming the SLW subglacial network participates in a 16-year drain and fill hydrologic cycle, the question remains as to whether patterns of incremental increase in organic matter and chemolithotrophic derived geochemical concentrations (sulfate, ammonia) are observed throughout the cycle.

Bibliography

Achberger, A. M., Christner, B. C., Michaud, A. B., Priscu, J. C., Skidmore, M. L., Vick-Majors, T. J., & Team, W. S. (2016). Microbial Community Structure of Subglacial Lake Whillans, West Antarctica. *Frontiers in Microbiology*, *7*, 1457. https://doi.org/10.3389/fmicb.2016.01457

Alder, V., Azzaro, M., Hucke-Gaete, R., Mosetti, R., Orgeira, J. L., Quartino, L., … Marschoff, E. R. (2016). Chapter 36H. Southern Ocean. *Chapter 36H. Southern Ocean*, 1–41.

Arrigo, K. R., Robinson, D. H., Worthen, D. L., Dunbar, R. B., DiTullio, G. R., VanWoert, M., & Lizotte, M. P. (1999). Phytoplankton community structure and the drawdown of nutrients and CO2 in the southern ocean. *Science (New York, N.Y.)*, *283*(5400), 365–367. https://doi.org/10.1126/SCIENCE.283.5400.365

Arrigo, K. R., van Dijken, G. L., & Bushinsky, S. (2008). Primary production in the Southern Ocean, 1997–2006. *Journal of Geophysical Research*, *113*(C8), C08004. https://doi.org/10.1029/2007JC004551

Arrigo, K. R., van Dijken, G., & Long, M. (2008). Coastal Southern Ocean: A strong anthropogenic CO2sink. *Geophysical Research Letters*, *35*(21). https://doi.org/10.1029/2008GL035624

Asper, V. (2003). The Distribution of Particulate Organic Carbon and its Dynamics in the Southern Ross Sea. In *Biogeochemistry of the Ross Sea Antarctic Research Series*. https://doi.org/10.1029/078ARS15

Azam, F., Beers, J. R., Campbell, L., Carlucci, A. F., Holm-Hansen, O., Reid, F. M. H., & Karl, D. M. (1979). Occurrence and Metabolic Activity of Organisms Under the Ross Ice Shelf, Antarctica, at Station J9. *Science*, *203*(4379), 451–453. https://doi.org/10.1126/science.203.4379.451

Carlson, C. A., & Hansell, D. A. (2003). The Contribution of Dissolved Organic Carbon and Nitrogen to the Biogeochemistry of the Ross Sea, *78*, 123–142. https://doi.org/10.1029/078ARS08

Christner, B. C., Priscu, J. C., Achberger, A. M., Barbante, C., Carter, S. P., Christianson, K., … Purcell, A. (2014). A microbial ecosystem beneath the West Antarctic ice sheet. *Nature*, *512*(7514), 310–313. https://doi.org/10.1038/nature13667

Clough, J. W., & Hansen, B. L. (1979). The Ross Ice Shelf Project. *Science*, *203*(4379), 433–434.

Egli, T. (2015). Microbial growth and physiology: a call for better craftsmanship. *Frontiers in Microbiology*, *06*, 287. https://doi.org/10.3389/fmicb.2015.00287

Gambi, M. C., Buia, M. C., Mazzella, L., Lorenti, M., & Scipione, M. B. (2000). Spatio-Temporal Variability in the Structure of Benthic Populations in a Physically Controlled System off Terra Nova Bay: The Shallow Hard Bottoms. In F. M. Faranda, L. Guglielmo, & A. Ianora (Eds.), *Ross Sea Ecology: Italiantartide Expeditions (1987--1995)* (pp. 527–538). Berlin, Heidelberg: Springer Berlin Heidelberg. https://doi.org/10.1007/978-3-642-59607-0_38

Hansell, D. A., & Carlson, C. A. (1998). Deep-ocean gradients in the concentration of dissolved organic carbon. *Nature*, *395*(6699), 263–266.

https://doi.org/10.1038/26200

Herndl, G. J., Reinthaler, T., Teira, E., van Aken, H., Veth, C., Pernthaler, A., & Pernthaler, J. (2005). Contribution of Archaea to total prokaryotic production in the deep Atlantic Ocean. *Applied and Environmental Microbiology*, *71*(5), 2303–2309. https://doi.org/10.1128/AEM.71.5.2303-2309.2005

Hood, E., Battin, T. J., Fellman, J., O'Neel, S., & Spencer, R. G. M. (2015). Storage and release of organic carbon from glaciers and ice sheets. *Nature Geoscience*, *8*(2), 91–96. https://doi.org/10.1038/ngeo2331

Horrigan, S. G. (1981). Primary production under the Ross Ice Shelf , Antarctica, *26*(2), 378–382.

Mangoni, O., Saggiomo, V., Bolinesi, F., Margiotta, F., Budillon, G., Cotroneo, Y., … Saggiomo, M. (2017). Phytoplankton blooms during austral summer in the Ross Sea, Antarctica: Driving factors and trophic implications. *Plos One*, *12*(4), 1–23. https://doi.org/10.1371/journal.pone.0176033

Martiny, A. C., Vrugt, J. A., & Lomas, M. W. (2014). Concentrations and ratios of particulate organic carbon, nitrogen, and phosphorus in the global ocean. *Scientific Data*, *1*, 140048. https://doi.org/10.1038/sdata.2014.48

Martiny, A. C., Vrugt, J. A., Primeau, F. W., & Lomas, M. W. (2013). Regional variation in the particulate organic carbon to nitrogen ratio in the surface ocean. *Global Biogeochemical Cycles*, *27*(3), 723–731. https://doi.org/10.1002/gbc.20061

Mikucki, J. A., Lee, P. A., Ghosh, D., Purcell, A. M., Mitchell, A. C., Mankoff, K. D., … Scherer, R. (2016). Subglacial Lake Whillans microbial biogeochemistry: a synthesis of current knowledge. https://doi.org/10.1098/rsta.2014.0290

Mosby, A. F. (2013). *Phytoplankton Growth Rates in the Ross Sea, Antarctica*. College of William and Mary in Virginia.

Nikaido, H., & Rosenberg, E. Y. (1981). Effect on solute size on diffusion rates through the transmembrane pores of the outer membrane of Escherichia coli. *The Journal of General Physiology*, *77*(2), 121–135. Retrieved from http://www.ncbi.nlm.nih.gov/pubmed/7021759

Rabouille, C., & Gaillard, J. -F. (1991). A coupled model representing the deep-sea organic carbon mineralization and oxygen consumption in surficial sediments. *Journal of Geophysical Research: Oceans*, *96*(C2), 2761–2776. https://doi.org/10.1029/90JC02332

Redfield, A. C., Ketchum, B. K., & Richards, F. A. (1963). The influence of organisms on the composition of sea-water. In M. N. Hill (Ed.), *The Sea: Ideas and Observations on Progress in the Study of the Seas* (pp. 26–77). New York, NY: John Wiley.

Smith, W. O., Nelson, D. M., DiTullio, G. R., & Leventer, A. R. (1996). Temporal and spatial patterns in the Ross Sea: Phytoplankton biomass, elemental composition, productivity and growth rates. *Journal of Geophysical Research: Oceans*, *101*(C8), 18455–18465. https://doi.org/10.1029/96JC01304

Vick-Majors, T. J. (2016). *Biogeochemical Processes in Antarctic Aquatic Environments: Linkages and Limitations*. Montana State University.

Vick-Majors, T. J., Achberger, A., Santibáñez, P., Dore, J. E., Hodson, T., Michaud, A.

B., … Priscu, J. C. (2016). Biogeochemistry and microbial diversity in the marine cavity beneath the McMurdo Ice Shelf, Antarctica. *Limnology and Oceanography*, *61*(2), 572–586. https://doi.org/10.1002/lno.10234

Vick-Majors, T. J., Michaud, A. B., Skidmore, M. L., Turetta, C., Christner, B. C., Christianson, K., … Priscu, J. C. (n.d.). Subglacial carbon and nutrient fluxes to the marine cavity under the Ross Ice Shelf, 1–25.

Vick-Majors, T. J., Mitchell, A. ., Achberger, A. ., Christner, B. ., Dore, J. E., Michaud, A. B., … Priscu, J. C. (2016). Physiological ecology of microorganisms in Subglacial Lake Whillans. *Frontiers in Microbiology*, *7*(October), 1–16. https://doi.org/10.3389/fmicb.2016.01705

APPENDIX

Table 4.1 The following table shows the tool, date and time of collection for each sample.

Tool	Time sample was collected	Date
CTD	*0434	9/Jan/2015
Niskin	1955	9/Jan/2015
Multicore	*0142	10/Jan/2015
WTS-LV	*0735	10/Jan/2015
GT probe	1900	10/Jan/2015
Piston Core	*0115	11/Jan/2015
CTD	2007	11/Jan/2015
Niskin	*0000	13/Jan/2015
Multicore	*0303	13/Jan/2015
Multicore	*0555	13/Jan/2015
WTS-LV	1000	13/Jan/2015
CTD and Niskin	1615	13/Jan/2015
Gravity corer	1703	13/Jan/2015
Piston Core	2332	13/Jan/2015
GT probe	1044	14/Jan/2015
WTS-LV and Niskin	1900	14/Jan/2015
Multicore	1015	15/Jan/2015
Niskin	1240	15/Jan/2015
Gravity corer	1723	15/Jan/2015
WTS-LV, Niskin, and Fishtrap	*0130	18/Jan/2015
Multicore	*0811	18/Jan/2015
Multicore	1839	18/Jan/2015
Fishtrap	*0100	19/Jan/2015

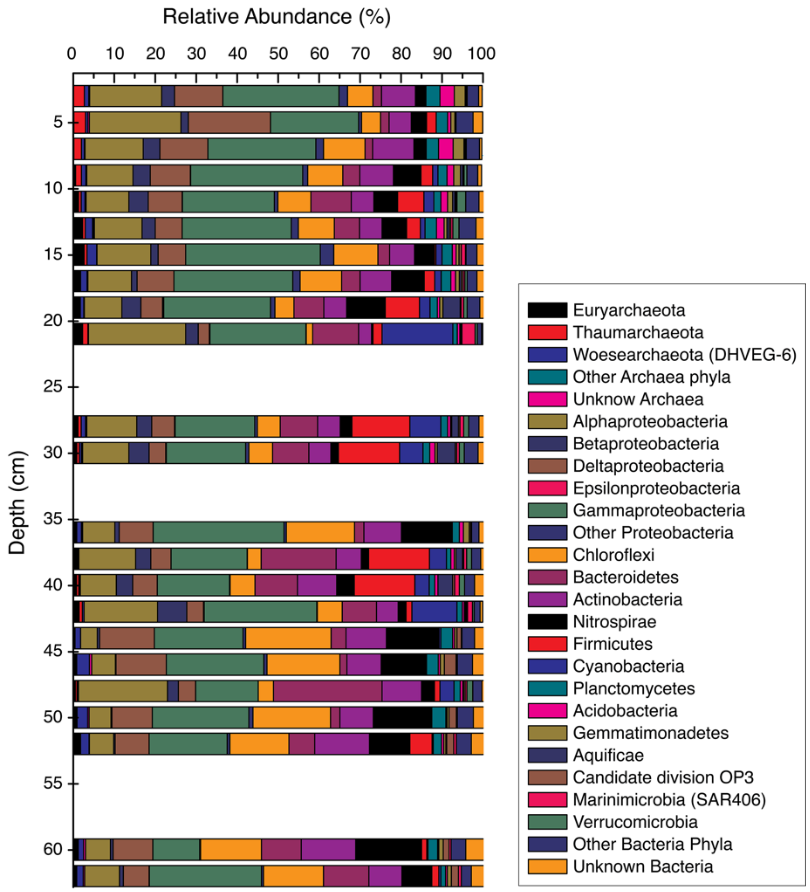

Figure 4.2 Relative abundance at the phylum level is shown above (Li, unpublished data)

<u>Marine Sediment Preparation for PC:PN Sediment Analysis</u>

<u>Sieving Sediments</u>

1. Gently break up a ~2.0 g plug of sediment with mortar and pestle.
2. Transfer sediments to a 250 µm sieve.
3. Wet sieve (using minimal milliQ water) sediments through a 250 µm sieve into a 250 mL beaker.
4. Repeat process with desired number of samples.

<u>Small fraction (<250µm), Acidification and Neutralization</u>

1. Transfer sediment slurry from 250 mL beaker to a 50 mL Falcon tube. Use more milliQ water from squeeze bottle to get all remaining sediments from beaker into Falcon.
2. Bring Falcons to ~20 mL. Vortex slurry for 20 seconds. Balance in centrifuge. Centrifuge 10 minutes at 10,000G.
3. Check pH and conductivity.
4. Pour off supernatant.
5. Add 1.0 mL of 3.0 N HCl. Vortex. Balance tubes.
6. Centrifuge*.
7. Check pH.
8. Pour off supernatant.
9. Add ~20 mL milliQ water to each Falcon. Vortex. Balance.
10. Centrifuge.
11. Check pH. Pour off supernatant.
12. Repeat cycle of multiple milliQ washes until pH stabilizes ~5.
13. Preheat incubator 105˚C.
14. Transfer sediments to pre-weighed tin boats.
15. Dry sediments at 105˚C for 24 hours.
16. Weigh sediments of mass, 200-250 mg, into pre-weighed CN tins.

<u>Large fraction (250-2000 µm), Acidification</u>

1. Transfer sediments to a clean, washed 20 mL scintillation vial.
2. Place burner in hood.
3. Place ~150mL of water in a 250 mL beaker with thermometer on ring stand set up to gauge temperature (see photo below). Maintain water about 60C. (about 4 on grey Corning Stirrer/Hot Plate, Priscu Lab)
4. Add 1.0 mL of 3 N HCl. Swirl.
5. Evaporate HCl for ~1.5-2 hours in scintillation vial to remove inorganic carbon. (No bubbling/fizzing during HCl occurred. HCl turned yellow after a few minutes.) Stir to prevent sediments from cooking to glass vial.

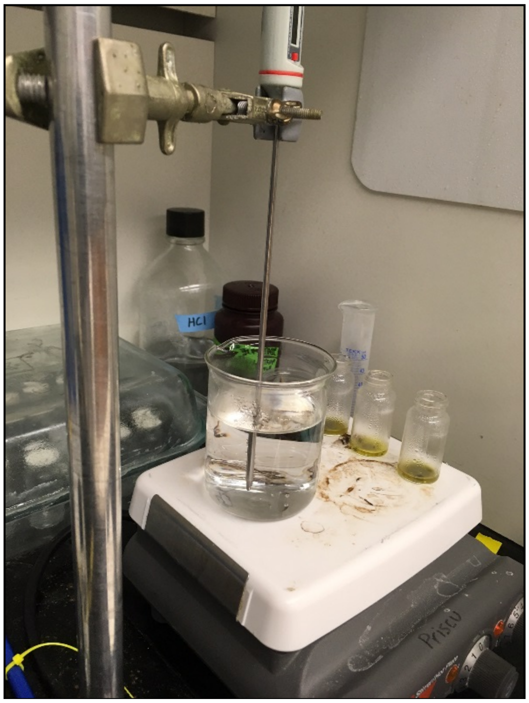
HCl

Table 4.2 Isotope, ion and ion ratio data.

	(‰)		(mM)										
Depth (cm)	**$\delta^{18}O$**	**δD**	**Chloride**	**Bromide**	**Sulfate**	**Sodium**	**Potassium**	**Calcium**	**Magnesium**	**Na.K**	**SO4.Cl**	**Br.Cl**	**Na.Cl**
5 m Cast Average	-2.28	3.62	529.03	0.88	22.77	492.16	10.75	11.45	58.45	45.96	0.04	0	0.93
3	-1.97	-12.1	549.87	0.84	32.36	519.88	12.04	11.14	55.24	43.19	0.06	0	0.95
5	-0.43	-4.7	644.68	1.1	30.58	586.48	12.12	13.69	68.7	48.39	0.05	0	0.91
7	-1.03	-4.54	633.55	1.07	30.21	576.17	12.6	13.45	66.61	45.73	0.05	0	0.91
9	-0.06	-0.21	606.45	1.01	30.32	557.73	12.04	13.01	63.84	46.32	0.05	0	0.92
11	-0.65	-2.66	672.74	1.11	34.29	618.57	13.71	14.62	69.74	45.1	0.05	0	0.92
13	-2.74	-20.19	517.2	0.83	26.48	478.06	10.6	11.31	53.42	45.08	0.05	0	0.92
15	-0.22	-2.05	584.83	0.96	31.4	538.55	11.64	13.05	61.34	46.27	0.05	0	0.92
17	-0.63	-4.08	542.36	0.89	29.17	503.83	10.77	11.77	55.31	46.79	0.05	0	0.93
19	0.2	0.45	NA	NA	NA	NA	NA	NA	NA	NA	NA	NA	NA
21	NA	NA	NA	NA	NA	NA	NA	NA	NA	NA	NA	NA	NA
28	-0.61	-2.22	567.95	0.94	28.74	528.14	11.89	12.66	58.17	44.42	0.05	0	0.93
30	-0.37	-1.5	530.5	0.88	28.6	497.53	11.22	11.76	53.65	44.34	0.05	0	0.94
32	-0.38	-1.83	540.1	0.89	29.31	510.72	11.07	12.25	55.05	46.14	0.05	0	0.95
34	-0.42	-1.97	539.4	0.89	28.78	510.16	11.08	12.3	54.55	46.05	0.05	0	0.95
36	-0.46	-1.97	531.85	0.88	28.81	501.95	11.07	12.04	53.95	45.35	0.05	0	0.94
38	-0.54	-2.44	528.44	0.87	28.7	499.79	10.83	11.95	53.17	46.15	0.05	0	0.95
40	-0.8	-8.01	532.71	0.88	28.79	502.34	11.15	11.96	53.86	45.04	0.05	0	0.94
42	-0.74	-4.88	545.81	0.88	28.8	511.27	11.21	12.26	55.46	45.62	0.05	0	0.94
44	-1.47	-6.45	543.57	0.9	28.91	513.94	11.41	12.29	54.8	45.03	0.05	0	0.95
46	-0.43	-3.46	552.94	0.91	29.15	519.66	11.3	12.2	56.33	45.99	0.05	0	0.94
48	-0.51	-3.81	561.98	0.93	29.29	526.64	10.94	13.24	57.93	48.12	0.05	0	0.94
50	-0.81	-4.61	553.95	0.91	29.15	518.71	10.89	12.96	56.96	47.62	0.05	0	0.94
52	-0.8	-4.58	548.19	0.89	28.98	509.7	10.92	12.65	56.11	46.66	0.05	0	0.93
54	-1.16	-5.74	539.13	0.89	28.41	505.58	10.78	12.91	55.47	46.88	0.05	0	0.94
56	-0.83	-5.03	546.95	0.9	28.69	512.64	10.94	12.87	56.13	46.84	0.05	0	0.94
58	-0.9	-5.53	541.37	0.96	28.53	NA	11	13.33	55.66	NA	0.05	0	NA
60	NA	NA	NA	NA	NA	NA	NA	NA	NA	NA	NA	NA	NA
62	-0.97	-6.3	537.81	0.89	28.72	505.18	10.62	12.5	55.1	47.57	0.05	0	0.94
64	-1.37	-9.29	545.03	0.9	28.66	511.85	11.27	13.03	55.36	45.43	0.05	0	0.94